

**Crustal Architecture, Cretaceous Rise and Igneous Activity of Sabine, Monroe and  
Jackson Uplifts, Northern Gulf of Mexico Basin**

---

A Thesis

Presented to the

Faculty of the Department of Earth and Atmospheric Sciences

University of Houston

---

In Partial Fulfillment

of the Requirements for the Degree

Master of Science

---

By

Sukru Gokhan Kose

December 2013

**Crustal Architecture, Cretaceous Rise and Igneous Activity of Sabine, Monroe and  
Jackson Uplifts, Northern Gulf of Mexico Basin**

---

Sukru Gokhan Kose

APPROVED:

---

Dr. Jonathan Snow, Chairman

---

Dr. Jolante Van Wijk, Co-Chairman

---

Dr. Shuhab Khan

---

Dr. Dale Bird

---

Dean, College of Natural Sciences and  
Mathematics

## **ACKNOWLEDGEMENT**

First and foremost, I am very grateful to my company, Turkish Petroleum Corporation (TPAO), who funded my graduate school education at the University of Houston and made this research study possible.

I would like to express my gratitude to my committee chair, Dr. Jonathan Snow for his guidance during my study. I would also like to express my deeply appreciation to my advisor, Dr. Jolante Van Wijk, who has supported and guided me throughout my thesis with her knowledge, patience, and encouragement. I am also very grateful to Dr. Dale Bird for his valuable comments, suggestions, and critical discussions during my interpretations. He has never left my questions unanswered and always showed me the best approaches to the problems. I also want to thank Dr. Shuhab Khan for his contributions to my study.

Finally, I would like to thank my family and friends for their unconditional love and support.

**Crustal Architecture, Cretaceous Rise and Igneous Activity of Sabine, Monroe and  
Jackson Uplifts, Northern Gulf of Mexico Basin**

---

A Thesis

Presented to the

Faculty of the Department of Earth and Atmospheric Sciences

University of Houston

---

In Partial Fulfillment

of the Requirements for the Degree

Master of Science

---

By

Sukru Gokhan Kose

December 2013

## **ABSTRACT**

Structural highs and lows that formed during the Cretaceous resulted in regional angular unconformities in the northern onshore Gulf of Mexico Basin. Some of the uplifts, with varying size and amplitude, are located where Cretaceous magmatism occurred. The Sabine, Monroe and Jackson Uplifts were formed during this period. The rising of the Sabine Uplift during the Late Cretaceous created major traps for oil and gas accumulation in East Texas Field and natural gas plays have been discovered related with the Monroe and Jackson structures.

The objectives of this study are: 1) to investigate crustal architecture of the area; 2) to locate subsurface Cretaceous igneous rocks; 3) to evaluate the Cretaceous tectonic events of the Sabine, Monroe and Jackson Uplifts; 4) to investigate the relationship between magmatism and uplift. To interpret these important structures and igneous bodies, gravity and magnetic anomaly data, and enhancements of these data were examined. Three 2D transects, ranging from 470 to 650 km-long, through the uplifts were constructed and modeled. Models were constrained by seismic, well and geological data.

Our results suggest that the crystalline crust of the northern onshore Gulf of Mexico Basin was variably extended beneath the Sabine, Monroe and Jackson Uplifts. There is a thick crust beneath Sabine Uplift with a shallow basement and deep Moho. The thickness

of the crust decreases to the south. From west to east interior basins are located between high standing structures and are characterized by thick accumulations of salt. Upper Cretaceous igneous activity modified and was superimposed upon the crustal and basinal structures. This activity was followed by partial erosion of the uplifted formations, resulting in angular unconformities. The Monroe and Jackson structures were locally uplifted during the Late Cretaceous. This age of uplifts and igneous rocks suggests that the rise of the structures during this time was associated with igneous activity. We interpreted the local rise of the Sabine Uplift, during the Woodbine and Eagle Ford Gulf Stages, as a result of the magmatism modeled in this study. Unraveling the complex relationship between this structuring and magmatism requires a solid understanding of the crustal architecture of the region.

## Table of Contents

LIST OF FIGURES.....	ix
CHAPTER I. INTRODUCTION.....	1
1.1.MOTIVATION AND OBJECTIVES .....	1
1.2. STUDY AREA .....	4
CHAPTER II. GEOLOGICAL AND TECTONIC SETTING .....	6
2.1. REGIONAL GEOLOGY.....	6
2.1.1. Drift and Rotation of Yucatan Block.....	8
2.2. NORTH-CENTRAL GULF OF MEXICO – INTERIOR ZONE.....	9
2.2.1. Sabine Uplift.....	10
2.2.2. Monroe Uplift .....	14
2.2.3. Jackson Dome .....	15
2.3. PREVIOUS WORK AND MODELS.....	17
2.3.1. Plutonic Dome Model and Volcanic Activity.....	18
2.3.2. Flexural Model .....	18
2.3.3. Anticline Model.....	20
2.3.4. Mantle Plume Model .....	20
CHAPTER III. DATA.....	23
3.1. GRAVITY DATA .....	23
3.2. MAGNETIC DATA.....	24
3.3. OTHER DATA .....	25
CHAPTER IV. METHODS.....	35
4.1. DATA ENHANCEMENT METHODS .....	35
4.1.1. Upward Continuation.....	36
4.2.2. First Vertical Derivative.....	36
4.2.3. Total Horizontal Gradient .....	37
4.2.4. Reduction to the Pole .....	38
4.2. FORWARD MODELING .....	40
4.2.1. Model Parameters .....	42
CHAPTER V. RESULTS AND INTERPRETATIONS .....	47

5.1. QUALITATIVE INTERPRETATIONS.....	47
5.1.1. Sabine Uplift.....	53
5.1.2. Monroe Uplift .....	54
5.1.3. Jackson Dome .....	55
5.2. FILTERED MAPS .....	56
5.3. 2-D GRAVITY MODELS.....	69
5.3.1. Model 1: L-101 (AA`) .....	73
5.3.2. Model 2: L-102 (BB`) .....	77
5.3.3. Model 3: L-103 (CC`) .....	82
5.4. CRUSTAL THICKNESS, DEPTH TO MOHO AND DEPTH TO BASEMENT MAPS.....	85
5.5. SUBSURFACE IGNEOUS ROCKS .....	88
CHAPTER VI .....	90
CHAPTER VI. DISCUSSION .....	90
6.1. INTERPRETATIONS AND MODELS .....	90
6.2. CRUSTAL STRUCTURE.....	94
6.3. STRUCTURAL EVOLUTION OF THE UPLIFTS.....	98
CHAPTER VII. CONCLUSION.....	106
CHAPTER VIII. REFERENCES.....	109

## LIST OF FIGURES

Figure 1.1: Map showing the location of study area.....	4
Figure 2.1: Four phases of the early evolution of the Gulf of Mexico Basin (from Buffler, 1991): A) Late Triassic – Early Jurassic Rifting; B) Middle Jurassic Crustal Extension; C) Formation of oceanic crust during Late Jurassic; D) Subsidence Phase during Early Cretaceous.....	7
Figure 2.2: Opening phases of the Gulf of Mexico Basin with a hotspot track A) Initial position as 160 Ma B) after oceanic crust and mantle plume track with a total of 42° of rotation. (Bird et al., 2005).....	9
Figure 2.3: Location map of Ups and Downs of Onshore Northern Gulf of Mexico Basin. The name of the basins and uplifts were labeled in the legend.....	11
Figure 2.4: Igneous activity around vicinity of Sabine Uplift, Monroe Uplift and Jackson Dome (Locations of the igneous rocks are gathered from Baksi, 1997; Ewing, 2009; Kidwell, 1951).....	13
Figure 2.5: Distribution of the wells in Monroe Uplift and Jackson Dome igneous material has been encountered (Baksi, 1997).....	15
Figure 2.6: Hypothetical cross-section goes over the Jackson Dome, shows the correlation between igneous body and short wavelength, high amplitude gravity and magnetic anomalies (Moody, 1949).....	17
Figure 2.7: Set of four curves showing calculated deflection of the lithosphere for varying effective elastic thickness (Nunn, 1990).....	19
Figure 2.7: Late Cretaceous-Early Tertiary structural and paleogeographic features in southwestern North America (Jackson and Laubach, 1988).....	21

Figure 2.8: Predicted paths of the Bermuda hotspot relative to North America based on data (Cox and Van Arsdale, 2002).....	21
Figure 2.9: Schematic illustration of passage of North America over the Bermuda plume during the Cretaceous super plume mantle event (Cox and Van Arsdale, 2002).....	22
Figure 3.1: Onshore Bouguer Gravity Data of area of interest.....	24
Figure 3.2: Magnetic Intensity Map of the area of interest.....	25
Figure 3.3: Location map of control points with basins and uplifts of the area.....	27
Figure 3.4: Result of a seismic refraction experiment along 94°W in east Texas (Hales et al., 1970).....	28
Figure 3.5: Structural cross-sections of sedimentary rocks, crust and upper mantle in Northern Gulf of Mexico (Worzel and Watkins, 1973). Locations of the profiles are shown on figure 3.3.....	29
Figure 3.6: Regional cross sections over Northeast Texas. A) E-W cross sections through East Texas Salt Basin and Sabine Uplift. B) N-S cross section over the same area. Locations of profiles are shown on each map over Texas State County Map (modified from Nichols et al., 1966).....	31
Figure 3.7: Published well-log data and lithological interpretations with a thickness of 3800 m in Carthage Field, Texas (Rogers, 1968).....	32
Figure 3.8: Moho depth and crustal thicknesses of the study area (modified from Sawyer et al., 1991).....	33
Figure 4.1: Gravity and horizontal gradient anomalies over a tabular source body (modified from Blakely, 1995).....	38
Figure 4.2: A magnetic anomaly a) before being reduced to the pole; b) after being reduced to the pole (modified from Blakely, 1995).....	39

Figure 4.3: Process chart of forward modeling. Measured anomaly is represented by M where calculated anomaly is represented by C (modified from Blakely, 1995).....	41
Figure 4.4: Generalized stratigraphic column and nomenclature of Northeast Texas (Nichols et al., 1966).....	43
Figure 4.5: Correlation of Mesozoic subsurface nomenclature of Northeast Texas with Arkansas and Louisiana (Nichols et al., 1966).....	44
Figure 5.1: Contoured Bouguer Gravity Anomaly Map (Contours are in mGal.).....	49
Figure 5.2: Interpreted anomalies of Sabine, Monroe and Jackson Uplifts on Bouguer Gravity Map. Black solid lines show the locations of 2-D gravity models.....	50
Figure 5.3: Contoured reduced to pole magnetic intensity map (Contours are in nT).....	51
Figure 5.4: Interpreted anomalies of Sabine, Monroe and Jackson Uplifts on reduced to pole magnetic anomaly map. Black solid lines show the locations of 2-D gravity models.....	52
Figure 5.5: A) 15 km upward continuation Bouguer gravity map B) 15 km upward continuation Bouguer gravity residual map.....	58
Figure 5.6: A) 15 km upward continuation reduced – to – pole magnetic intensity map B) 15 km upward continuation reduced – to – pole magnetic intensity residual map.....	59
Figure 5.7: Residual Maps of 15 km upward magnetic and gravity data. Assigned numbers are interpreted anomalies over Sabine, Monroe and Jackson Uplifts. Black solid lines show the locations of 2-D gravity models.....	60
Figure 5.8: Total horizontal gradient (THG) of Bouguer Gravity Data. Assigned numbers are interpreted anomalies over Sabine, Monroe and Jackson Uplifts. Black solid lines show the locations of 2-D gravity models.....	61

Figure 5.9: Total horizontal gradient (THG) of Reduced – to – pole magnetic intensity.....	62
Figure 5.10: Total horizontal gradient (THG) of Reduced – to – pole magnetic intensity with interpreted anomalies of Sabine, Monroe and Jackson Uplifts. Black solid lines show the locations of 2-D gravity models.....	63
Figure 5.11: Analytic Signal of Bouguer gravity data.....	64
Figure 5.12: 2-D Gravity model locations through the interpreted anomalies of Sabine, Monroe and Jackson Uplifts on the analytic signal map of Gravity data.....	65
Figure 5.13: Analytic signal of reduced – to – pole magnetic intensity data.....	66
Figure 5.14: 2-D Gravity model locations through the interpreted anomalies of Sabine, Monroe and Jackson Uplifts on the analytic signal map of magnetic data.....	67
Figure 5.15: 100 km low pass of a) Bouguer gravity data; b) reduced – to – pole magnetic intensity data.....	68
Figure 5.16: 2-D gravity model locations.....	71
Figure 5.17: Properties of 2-D gravity model layers.....	71
Figure 5.18: Topography of the area (GTOPO 30 digital elevation model was used to generate the map).....	72
Figure 5.19: Crustal view of preferred 2-D gravity model for profile L-101 (see figure 5.17 for legend); A)Observed reduced – to – pole magnetic anomalies; B) Observed and calculated gravity values in mGal; C)1,5 times vertically exaggerated version of final model; D) No vertical exaggeration. Locations of the assigned numbers are shown in anomaly and filter maps.....	75

Figure 5.20: Basin view of preferred 2-D gravity model for profile L-101 (see figure 5.11 for legend); A) Observed and calculated gravity values in mGal; B) Basin view of model – 6 times vertically exaggerated C) No vertical exaggeration.....	76
Figure 5.21: Crustal view of preferred 2-D gravity model for profile L-102 (see figure 5.17 for legend); A)Observed reduced – to – pole magnetic anomalies; B) Observed and calculated gravity values in mGal; C)2,5 times vertically exaggerated version of final model; D) No vertical exaggeration. Locations of the assigned numbers are shown in anomaly and filter maps.....	79
Figure 5.22: Basin view of preferred 2-D gravity model for profile L-102 (see figure 5.11 for legend); A) Observed and calculated gravity values in mGal; B) Basin view of model – 6 times vertically exaggerated; C) No vertical exaggeration.....	80
Figure 5.23: Cross – section through Jackson Dome, constructed by well data (Dockery, 1997).....	81
Figure 5.24: Crustal view of preferred 2-D gravity model for profile L-103 (see figure 5.17 for legend); A)Observed reduced – to – pole magnetic anomalies; B) Observed and calculated gravity values in mGal; C)2 times vertically exaggerated version of final model; D) No vertical exaggeration. Locations of the assigned numbers are shown in anomaly and filter maps.....	83
Figure 5.25: Basin view of preferred 2-D gravity model for profile L-103 (see figure 5.11 for legend); A) Observed and calculated gravity values in mGal; B) Basin view of model – 6 times vertically exaggerated C) Crustal view – no vertical exaggeration.....	84
Figure 5.26: Crustal Thickness Map of the area.....	86
Figure 5.27: Depth to Moho Map.....	87
Figure 5.28: Depth to Basement Map.....	87

Figure 5.28: Subsurface Igneous Rocks of the Sabine Uplift, Monroe Uplift and Jackson Dome.....	89
Figure 6.1: Alternative 2 – D gravity models for model 1: L-101; A) Gravity anomalies without igneous bodies; B) Our preferred model with igneous bodies; C) Gravity anomalies with an uplifted crust beneath Sabine Uplift.....	92
Figure 6.2: Crustal thickness map of CRUST 2.0 for the area.....	97
Figure 6.3: Crustal thickness map by Sawyer et. al,1991 (Contours are in km).....	97
Figure 6.4: Tectonostratigraphic chart of the uplifts. Depositional history and dated age of igneous rocks were obtained from previous studies (Mancini et. al, 2005; Mancini et. al, 2008; Halbouty and Halbouty, 1982; Nichols et. al, 1968, Ewing, 2009; Baksi, 1997; Sundeen and Cook, 1977; Salvador, 1991).....	100
Figure 6.5: Paleogeography of the region during Late Cenomanian – Turonian (modified from Salvador, 1991).....	101
Figure 6.6: Rise of the Sabine Uplift based on the position of James Formation and cross – section with datum on base of Austin Chalk. Truncation of Woodbine Formation created stratigraphic trap of East Texas Field (modified from Halbouty and Halbouty, 1982).....	103
Figure 6.7: Interpretative cross section through Monroe Uplift. The lower unconformity where Upper Cretaceous rocks are overlying older Lower Cretaceous rocks unconformably is a regional unconformity. The upper unconformity where Monroe Gas Rock is overlying Cretaceous and Jurassic rocks unconformably is a result of a local rise of this structure (modified from Johnson, 1958).....	104
Figure 6.8: Cross – section through Jackson Dome (modified from Dockery, 1997)....	105

# **CHAPTER I**

## **INTRODUCTION**

### **1.1.MOTIVATION AND OBJECTIVES**

Rifting in the Gulf of Mexico was initiated in the Late Triassic by the relative motion of Africa, North America and South America. During the mid-Jurassic main phase of rifting the entire basin was subject to extension resulting in rifting and thinning of the crust (Buffler, 1991, Sawyer et. al, 1991). Sea-floor spreading began in the Late Jurassic and oceanic crust was formed at the central deepest part of the basin during this time. During the last phase of evolution of the basin the Gulf of Mexico took its final form (Bird et. al, 2005). The basin had been tectonically quiet during the Late Jurassic and Early Cretaceous. The tectonic stability of the Gulf of Mexico Basin was interrupted by significant uplifts, regional and local unconformities, and igneous activity in the Late Cretaceous (Salvador, 1991). The Sabine, Monroe and Jackson Uplifts, which are the focus of this study, were formed or at least re-activated during this period. Some of the

models that have been proposed and discussed in order to explain evolutions of these structures are i) crustal heating and thermal doming caused by deep-seated igneous rocks; ii) flexural isostasy between two crustal blocks of different thicknesses; iii) formation of anticlinal structures caused by compressional far-field stresses; iv) heating of lithosphere by moving of a plate over fixed mantle plume; v) direct uplift due to magma chambers or volcanic activity (Nunn, 1990; Jackson and Laubach, 1988; Jackson and Laubach, 1990; Ewing, 2009; Cox and Van Arsdale, 2002).

The structural elements of the Onshore Northern Gulf of Mexico Basin have economic importance due to their relations with oil and gas fields. Rising of the Sabine Uplift during Late Cretaceous provide major traps for oil and gas accumulation in East Texas Field and natural gas plays have been discovered related with Monroe and Jackson structures. Understanding of the crustal architecture of the region and relationship between the structural elements and the interior basins are crucial. There are still different ideas about crustal architecture, structural elements of the basin, and presence or absence of magmatism in some of the areas. The size and amplitude of these domal uplifts vary.

The Sabine Uplift is located in northeastern Texas and northwestern Louisiana. It is a broad, domal feature and it is defined by an unconformity at the base of the Austin Group (Santonian – Coniacian). At the beginning of the Late Cretaceous, the area was uplifted relative to adjacent East Texas basin resulting in partial erosion of Eagle Ford and Woodbine Groups. The approximate diameter of the Sabine Uplift is 150 kilometers (Halbouty and Halbouty, 1982; Nicholas et al, 1968).

The Monroe Uplift is located in northeast Louisiana, southeastern Arkansas, and west-central Mississippi. It is a roughly circular dome-like feature. It formed during Late Cretaceous time and is marked by the truncation of the Tuscaloosa Formation (stratigraphic equivalent of the Woodbine Formation in East Texas) in an area 130 kilometers in diameter (Johnson, 1958). This event resulted in more than 500 meters of uplift and erosion. A major carbonate reservoir rock, the Monroe Gas Rock, was deposited over the uplifted area (Jackson and Laubach, 1988; Ewing, 2009).

Jackson Dome is a structural feature at the northeastern edge of the Mississippi Salt Basin and it is geographically located below the City of Jackson, Mississippi. The dome is roughly circular and its diameter is around 40 km. Uplifted formations including Upper Jurassic and Cretaceous, were tilted and eroded resulting in an angular unconformity (Saunders and Harrelson, 1992).

The objectives of this study can be summarized as followings: 1) to investigate crustal structures of the area; 2) to locate subsurface Mesozoic igneous rocks; 3) to evaluate the Cretaceous tectonic events of the Sabine, Monroe and Jackson Uplifts; 4) to investigate the relationship between igneous rocks and domal uplifts. To interpret these important structures and igneous bodies, gravity and magnetic anomaly data, and enhancements of these data will be examined. Three 2D transects, ranging from 470 to 650 km-long, through the uplifts will be constructed and modeled. Open-file gravity and magnetic data, integrated with seismic data, regional cross sections, well logs, velocity profile studies

and geological information including; paleogeographic maps, age and petrology of the igneous rocks, and depositional history will be used during the study.

## 1.2. STUDY AREA

The study area is located on the Onshore Northern Gulf of Mexico Basin. Investigations during this study were partly conducted in States of Texas, Louisiana, Mississippi, and

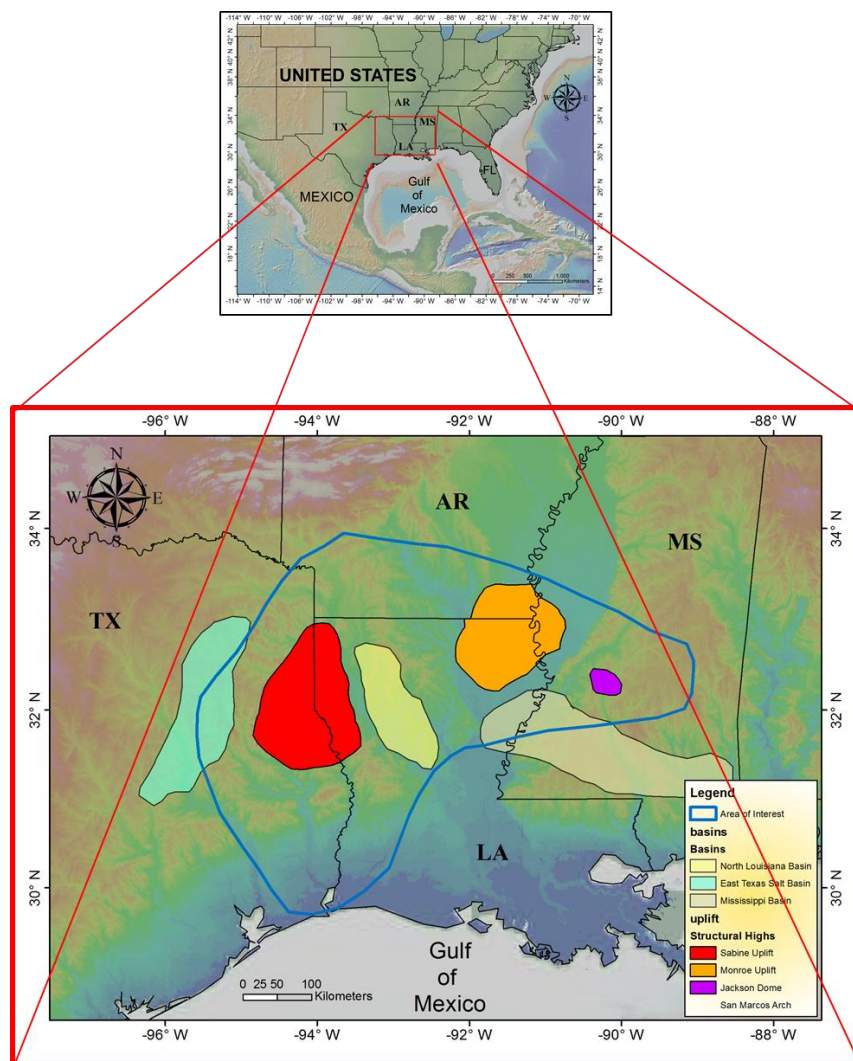


Figure 1.1: Map showing the location of study area.

Arkansas. Figure 1.1 shows the location of the study area. The Sabine, Monroe and Jackson Uplifts are shown and labeled. This study is focussed on but not limited to these structures. The blue line outlines the boundary of the area that was covered during the analysis and interpretations.

## **CHAPTER II**

### **GEOLOGICAL AND TECTONIC SETTING**

#### **2.1. REGIONAL GEOLOGY**

Rifting in the Gulf of Mexico was initiated by the relative motion of Africa, North America and South America in the Late Triassic. It has been described as a four-phase evolution (Figure 2.1; Buffler, 1991). During the first phase (Late Triassic – Early Jurassic), brittle deformation of the crust resulted in formation of grabens and half grabens filled by mainly non-marine clastics including red beds and volcanics. Major crustal deformation did not occur at this time (Salvador, 1991; Sawyer et.al., 1991).

During the mid-Jurassic phase of rifting the entire basin was subject to main extension resulting in rifting and thinning of crust. Crustal thinning progressed to the formation of transitional crust. The central part of the basin was exposed to more crust and lithosphere attenuation, while surrounding regions experienced relatively limited thinning (Sawyer et

al., 1991). As extension and subsidence were in progress during Late Middle Jurassic to early Late Jurassic, a broad salt deposition occurred mainly in the central part and on the surrounding thick transitional crust while waters were spilled out (Buffler, 1991; Sawyer et al., 1991).

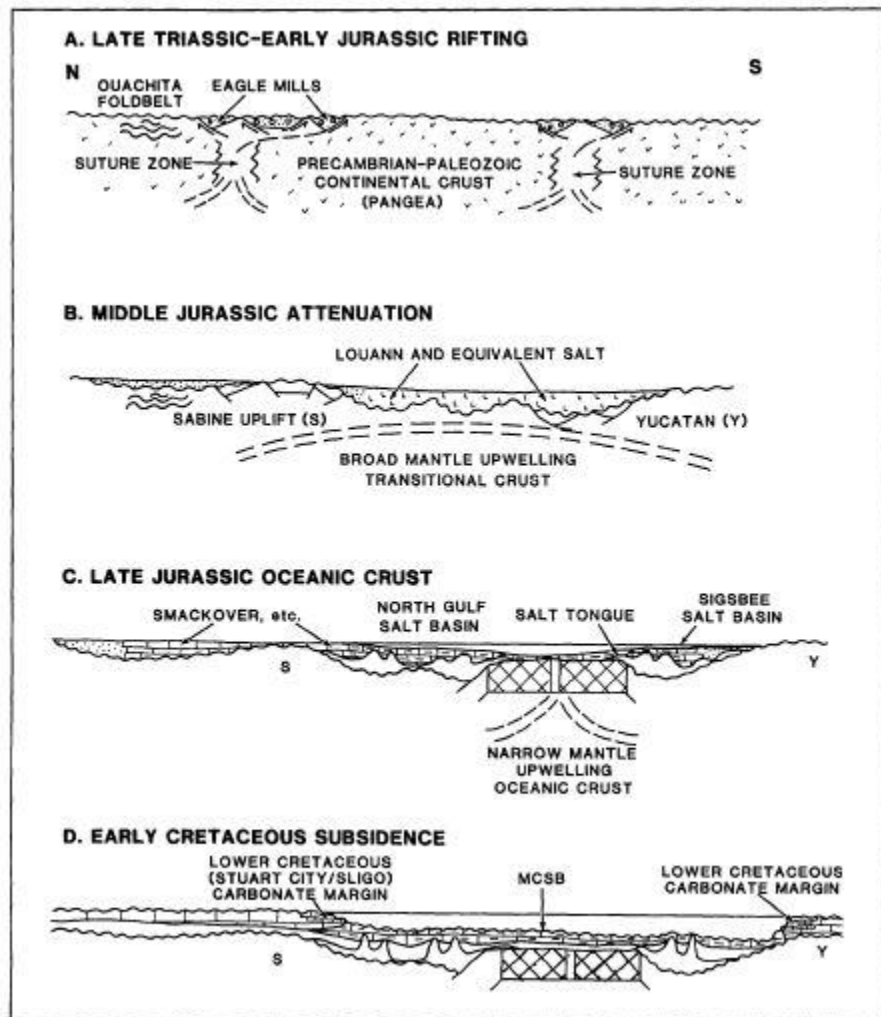


Figure 2.1: Four phases of the early evolution of the Gulf of Mexico Basin (from Buffler, 1991): A) Late Triassic – Early Jurassic Rifting; B) Middle Jurassic Crustal Extension; C) Formation of oceanic crust during Late Jurassic; D) Subsidence Phase during Early Cretaceous.

Sea-floor spreading began in the Late Jurassic and oceanic crust was formed at the central deepest part of the basin during this time (Bird et al., 2005; Salvador, 1991; Sawyer et al., 1991). At this time continental extensional tectonic deformation stopped while the basin continued to subside. The new oceanic crust was filled up by water up to several kilometers (Figure 2.1).

During the last phase of evolution of the basin, the Gulf of Mexico took its final form in the Early Cretaceous and its present day configuration was locked except for second-order structural features (Bird et al., 2005). Continuous subsidence enabled deposition of carbonate platforms. Except for continuous sedimentation and subsidence in the center of the basin and salt deformation, the basin was tectonically quiet during this phase.

During the Cretaceous post-rift stage, structural highs and lows were formed resulting in regional angular unconformities in the northern onshore Gulf of Mexico Basin. Broad igneous activity also occurred during this time (Ewing, 2009).

#### **2.1.1. Drift and Rotation of Yucatan Block**

As extension proceeded between Late Middle to Early Late Jurassic, the continental crust extended and thinned and the Yucatan block moved away from the North American Plate. This event coincides with the beginning of sea-floor spreading and oceanic crust formation (Salvador, 1991). There is a consensus on southward displacement models of Yucatan Block which require a counterclockwise rotation (Salvador, 1991; Bird et al.,

2005; Salvador, 1987). On the other hand, there are different explanations for the details of rotation such as total rotation amount and pole. Keathley Canyon and Yucatan Parallel anomalies were interpreted as hot spot tracks, which are produced by a single mantle plume according to Bird et al. (2005). Bird et al. (2005) proposed that during continental extension Yucatan Block had been involved in  $22^\circ$  of counterclockwise rotation and followed by another  $20^\circ$  of counterclockwise rotation with sea-floor spreading (figure 2.2).

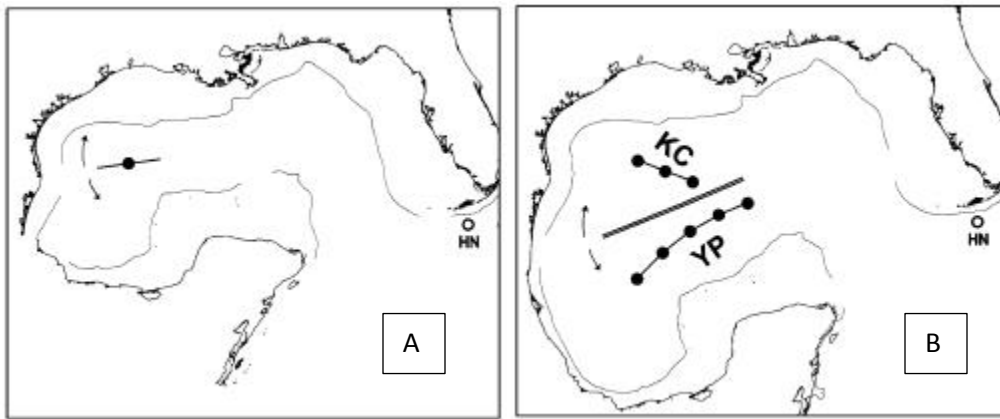


Figure 2.2: Opening phases of the Gulf of Mexico Basin with a hotspot track A) Initial position as 160 Ma B) after oceanic crust and mantle plume track with a total of  $42^\circ$  of rotation. (Bird et al., 2005)

## 2.2. NORTH-CENTRAL GULF OF MEXICO – INTERIOR ZONE

Basement structures of the onshore northern Gulf of Mexico basin vary in north – south and east - west. There are structural highs and lows in the area with differential crustal

attenuation. Those high basement blocks separate deep basins and both of them strongly affected the depositional system and basin history after rifting had ceased (Ewing, 2009).

The interior Zone of the North-Central Onshore Gulf of Mexico Basin has several structurally positive and negative features which are formed after formation of the Gulf of Mexico Basin. The Sabine Uplift and Monroe Uplift (Figure 3) are two of the major structural highs which are bounded by deep basins; the East Texas Salt Basin - North Louisiana Salt Basin and North Louisiana Salt Basin – Mississippi Interior Salt Basin, respectively (Figure 2.3).

### **2.2.1. Sabine Uplift**

The Sabine Uplift is a structural high, located at the border of northeast Texas and northwest Louisiana, located between the East Texas Salt Basin and the North Louisiana Salt Basin (Figure 2.3). Its shape on the surface is defined by Paleocene and Eocene strata which are surrounded by younger rocks (Ewing, 1991; Jackson and Laubach, 1988). The area is characterized by a thin Jurassic salt layer, and a moderately extended thick continental basement block which is relatively less subsided than the surrounding areas (Ewing, 2010; Sawyer et al., 1991).

After deposition of salt all over the area, there was not a structural high on the Sabine Uplift area (Salvador 1987, in Jackson and Laubach, 1990). Moreover, it was a structural

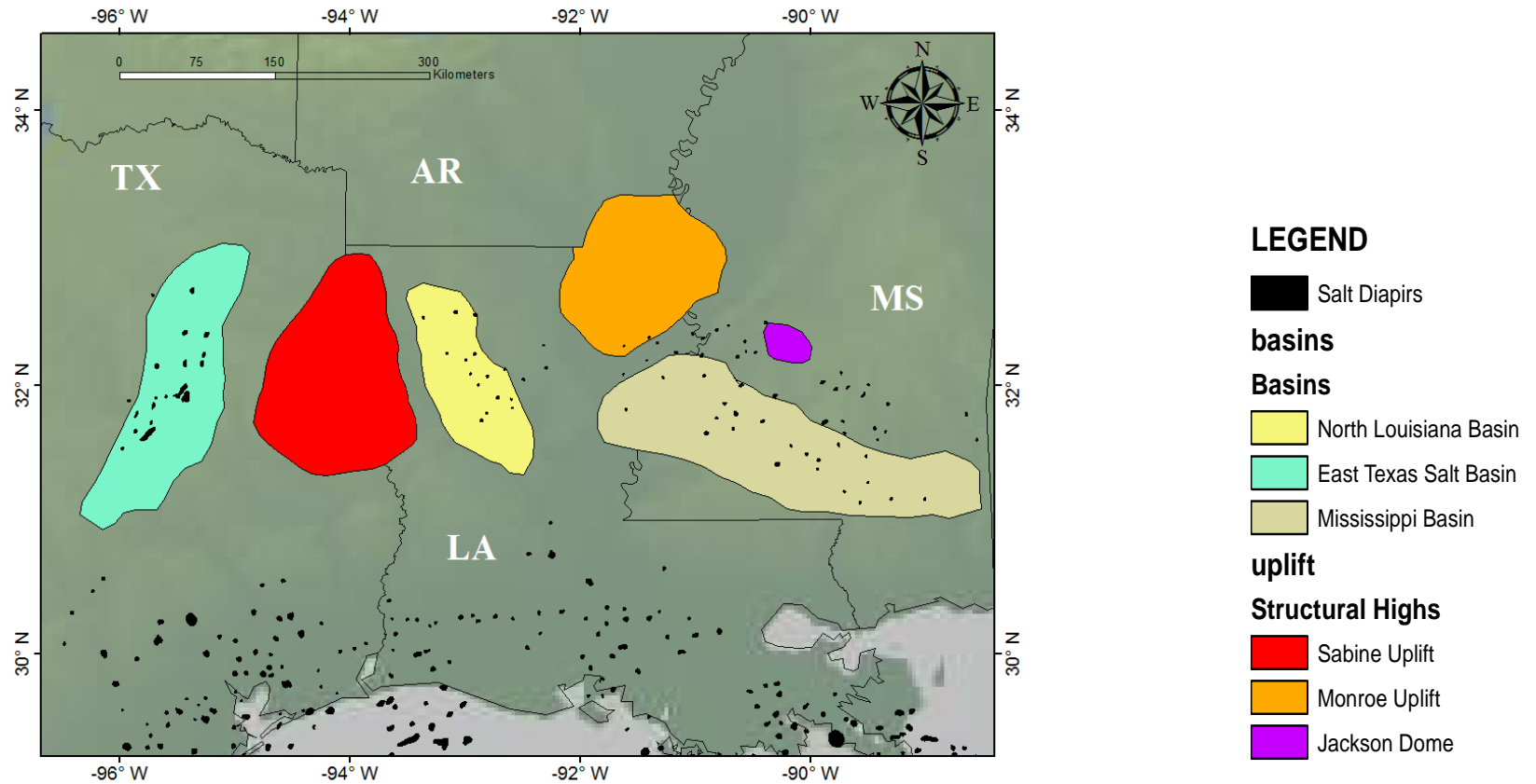


Figure 2.3: Location map of Uplifts and Basins of the Onshore Northern Gulf of Mexico Basin.

low by Late Jurassic where lower Cretaceous units have a constant thickness along the future uplift area (Jackson and Laubach, 1988).

A regional unconformity at the east Texas Basin through North Louisiana indicates the regional elevation of lower Cretaceous and Jurassic strata during Middle Cretaceous time resulting with the erosion of upper Cretaceous Woodbine and Eagle Ford Strata in the area (Jackson and Laubach, 1988).

Mesozoic igneous activity of the onshore Northern Gulf of Mexico Basin was studied and discussed in several studies and local reports (Byerly, 1991; Kidwell, 1951; Moody, 1949; Griffin, 2010; Ewing, 2009; Baksi, 1997; Nichols et al., 1968). Although there are not sufficient outcrops in the area, igneous rocks have been observed and sampled in deep exploration wells. In addition, geophysical signatures were interpreted and discussed as an evidence of subsurface igneous activity. The diabase rocks of the northern Gulf of Mexico Basin were encountered in 13 deep wells from Northeast Texas through Southern Arkansas; two of which have been discovered in Northeast Texas around the Sabine Uplift (Kidwell, 1951; Moody, 1949).

The Sabine Uplift shows little Cretaceous igneous activity and there are sparse locations where igneous rocks have been encountered. However, geophysical data were interpreted as possible buried igneous bodies in the area (Figure 4) (Ewing, 2009). In addition, there are also indirect evidences for igneous activity, for example; in Shelby County area hydrothermal alteration and base metal occurrences were reported which is in need of a source as a deep intrusion (Ewing, 2009). One intrusive rock was reported by Kidwell

(1951) in Sabine Uplift of Northwest Louisiana where trachybasalt occurrence was observed below the Louann Salt at a depth of around 3,500 meters. This sample might be counted as evidence of the idea proposed by Ewing (2009) which explains the possibility of trapped igneous materials beneath the ductile salt.

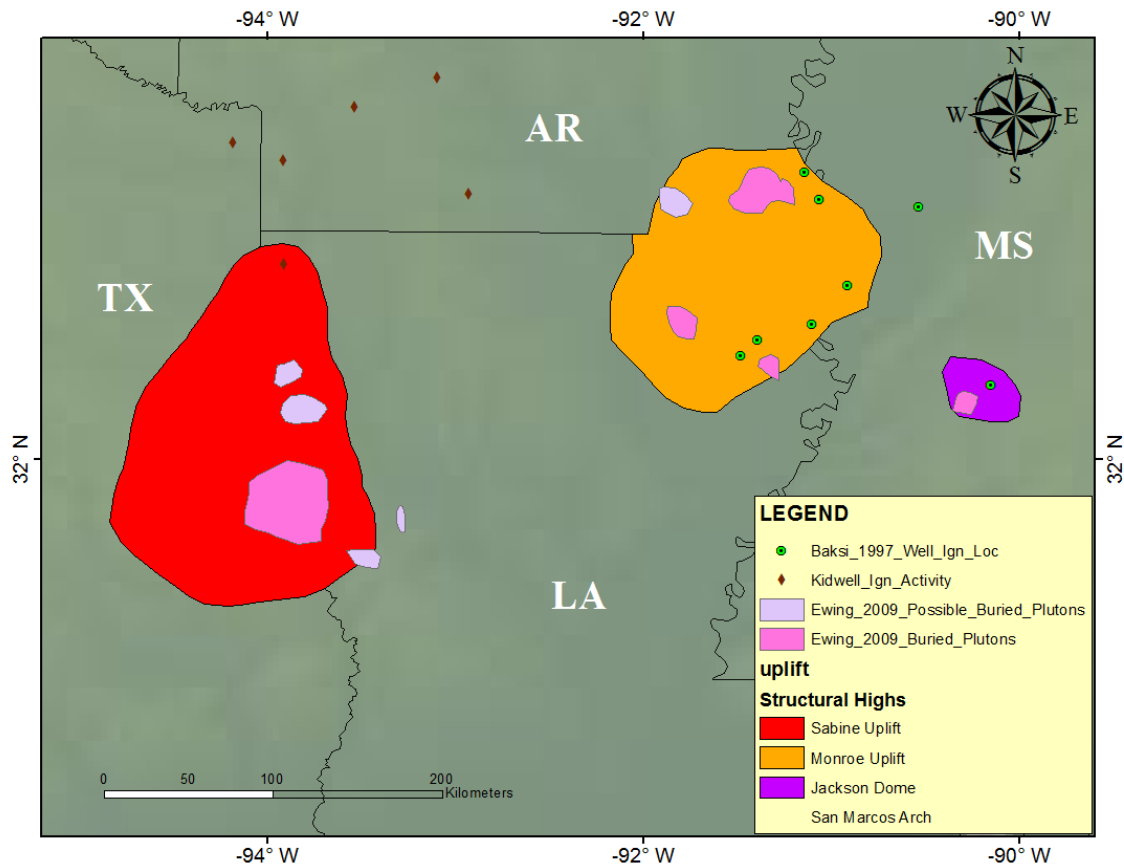


Figure 2.4: Igneous activity around vicinity of Sabine Uplift, Monroe Uplift and Jackson Dome (Locations of the igneous rocks are gathered from Baksi, 1997; Ewing, 2009; Kidwell, 1951).

### **2.2.2. Monroe Uplift**

The Monroe Uplift is located in parts of mainly north-east Louisiana, south-central Mississippi and southern Arkansas (Figure 2.2), defined by pinch out of Tuscaloosa strata with a diameter of approximately 130 km. The unconformities in the area exist between Lower Paleocene and thin upper Cretaceous units which are unconformably underlain by lower Cretaceous Units (Jackson and Laubach, 1988; Johnson, 1958; Ewing, 2009).

Mesozoic igneous activity of the onshore Northern Gulf of Mexico Basin was studied and discussed in several studies and local reports (Byerly, 1991; Kidwell, 1951; Moody, 1949; Griffin, 2010; Ewing, 2009; Baksi, 1997; Nichols et al., 1968). There is a different scenario about igneous activity in the Monroe Uplift when we compare it with the Sabine Uplift. The Monroe Uplift has largest volume of magma and greatest compositional diversity in the Northern Gulf of Mexico Basin and at least four major igneous rock groups were defined so far: i) intermediate rocks; ii) alkaline rocks; iii) basalts; iv) lamprophyres (Ewing, 2009; Kidwell, 1951). Igneous rocks are encountered in more than 50 wells in and around the Monroe Uplift (Figure 2.5) (Baksi, 1997). Dated samples from exploration wells were plotted in Figure 2.4 and the age of rocks vary between 94 – 66 Ma (Baksi, 1997). It is not well understood why igneous activity occurred but there appears to be a relation between igneous activity and the movement of the uplift in the area (Salvador, 1991; Kidwell, 1951). Pyroclastic rocks are also widespread. One of the

wells in Monroe Gas Field of Northeastern Louisiana drilled about 500 meters of trachytic tuff sequences.

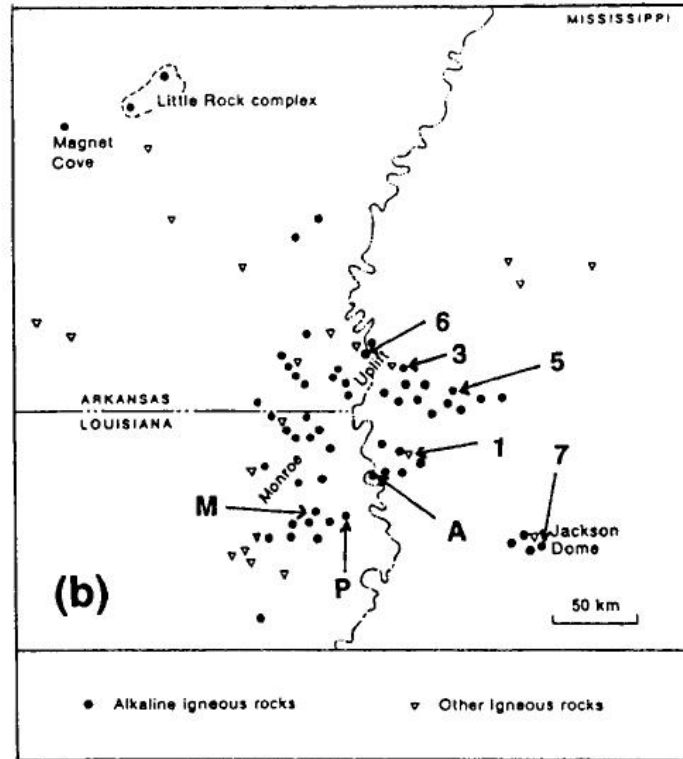


Figure 2.5: Distribution of the wells in Monroe Uplift and Jackson Dome igneous material has been encountered (Baksi, 1997).

### 2.2.3. Jackson Dome

Jackson Dome is a structural feature at the northeastern edge of the Mississippi Salt Basin and it is geographically located below the City of Jackson, Mississippi. The dome is roughly circular and its diameter is around 40 km (Figure 2.3). The fields on the Jackson

Dome have been producing significant natural gas and minor crude oil since 1930s. Jackson Dome has a similar structural style with the most of the salt domes in the Gulf Coast. It has a core built by igneous rocks of Cretaceous age instead of salt stacks (Saunders and Harrelson, 1992; Ewing, 2009). Jurassic strata uplifted 2000 m. above the surrounding area. There was abundant igneous activity in the Late Cretaceous which was followed by deposition of reefal carbonates, called as Jackson Gas Rock, associated with the uplift (Ewing, 1991).

Igneous rocks were encountered in more than 200 samples which includes drill cores from 7 wells at the center of the dome (Figure 2.5). Geochronology results show different results in the area between 79 - 69 Ma (Baksi, 1997; Saunders and Harrelson, 1992). Igneous rocks of Jackson Dome have distinct gravity and magnetic high anomaly as all the igneous vicinities in the north-central Gulf of Mexico Basin (Figure 2.6).

The igneous rocks in the area could be explored by using gravity and magnetic data, because circular high gravity and magnetic anomalies in the area could be interpreted as deeply buried, highly differentiated stocks. Moreover, igneous rocks have been penetrated in deep wells where there are circular or ellipsoidal positive gravity anomalies of 20 or more mGal. This is also illustrated by an example on a 2-D profile which is crossing the Jackson Dome, which is a known igneous field where considerable uplifting occurred (Moody, 1949) (Figure 2.6).

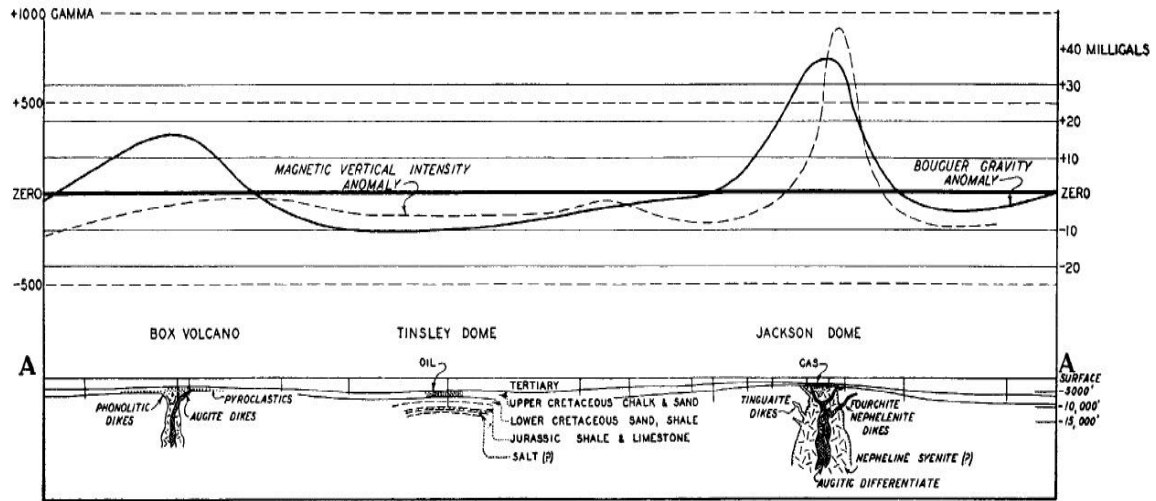


Figure 2.6: Hypothetical cross-section goes over the Jackson Dome, shows the correlation between igneous body and short wavelength, high amplitude gravity and magnetic anomalies (Moody, 1949).

### 2.3. PREVIOUS WORK AND MODELS

The Jurassic crustal structure and basement blocks, Cretaceous uplifts and igneous activities and models that were proposed to explain the structural evolution for the uplifts in the Northern Gulf of Mexico were reviewed and discussed by Ewing (2009). Although all uplifts have different characteristics we can generalize the models for the genesis of uplifts in the area. The structural models and previous studies about the Sabine and Monroe Uplifts are summarized below:

### **2.3.1. Plutonic Dome Model and Volcanic Activity**

The Plutonic Dome Model suggests that an intruded deep seated pluton might cause thermal expansion and doming resulting in structural highs (Jackson and Laubach, 1988). Evidence of Mesozoic igneous activity in the Northern Gulf of Mexico Basin, especially during Cretaceous time, supports this model (Figure 4) (Moody, 1949; Kidwell, 1951; Baksi, 1997; Ewing, 2009). In addition, outcrops and subsurface shape of uplifts are roughly circular which is characteristic for domes caused by igneous activity whereas compressed arches are in linear shape (Figure 2.4). However, the distribution of the volcanic material and timing of the vertical movement of the arches do not fit for all the domes. For example, the abundance of volcanic material on and around Monroe Uplift is not found on the Sabine Uplift. It is proposed by Ewing (2009) that the Sabine Area shows little igneous activity, but it might also contains buried plutons that have related age relationships with the movement of the arch. Ewing (2009) also proposed that ductile salt bodies might have behaved as a trap for the igneous material.

### **2.3.2. Flexural Model**

Nunn (1990) proposed that large sub-circular uplifts might be explained by the thermal rejuvenation hypothesis which refers to flexure of weakened lithosphere due to rise of warm mantle. Median magnitudes of the present day uplifts (300 km in diameter and 500 m in height - Ewing, 2009) are not so different than what we see in the area. In addition, the Sabine and Monroe Uplifts are bounded by deep basins which have thick sedimentary

depositions. In this case, the loading effect of sedimentary section might cause bending of the elastic lithosphere resulting in a bulge at the flanks of the subsided basin (Figure 2.7).

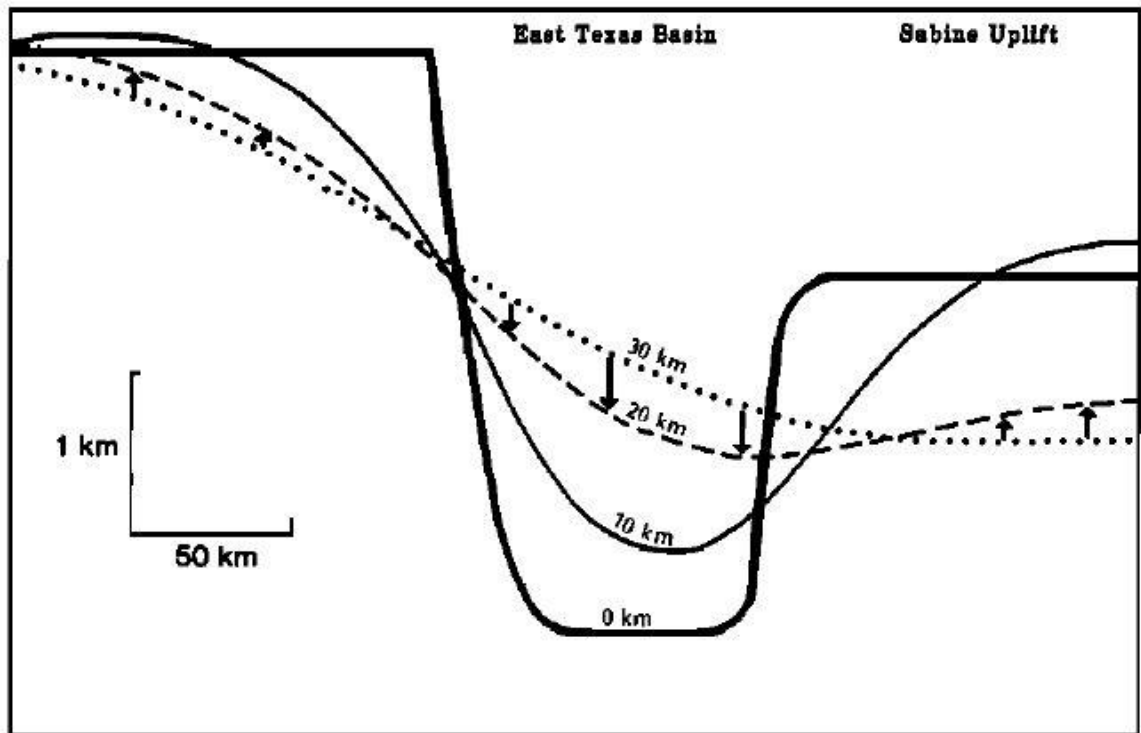


Figure 2.7: Set of four curves showing calculated deflection of the lithosphere for varying effective elastic thickness (from Nunn, 1990).

It is simple to quantify and test this model, and Nunn (1990) found a good fit between their results and present day observations. However, Jackson and Laubach (1988) suggested that when the timing of the uplifts is considered, Cretaceous sedimentary loads are insufficient to cause the vertical movement of the arch. In addition, major sedimentary deposition in the Northern Gulf of Mexico Basin did not start until Tertiary.

Moreover, the main disadvantage of this model for the Sabine Uplift is the lack of isostatic rise of deep warm mantle as a mantle plume track. Age progression of the Bermuda Hot Spot is also not well identified for the adjacent areas including Monroe Uplift (Figure, 2.8).

### **2.3.3. Anticline Model**

This model is proposed by Jackson and Laubach (1988; 1990) and it explains the formation of Sabine Uplift as a result of tectonic compression (Figure 2.7).

A compressional regime during the convergence between North American and Pacific Plates in the Cretaceous coincides with the vertical movement of the uplifts. The main disadvantage of this model is that there is no available data to test it so it remains speculative (Jackson and Laubach, 1988; Nunn, 1990). In addition, the tectonic elements associated with compressional regimes such as folds, thrust faults and inverted faults are absent around the area.

### **2.3.4. Mantle Plume Model**

Cox and Van Arsdale (2002) reviewed the early predicted models for the Bermuda Hotspot (Figure 8) and also they proposed that moving of Northern America Plate over Bermuda plume caused to form uplifting of the Mississippi Valley Graben in the Cretaceous, resulting in Mississippi Embayment (Figure 2.9).

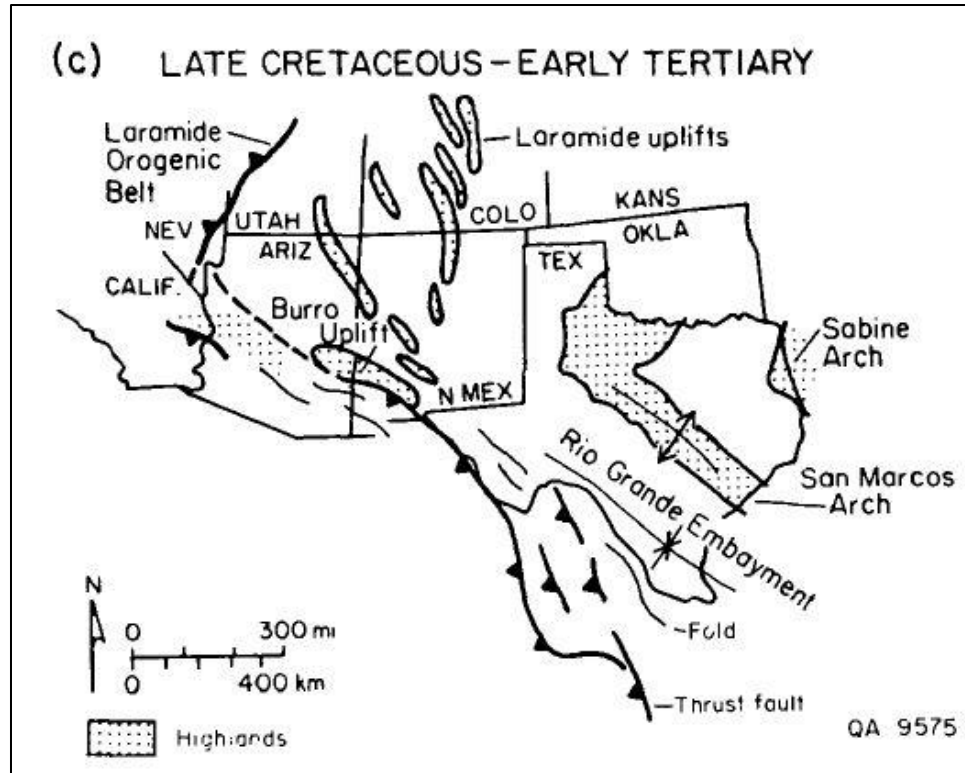


Figure 2.7: Late Cretaceous-Early Tertiary structural and paleogeographic features in southwestern North America (from Jackson and Laubach, 1988).

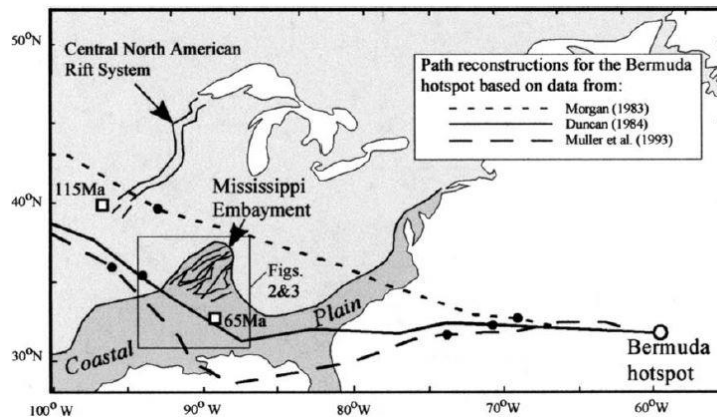


Figure 2.8: Predicted paths of the Bermuda hotspot relative to North America based on data (from Cox and Van Arsdale, 2002).

This model is also interrelated with first two models discussed above. However, a complete age progression is not well observed in the area. In order to prove this model, more high resolution geochemistry data would be needed.

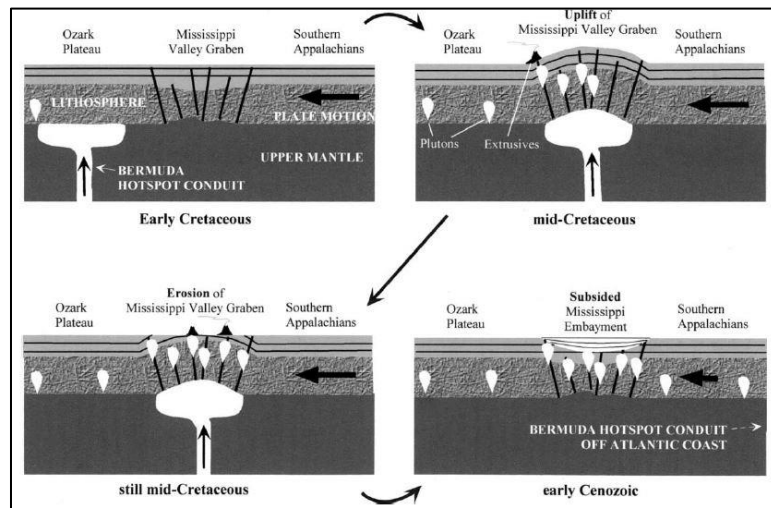


Figure 2.9: Schematic illustration of passage of North America over the Bermuda plume during the Cretaceous super plume mantle event (from Cox and Van Arsedale, 2002)

## **CHAPTER III**

### **DATA**

Geological and geophysical data from different sources have been integrated during the study. Integrated data include onshore Bouguer gravity, onshore magnetic, available seismic data, well information, velocity profiles, published local and regional cross sections, maps and reports. During the qualitative interpretations, mainly gravity and magnetic anomaly data, and enhancements of these data were examined. Integration of geological and geophysical data was used during the modeling stage as constraints to obtain geologically reasonable results.

#### **3.1. GRAVITY DATA**

Open-file Decade of North American Geology (DNAG) gravity data were used in this study. Maps and models were constructed by using this Bouguer gravity grid data which has 0.04 degree grid cell dimension of about 4 km spacing. Grid limits for longitude and latitude extend from 170E to 10.75W and from 5.17N to 81.17N, respectively. The area

of interest for the study (roughly -96 to -88 for longitude; 30 to 34 degrees for latitude) was clipped from the original grid data. Bouguer gravity map of the area was generated by using Oasis Montaj Software, which are shown in figure 3.1.

### 3.2. MAGNETIC DATA

Open-file North American Magnetic Anomaly Map (reprocessed DNAG), which is 1 km aeromagnetic grid, was used in the study. North America is fully covered by this grid. The onshore part of the data was mainly acquired by aeromagnetic surveys. The same area of interest with the gravity data for the study was clipped from original data. Magnetic map was generated by using Oasis Montaj Software, which are shown in figure 3.2.

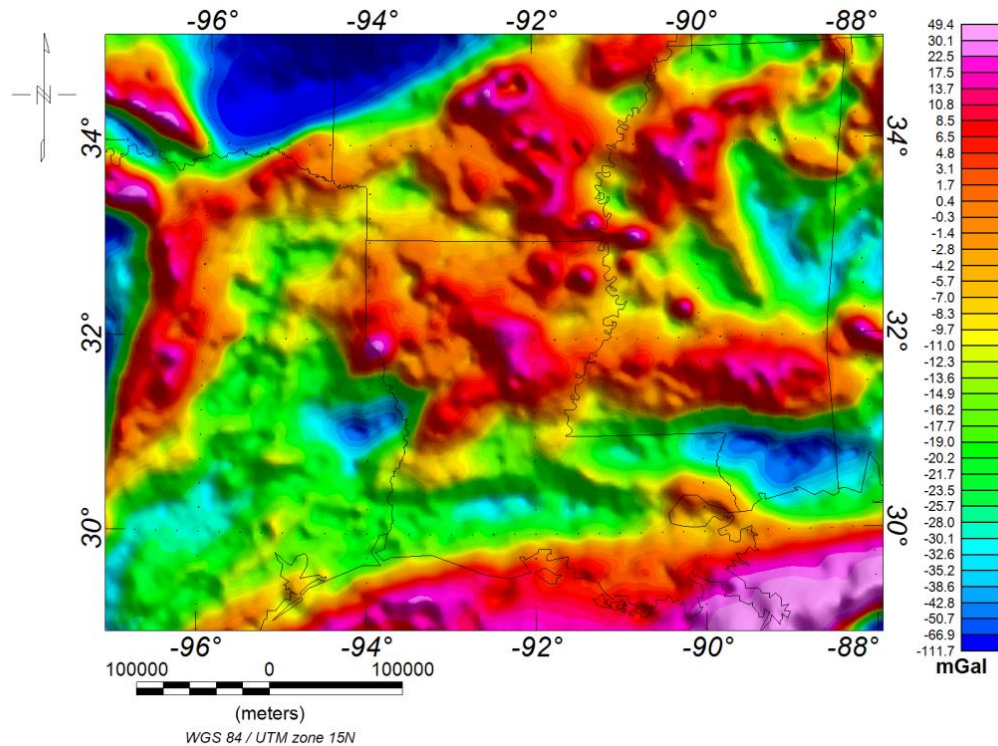


Figure 3.1: Onshore Bouguer Gravity Data of area of interest

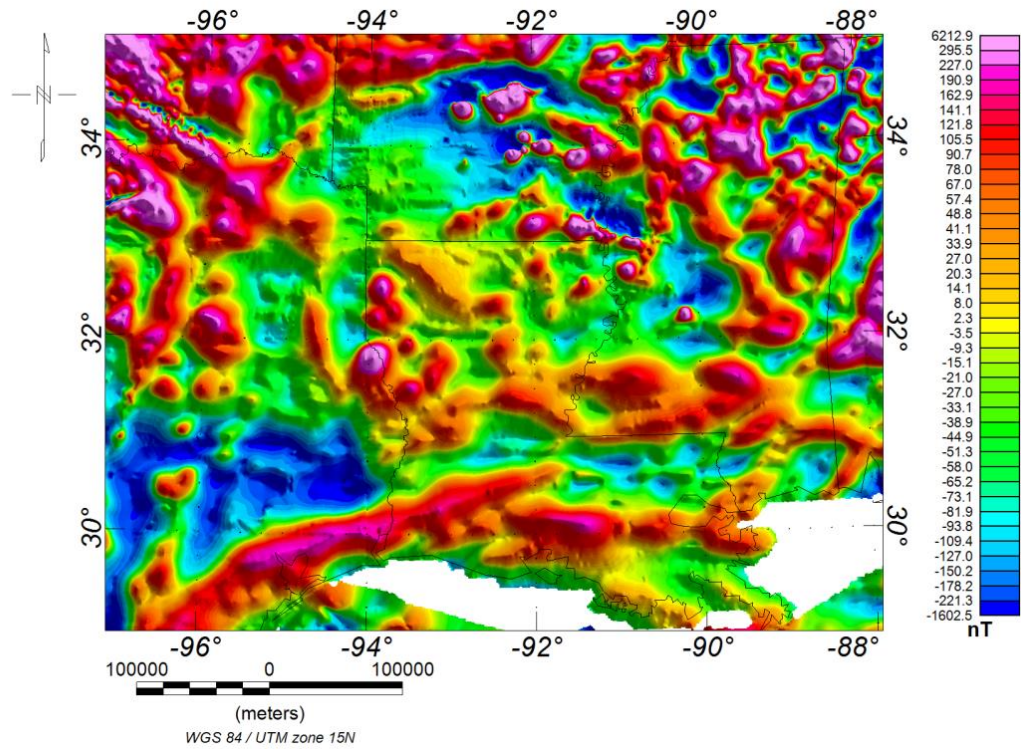


Figure 3.2: Magnetic Intensity Map of the area of interest

### 3.3. OTHER DATA

In addition to gravity and magnetic data, other types of supporting data; including seismic refraction data, regional cross sections, well logs, velocity profile studies and geological information including; paleogeographic maps, age and petrology of the igneous rocks, and depositional history, were used during this study. Those kinds of data should be used as control in order to get more accurate and geologically plausible results during forward

modeling stage. Therefore available data, could be used as control points, have been researched and gathered.

Main studies used as constraints are digitized and mapped (Baksi, 1997; Ewing, 1991; Ewing, 2009; Hales, 1970; Kidwell, 1951; Kruger and Keller, 1989; Keller et. al., 1989; Moody, 1949; Salvador, 1991; Sawyer, 1991; Worzel and Watkins, 1973). Some of these studies are shown below and the location of each study shown in figure 3.3.

During the modeling stage to make an appropriate analysis, control data were used to determine basement depth, Moho depth, crustal thicknesses, sedimentary rock thicknesses, possible igneous rock and salt diapir locations. Constant density and magnetic properties were assigned to each layer to make the models consistent and geometries were allowed to be modified with constraints.

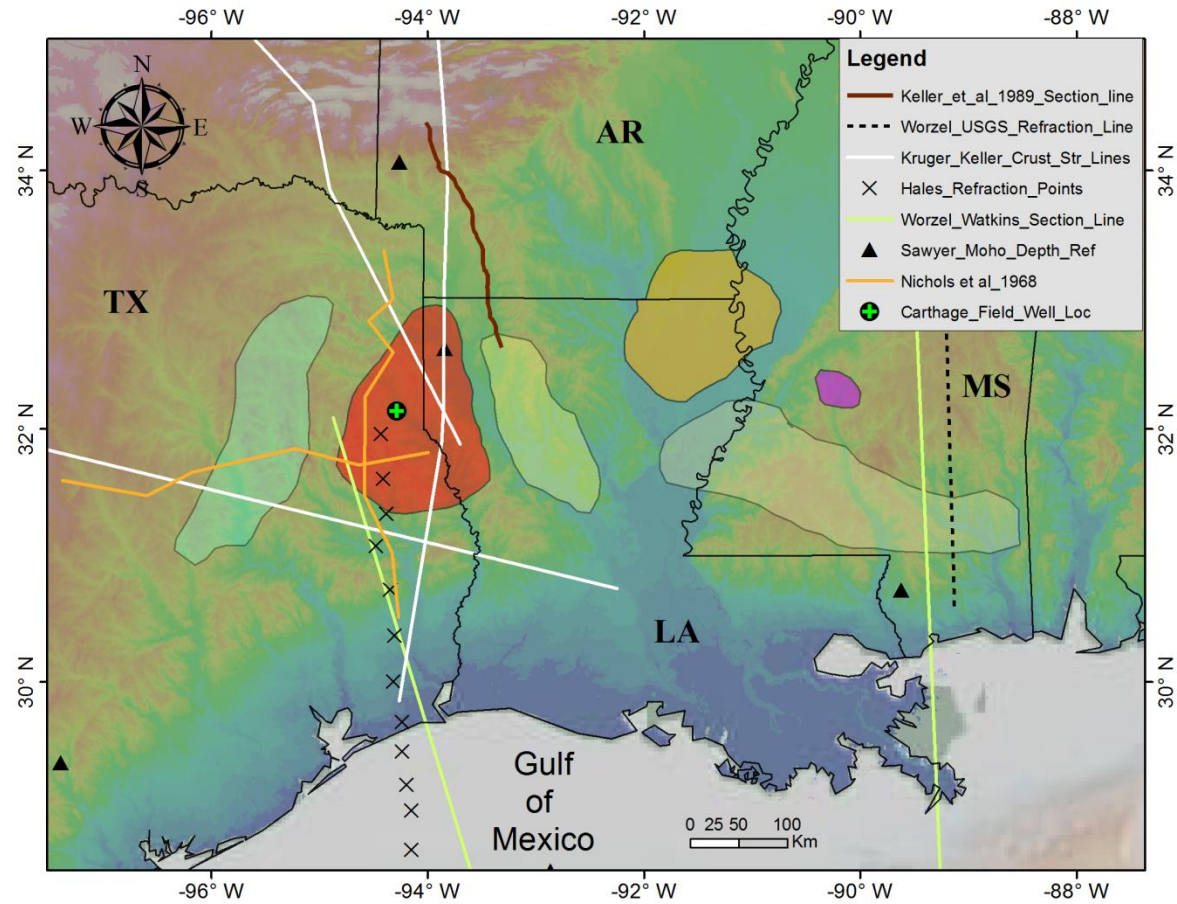


Figure 3.3: Location map of control points with basins and uplifts of the area.

- North – South seismic refraction profile from Hales et al., 1970 :

This transect is a result of a seismic refraction experiment which was made along 94°W by Hales et al., 1970, located at east Texas. This model covers roughly 300 km of land and 400 km of sea through the profile. In our models, only the onshore stations were used.

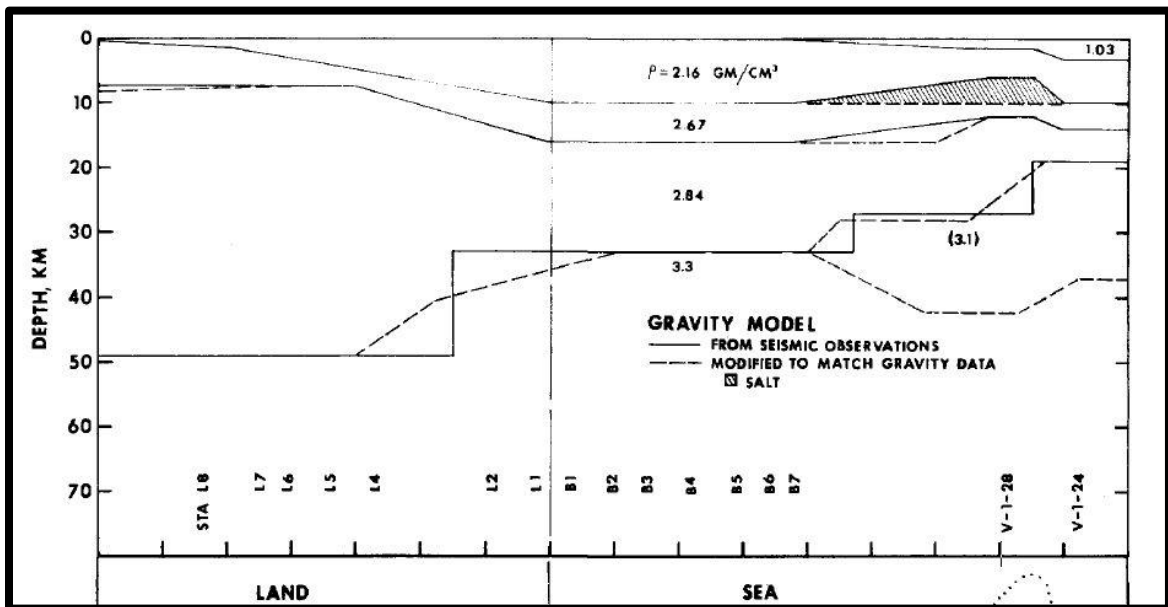


Figure 3.4: Result of a seismic refraction experiment along 94°W in east Texas (Hales et al., 1970).

- East Texas and Mississippi crustal cross sections by Worzel and Watkins, 1973;

This study illustrates crustal structures of East Texas, South Texas, Mississippi and adjacent areas of Gulf Coast Plain (Figure 3.3). Three profiles were constructed from onshore Gulf of Mexico to the Sigsbee Deep (Figure 3.5). After synthesis of available data on the area crustal structures were defined and modeled. According to the results,

sedimentary section of the area has a velocity of 5.2 – 6.0 km/sec with thicknesses of ranging up to 17 km. Upper and lower crust velocities are 5.8 – 6.0 km/sec and 6.45 – 6.9 km/sec with thicknesses of 12-20 km and 15 – 20 km, respectively.

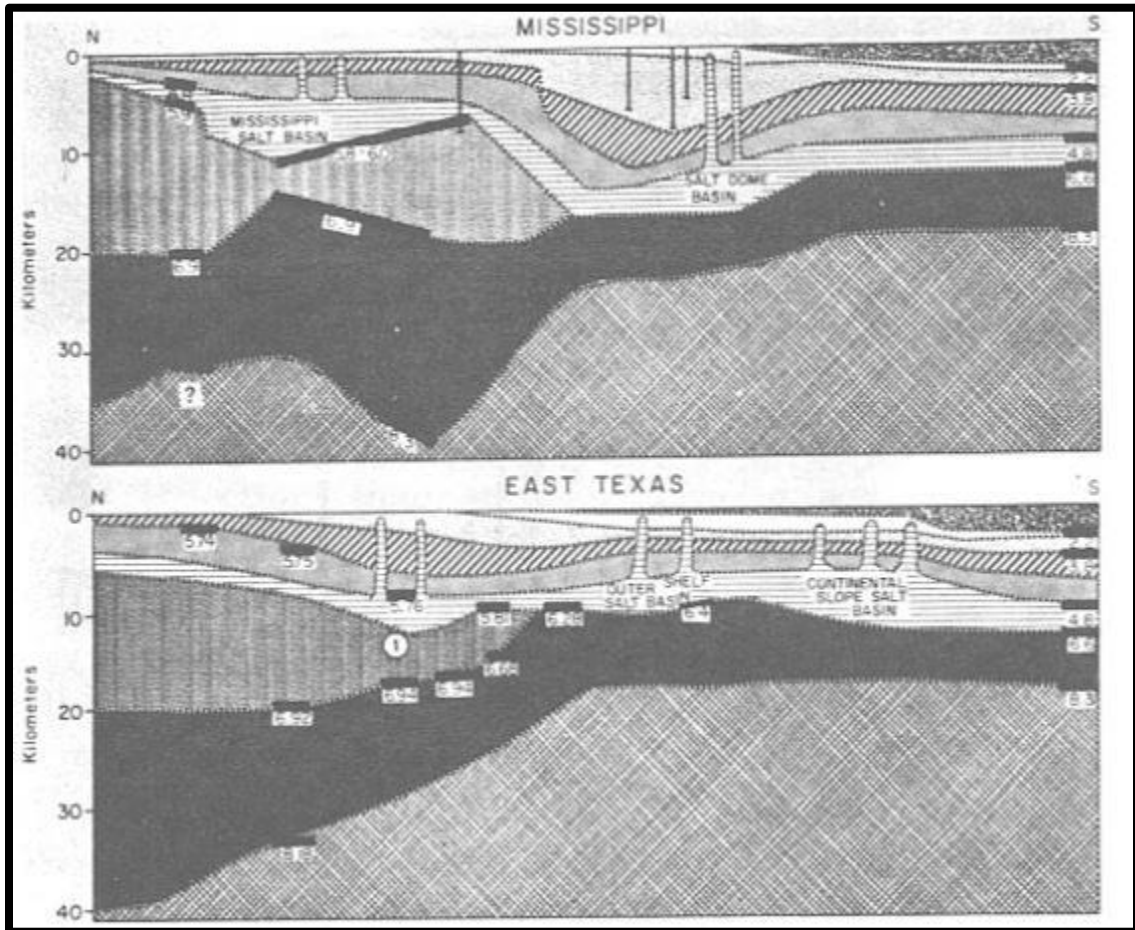


Figure 3.5: Structural cross-sections of sedimentary rocks, crust and upper mantle in Northern Gulf of Mexico (Worzel and Watkins, 1973). Locations of the profiles are shown on figure 3.3.

- East Texas Stratigraphy and Regional Cross-Sections from Nichols et al., 1966:

Stratigraphy of East Texas was studied by Nichols et al., 1966 by using relatively deep wells penetrated in the area. Regional cross-sections were constructed through the area with well control (Figure 3.6). Thicknesses of sedimentary packages, structure of the basement around East Texas Salt Basin and Sabine Uplift were used during the forward modeling stage.

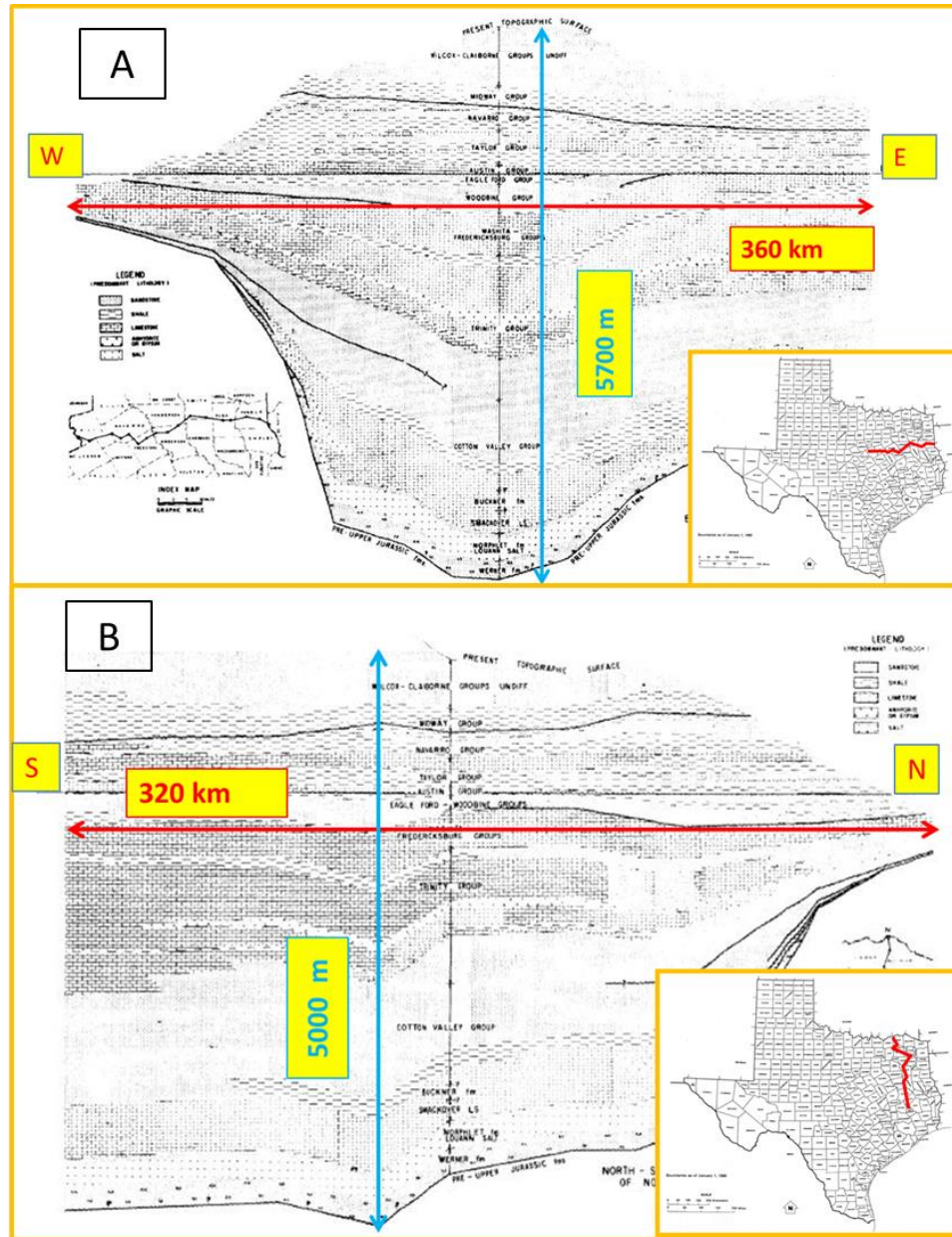


Figure 3.6: Regional cross sections over Northeast Texas. A) E-W cross sections through East Texas Salt Basin and Sabine Uplift. B) N-S cross section over the same area. Locations of profiles are shown on each map over Texas State County Map (modified from Nichols et al., 1966).



- Moho Depth and Crust Thickness Contour Maps ( Sawyer et al., 1991):

Based on subsidence analysis and Moho depth observations, estimated crustal thickness (figure 3.8 b) and Moho depth contour (figure 3.8 a) maps were made by Sawyer et al., 1991. By combining results of this study with location of structures on our study area, the maps were constructed as shown below.

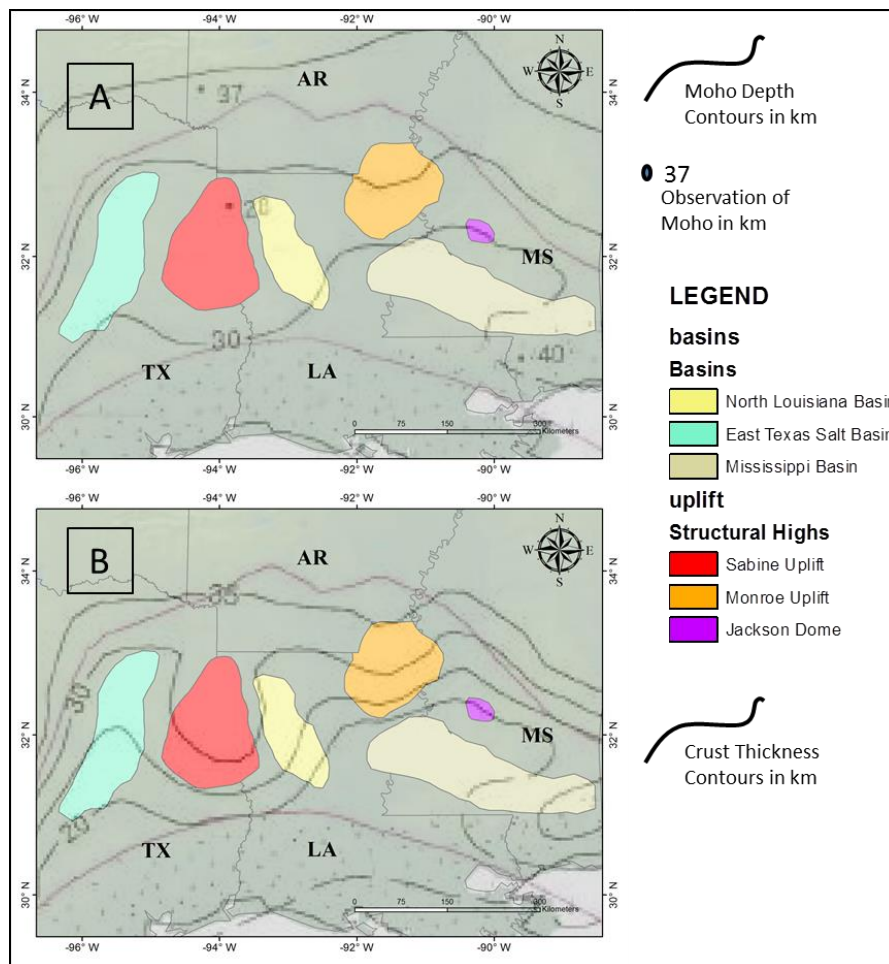


Figure 3.8: Moho depth and crustal thicknesses of the study area (modified after Sawyer et al., 1991)

Main integrated control point data are shown on figure 3.3 but not limited with those data. Some other sources, which were used during forward modeling, are discussed in this study. Moreover, control data related with igneous rocks are mentioned in the geology chapter and not discussed in this chapter again to avoid repeating.

## **CHAPTER IV**

### **METHODS**

#### **4.1. DATA-ENHANCEMENT METHODS**

Data-enhancement methods are applied to separate anomalies by wavelength. By doing this, interested anomaly features can be enhanced and isolated to make a better interpretation. To get smoother anomalies by avoiding shallower source bodies, upper continuation filter was used for gravity data. Then by subtracting the result from original data, residual maps were obtained. Total horizontal gradient map was constructed by using derivative of Bouguer gravity data in x and y direction. First vertical derivative map was also prepared by using the derivative of gravity data in z direction. Reduce to Pole Filter (RTP) was used for magnetic data by using calculated international geomagnetic reference field (IGRF). Data enhancement methods for magnetic data were applied to the data obtained after RTP.

#### **4.1.1. Upward Continuation**

Upward continuation transforms the potential field acquired on a given surface to another field that would be measured on a higher surface. This filter minimizes the effect of the anomalies produced by shallow sources in order to accentuate the anomalies of deep source bodies (Blakely, 1995).

To isolate the residual field, regional field obtained after upward continuation can be subtracted from the total field (Jacobsen, 1987).

In this study, upward continuation method was used for both magnetic and gravity data. Residual maps were also constructed for 5,000; 10,000; 15,000 meters. Filtered and residual maps of upward continuation are very helpful. Filtered maps enhance the dominance of anomalies produced by deep seated structures like crustal and Moho structures. On the other hand, residual maps effectively display the anomalies produced by shallower sources after suppressing the effect of deep seated structures.

#### **4.2.2. First Vertical Derivative**

First vertical derivative measures the rate of vertical change of potential field in the vertical direction. It can be an alternative way to residual maps by enhancing the shorter wavelength features relatively to those with longer wavelengths.

Upward continuation method also amplifies the shallower features by increasing the amplitude of the high frequencies whereas first vertical does the same task by suppressing the long wavelength anomalies.

This data enhancement method can be used for both gravity and magnetic data. However, it must be applied to the magnetic data after applying Reduce to the Pole (RTP) to the gridded magnetic data.

#### **4.2.3. Total Horizontal Gradient**

Total horizontal gradient method is an effective way to identify edges of the source bodies. The edges of the body are highlighted by the steepest horizontal gradient of a gravity anomaly  $g_z(x, y)$  produced by a source body (Blakely, 1995) (Figure 4.1).

Total horizontal gradient is calculated by using derivatives of the gravity and RTP data in x and y directions as below:

$$THG = \sqrt{d_x^2 + d_y^2}$$

The horizontal gradient maxima should be located over the edges of the source which produce anomalies (Figure 4.1).

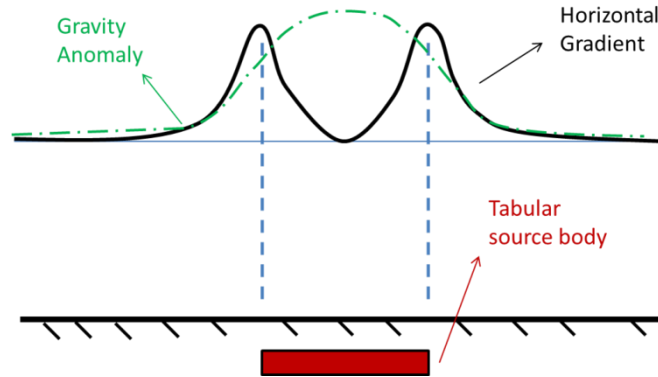


Figure 4.1: Gravity and horizontal gradient anomalies over a tabular source body (modified from Blakely, 1995).

#### 4.2.4. Reduction to the Pole

The shape of the magnetic anomalies can vary according to its location on the earth on the basis of inclination and declination of the ambient magnetic field. Reduction to Pole (RTP) is a data processing method which recalculates the Earth's magnetic field as if it was located at the North Pole where both magnetization and main magnetic field are vertical. Therefore, this method enables to locate anomaly directly above its causative body (Blakely, 1995) (Figure 4.2).

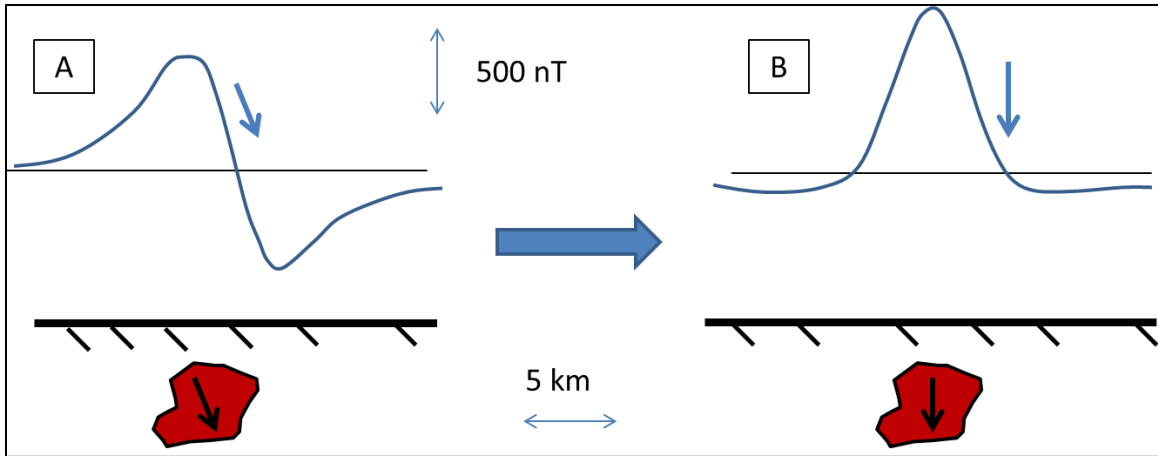


Figure 4.2: A magnetic anomaly a) before being reduced to the pole; b) after being reduced to the pole (modified from Blakely, 1995).

Reduction to the pole filter can be explained as below:

$$L(\theta) = \frac{1}{[\sin(I) + i \cos(I) \cos(D - \theta)]^2}$$

Where;

$\Theta$  is the wavenumber direction,

$I$  is the magnetic inclination

$D$  is the magnetic declination (Macleod et al., 1994)

Inclination and declination of the area are calculated according to International Geomagnetic Reference Field (IGRF).

This method is not suggested for the areas at less than 15° magnetic latitudes (Milligan and Gunn, 1997)

All data enhancement methods discussed above were applied to the magnetic data after applying RTP.

## **4.2. FORWARD MODELING**

In forward modeling, a designated model for the source body is constructed based on geological and geophysical knowledge by using initial model parameters. Anomaly of the model is calculated. And then, the calculated model anomaly is compared with observed anomaly which is data collected in the field. The next step in the forward modeling is to adjust and modify model parameters in order to improve the fit between observed and calculated anomaly. Until we get the best fit, these steps are repeated by considering control point data (Figure 4.3) (Blakely, 1995).

After comparison of the anomalies, model parameters or model geometry can be changed. In this study, model parameters as density and magnetic properties of layers were held constant to keep models consistent.

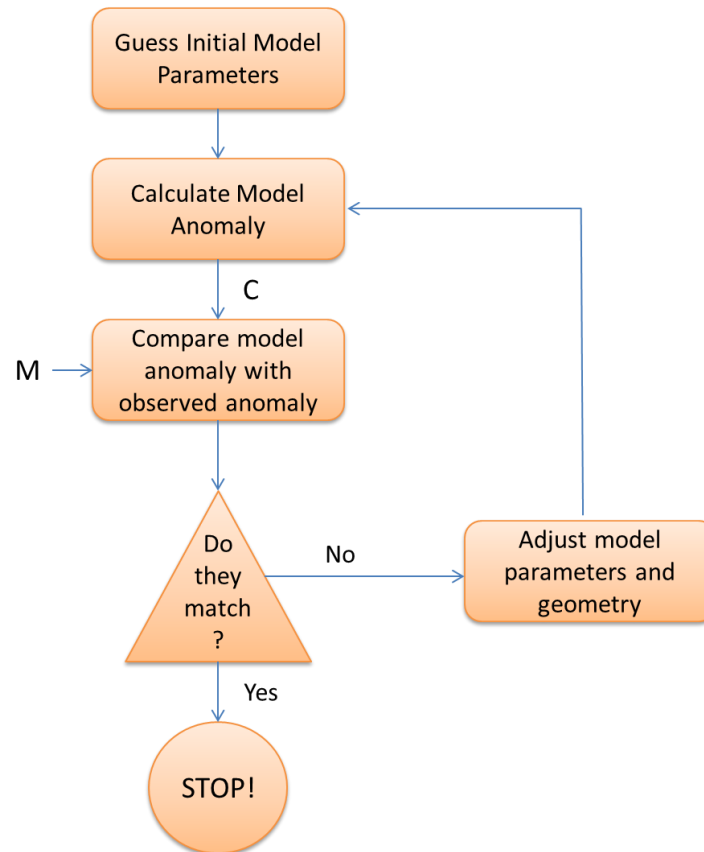


Figure 4.3: Process chart of forward modeling. Measured anomaly is represented by M where calculated anomaly is represented by C (modified from Blakely, 1995).

In order to reduce the variability of geometries, the most important process is to use control data as seismic reflection and refraction, well data, other geological and geophysical information with previous potential field studies. Although forward modeling interpretations are non-unique, geologically reasonable results can be obtained with a low margin of error by using control data.

#### 4.2.1. Model Parameters

During the forward modeling stage, initial model and layer properties were prepared by using control data and published papers as discussed in the previous chapter (Christensen, 1989; Hales et al., 1970; Ginzburg et al., 1983; Nichols et al., 1966; Sawyer et al., 1991; Worzel and Watkins, 1973; Kruger and Keller, 1989; Rogers, 1968). The model has four main layers which have also sublayers. Main layers which produce and contrast density differences are sedimentary rocks, crust, mantle and igneous rocks.

Subsurface geology and sedimentary rocks of the northeast Texas area are studied by Nichols et al., 1966 in detail with many numerous well data. Stratigraphic nomenclature and sedimentary rocks of Cenozoic and Mesozoic Eras are shown on figure 4.4. Moreover, they correlated the Mesozoic subsurface geology of the Northeast Texas with Arkansan subsurface and Louisiana subsurface (Figure 4.5). Therefore, by using this information sedimentary layers are generalized over the area. Sedimentary rocks are divided into five main layers with integration the studies for the study area. They are unconsolidated sediments, Cenozoic sedimentary rocks, Cretaceous sedimentary rocks, salt, and pre-Cretaceous sedimentary rocks. Unconsolidated sediments have a density value of  $2.1 \text{ g/cm}^3$  and it is a thin layer starting from surface. This layer is slightly thickening from North to South. Cenozoic sedimentary rocks are composed of mainly clastic rocks and they are on the relatively shallower parts of the basin. This layer has a density value of  $2.25 \text{ g/cm}^3$  in the models. Since increasing temperature and pressure at the deeper part of earth causes more compaction, density of the rocks also increase

MESOZOIC ERA									
CRETACEOUS SYSTEM					TERTIARY SYSTEM				
COMANCHE SERIES					Eocene Series				
ALBION STAGE					PALEOCENE SERIES				
WASHITA GROUP					DANIAN → THANNETIAN				
GEORGETOWN					MAESTRCHT				
FREDERICKSBURG GROUP					CAMPAIAN				
					TAYLOR GROUP				
					UPPER				
					LOWER				
					AUSTIN GROUP				
					EAGLE FORD GROUP				
					EAGLE FORD FORMATION				
					WOODBINE GROUP				
					LEWISVILLE Fm.				
					DEXTER Fm.				
					MANESS SHALE				
					BUDA LIMESTONE				
					GRAYSON SHALE				
					MAIN STREET LIMESTONE				
					WENO-PAW PAW LIMESTONE				
					DENTON SHALE				
					FORT WORTH LIMESTONE				
					DUCK CREEK LIMESTONE				
					KIAMICHI SHALE				
					GOODLAND LS.-EDWARDS LS.				
					WOLFE CITY SAND				
					GOBER CHALK				
					AUSTIN "CHALK"				
					TOKIO Fm.				
					SUBCLARKVILLE SAND				
					COCKER SAND (BLADOCK SAND)				
					HARRIS SAND				
					UPPER				
					LOWER				
					UPPER NAVARRO				
					KEMP GLAY				
					CORNICANA MARL				
					MACATOCH SAND				
					NEVLANDVILLE MARL				
					UPPER				
					LOWER				
					UPPER NAVARRO				
					KEMP GLAY				
					CORNICANA MARL				
					MACATOCH SAND				
					NEVLANDVILLE MARL				
					UPPER				
					LOWER				
					UPPER NAVARRO				
					KEMP GLAY				
					CORNICANA MARL				
					MACATOCH SAND				
					NEVLANDVILLE MARL				
					UPPER				
					LOWER				
					UPPER NAVARRO				
					KEMP GLAY				
					CORNICANA MARL				
					MACATOCH SAND				
					NEVLANDVILLE MARL				
					UPPER				
					LOWER				
					UPPER NAVARRO				
					KEMP GLAY				
					CORNICANA MARL				
					MACATOCH SAND				
					NEVLANDVILLE MARL				
					UPPER				
					LOWER				
					UPPER NAVARRO				
					KEMP GLAY				
					CORNICANA MARL				
					MACATOCH SAND				
					NEVLANDVILLE MARL				
					UPPER				
					LOWER				
					UPPER NAVARRO				
					KEMP GLAY				
					CORNICANA MARL				
					MACATOCH SAND				
					NEVLANDVILLE MARL				
					UPPER				
					LOWER				
					UPPER NAVARRO				
					KEMP GLAY				
					CORNICANA MARL				
					MACATOCH SAND				
					NEVLANDVILLE MARL				
					UPPER				
					LOWER				
					UPPER NAVARRO				
					KEMP GLAY				
					CORNICANA MARL				
					MACATOCH SAND				
					NEVLANDVILLE MARL				
					UPPER				
					LOWER				
					UPPER NAVARRO				
					KEMP GLAY				
					CORNICANA MARL				
					MACATOCH SAND				
					NEVLANDVILLE MARL				
					UPPER				
					LOWER				
					UPPER NAVARRO				
					KEMP GLAY				
					CORNICANA MARL				
					MACATOCH SAND				
					NEVLANDVILLE MARL				
					UPPER				
					LOWER				
					UPPER NAVARRO				
					KEMP GLAY				
					CORNICANA MARL				
					MACATOCH SAND				
					NEVLANDVILLE MARL				
					UPPER				
					LOWER				
					UPPER NAVARRO				
					KEMP GLAY				
					CORNICANA MARL				
					MACATOCH SAND				
					NEVLANDVILLE MARL				
					UPPER				
					LOWER				
					UPPER NAVARRO				
					KEMP GLAY				
					CORNICANA MARL				
					MACATOCH SAND				
					NEVLANDVILLE MARL				
					UPPER				
					LOWER				
					UPPER NAVARRO				
					KEMP GLAY				
					CORNICANA MARL				
					MACATOCH SAND				
					NEVLANDVILLE MARL				
					UPPER				
					LOWER				
					UPPER NAVARRO				
					KEMP GLAY				
					CORNICANA MARL				
					MACATOCH SAND				
					NEVLANDVILLE MARL				
					UPPER				
					LOWER				
					UPPER NAVARRO				
					KEMP GLAY				
					CORNICANA MARL				
					MACATOCH SAND				
					NEVLANDVILLE MARL				
					UPPER				
					LOWER				
					UPPER NAVARRO				
					KEMP GLAY				
					CORNICANA MARL				
					MACATOCH SAND				
					NEVLANDVILLE MARL				
					UPPER				
					LOWER				
					UPPER NAVARRO				
					KEMP GLAY				
					CORNICANA MARL				
					MACATOCH SAND				
					NEVLANDVILLE MARL				
					UPPER				
					LOWER				
					UPPER NAVARRO				
					KEMP GLAY				
					CORNICANA MARL				
					MACATOCH SAND				
					NEVLANDVILLE MARL				
					UPPER				
					LOWER				
					UPPER NAVARRO				
					KEMP GLAY				
					CORNICANA MARL				
					MACATOCH SAND				
					NEVLANDVILLE MARL				
					UPPER				
					LOWER				
					UPPER NAVARRO				
					KEMP GLAY				
					CORNICANA MARL				
					MACATOCH SAND				
					NEVLANDVILLE MARL				
					UPPER				
					LOWER				
					UPPER NAVARRO				
					KEMP GLAY				
					CORNICANA MARL				
					MACATOCH SAND				
					NEVLANDVILLE MARL				
					UPPER				
					LOWER				
					UPPER NAVARRO				
					KEMP GLAY				
					CORNICANA MARL				
					MACATOCH SAND				
					NEVLANDVILLE MARL				
					UPPER				
					LOWER				
					UPPER NAVARRO				
					KEMP GLAY				
					CORNICANA MARL				
					MACATOCH SAND				
					NEVLANDVILLE MARL				
					UPPER				
					LOWER				
					UPPER NAVARRO				
					KEMP GLAY				
					CORNICANA MARL				
					MACATOCH SAND				
					NEVLANDVILLE MARL				
					UPPER				
					LOWER				
					UPPER NAVARRO				
					KEMP GLAY				
					CORNICANA MARL				
					MACATOCH SAND				
					NEVLANDVILLE MARL				
					UPPER				
					LOWER				
					UPPER NAVARRO				
					KEMP GLAY				
					CORNICANA MARL				
					MACATOCH SAND				
					NEVLANDVILLE MARL				
					UPPER				
					LOWER				
					UPPER NAVARRO				
					KEMP GLAY				
					CORNICANA MARL				
					MACATOCH SAND				
					NEVLANDVILLE MARL				
					UPPER				
					LOWER				
					UPPER NAVARRO				
					KEMP GLAY				
					CORNICANA MARL				
					MACATOCH SAND				
					NEVLANDVILLE MARL				
					UPPER				
					LOWER				
					UPPER NAVARRO				
					KEMP GLAY				
					CORNICANA MARL				
					MACATOCH SAND				
					NEVLANDVILLE MARL				
					UPPER				
					LOWER				
					UPPER NAVARRO				
					KEMP GLAY				
					CORNICANA MARL				
					MACATOCH SAND				
					NEVLANDVILLE MARL				
					UPPER				
					LOWER				
					UPPER NAVARRO				
					KEMP GLAY				
					CORNICANA MARL				
					MACATOCH SAND				
					NEVLANDVILLE MARL				
					UPPER				
					LOWER				
					UPPER NAVARRO				
					KEMP GLAY				
					CORNICANA MARL				
					MACATOCH SAND				
					NEVLANDVILLE MARL				
					UPPER				
					LOWER				
					UPPER NAVARRO				
					KEMP GLAY				
					CORNICANA MARL				
					MACATOCH SAND				
					NEVLANDVILLE MARL				
					UPPER				
					LOWER				
					UPPER NAVARRO				
					KEMP GLAY				
					CORNICANA MARL				
					MACATOCH SAND				
					NEVLANDVILLE MARL				
					UPPER				
					LOWER				
					UPPER NAVARRO				
					KEMP GLAY				
					CORNICANA MARL				
					MACATOCH SAND				
					NEVLANDVILLE MARL				
					UPPER				
					LOWER				
					UPPER NAVARRO				
					KEMP GLAY				
					CORNICANA MARL				
					MACATOCH SAND				
					NEVLANDVILLE MARL				
					UPPER				
					LOWER				
					UPPER NAVARRO				
					KEMP GLAY				
					CORNICANA MARL				
					MACATOCH SAND				
					NEVLANDVILLE MARL				
					UPPER				
					LOWER				
					UPPER NAVARRO				
					KEMP GLAY				
					CORNICANA MARL				
					MACATOCH SAND				
					NEVLANDVILLE MARL				
					UPPER				
					LOWER				
					UPPER NAVARRO				
					KEMP GLAY				
					CORNICANA MARL				
					MACATOCH SAND				
					NEVLANDVILLE MARL				
					UPPER				
					LOWER				
					UPPER NAVARRO				
					KEMP GLAY				
					CORNICANA MARL				
					MACATOCH SAND				
					NEVLANDVILLE MARL				
					UPPER				
					LOWER				
					UPPER NAVARRO				
					KEMP GLAY				
					CORNICANA MARL				
					MACATOCH SAND				
					NEVLANDVILLE MARL				
					UPPER				
					LOWER				
					UPPER NAVARRO				
					KEMP GLAY				
					CORNICANA MARL				
					MACATOCH SAND				
					NEVLANDVILLE MARL				
					UPPER				
					LOWER				
					UPPER NAVARRO				
					KEMP GLAY				
					CORNICANA MARL				
					MACATOCH SAND				
					NEVLANDVILLE MARL				
					UPPER				
					LOWER				
					UPPER NAVARRO				
					KEMP GLAY				
					CORNICANA MARL				
					MACATOCH SAND				
					NEVLANDVILLE MARL				
					UPPER				
					LOWER				
					UPPER NAVARRO				
					KEMP GLAY				
					CORNICANA MARL				
					MACATOCH SAND				
					NEVLANDVILLE MARL				
					UPPER				
					LOWER				
					UPPER NAVARRO				
					KEMP GLAY				
					CORNICANA MARL				
					MACATOCH SAND				
					NEVLANDVILLE MARL				
					UPPER				
					LOWER				
					UPPER NAVARRO				
					KEMP GLAY				
					CORNICANA MARL				
					MACATOCH SAND				
					NEVLANDVILLE MARL				
					UPPER				
					LOWER				
					UPPER NAVARRO				
					KEMP GLAY				
					CORNICANA MARL				
					MACATOCH SAND				
					NEVLANDVILLE MARL				
					UPPER				
					LOWER				
					UPPER NAVARRO				
					KEMP GLAY				
					CORNICANA MARL				
					MACATOCH SAND				
					NEVLANDVILLE MARL				
					UPPER				
					LOWER				
					UPPER NAVARRO				
					KEMP GLAY				
					CORNICANA MARL				
					MACATOCH SAND				
					NEVLANDVILLE MARL				
					UPPER				
					LOWER				
					UPPER NAVARRO				
					KEMP GLAY				
					CORNICANA MARL				
					MACATOCH SAND				
					NEVLANDVILLE MARL				
					UPPER				
					LOWER				
					UPPER NAVARRO				
					KEMP GLAY				
					CORNICANA MARL				
					MACATOCH SAND				
					NEVLANDVILLE MARL				
					UPPER				
					LOWER				
					UPPER NAVARRO				
					KEMP GLAY				
					CORNICANA MARL				
					MACATOCH SAND				
					NEVLANDVILLE MARL				
					UPPER				
					LOWER				
					UPPER NAVARRO				
					KEMP GLAY				
					CORNICANA MARL				
					MACATOCH SAND				
					NEVLANDVILLE MARL				
					UPPER				
					LOWER				
					UPPER NAVARRO				
					KEMP GLAY				
					CORNICANA MARL				
					MACATOCH SAND				
					NEVLANDVILLE MARL				
					UPPER				
					LOWER				
					UPPER NAVARRO				
					KEMP GLAY				
					CORNICANA MARL				
					MACATOCH SAND				
					NEVLANDVILLE MARL				
					UPPER				
					LOWER				
					UPPER NAVARRO				

GULF STATES				EAST TEXAS SUBSURFACE	ARKANSAS SUBSURFACE	LOUISIANA SUBSURFACE
				UPPER NAVARRO	ARKADELPHIA MARL	ARKADELPHIA MARL
				KEMP CLAY		
				CORSICANA MARL		
				NACATOCH SAND	NACATOCH fm.	NACATOCH fm.
				NEYLANDVILLE MARL	SARATOGA CHALK	SARATOGA CHALK
				UPPER TAYLOR	MARLBROOK MARL	MARLBROOK MARL
				PECAN GAP CHALK	ANNONA CHALK (RES.) OZAN fm	ANNONA CHALK (RES.) OZAN fm
				WOLFE CITY SAND	BUCKRANGE SAND	BUCKRANGE SAND
				LOWER TAYLOR	BROWNSTOWN fm	BROWNSTOWN fm.
				GOBER CHALK	B. GOBER CHALK	
				AUSTIN "CHALK"	TOKIO fm.	TOKIO fm.
				ECTOR CHALK		ECTOR CHALK
				SUBCLARKVILLE SAND		
				COKE SAND (BLACK SAND)	EAGLE FORD fm.	EAGLE FORD fm.
				HARRIS SAND		
				LEWISVILLE fm	LEWISVILLE fm.	LEWISVILLE fm.
					OR UPPER TUSCALOOSA fm.	OR UPPER TUSCALOOSA fm.
					EULESS fm	EULESS fm
					OR LOWER TUSCALOOSA fm	OR LOWER TUSCALOOSA fm.
				DEXTER fm.		DANTZLER fm.
UPPER JURASSIC SERIES				EAST TEXAS SUBSURFACE	ARKANSAS SUBSURFACE	LOUISIANA SUBSURFACE
				WASHITA GR.		
				MAHES SH		
				BUCK LS		
				GEORGE TOWN		
				WENCO-PAWPAW LS	ABSENT OR UNDIFF.	ABSENT OR UNDIFF.
				DENTON SH		
				FORT WORTH LS		
				DUCK CREEK LS		
				KIAMOCHI SH		
				GOODLAND LS		
				PALUXY fm.	PALUXY facies	PALUXY facies
				UPPER GLEN ROSE fm.	MOORINGSPOINT fm.	MOORINGSPOINT fm.
				MASSIVE ANHYDRITE		
				FERRY LAKE ANHYDRITE	FERRY LAKE ANHYDRITE	FERRY LAKE ANHYDRITE
				RODESSA mbr.	RODESSA fm.	RODESSA fm.
				JAMES LS	JAMES LS	JAMES LS
				PINE ISLAND SH	PINE ISLAND fm	PINE ISLAND fm
				PETTET LS	SLIGO fm	SLIGO fm
				TRAVIS PLAK fm.	HOSSTON fm.	HOSSTON fm.
				SCHULER fm.	SCHULER fm.	SCHULER fm.
				BOSSIER fm.	BOSSIER fm.	BOSSIER fm.
				BUCKNER fm.	BUCKNER fm.	BUCKNER fm.
				SMACKOVER LS.	SMACKOVER LS.	SMACKOVER LS.
				NORPHLET fm.	NORPHLET fm.	NORPHLET fm.
				LOUANN SALT	LOUANN SALT	LOUANN SALT
				WERNER fm.	WERNER fm.	WERNER fm.
				EAGLE MILLS fm.	EAGLE MILLS fm.	EAGLE MILLS fm.

Figure 4.5: Correlation of Mesozoic subsurface nomenclature of Northeast Texas with Arkansas and Louisiana (Nichols et al., 1966).

proportional to the depth. This simple assumption was also considered for model parameters. Cretaceous sedimentary rocks of northeast Texas and its time equivalent rocks of Louisiana and Northwestern Mississippi are dominantly composed of carbonate rocks with minor shale and evaporate rocks. This layer has a density of  $2.50 \text{ g/cm}^3$ . Salt layer has a density of  $2.16 \text{ g/cm}^3$  and it represents mainly Louann Salt layer deposited on a broad area in the Gulf of Mexico Basin. Pre-Cretaceous sedimentary rock layer is composed of dominantly with low density clastic rocks. It has a density of  $2.50 \text{ g/cm}^3$  because it is located at the deepest part of the basin.

In this study crustal layer of the models is composed of two sublayers as Upper and Lower Crusts because there is limited information about middle crust in the study area. In addition, only two crustal layers are used in most of the previous studies, those were used to construct initial models (Kruger and Keller, 1989; Worzel and Watkins, 1973; Hales et al., 1970). Upper crust layer is assumed to be a magnetic layer with a density value of  $2.7 \text{ g/cm}^3$  due to its composition. On the other hand, lower crustal layer has a density value of  $3.00 \text{ g/cm}^3$ . Geothermal gradient increases with depth which cause increasing of the temperature through the Earth's deeper parts. Since rocks are losing their magnetic properties when they reach to the Curie point,  $600 \text{ C}$ , the layers below the upper crust are assumed to be formed by non-magnetic layers. Therefore, lower crust layer of the models have no magnetization.

Upper mantle layer has a density of  $3.30 \text{ g/cm}^3$ .

Igneous rocks of the models have different density values according to their composition between  $2.7 - 2.9 \text{ g/cm}^3$ . All of them are assumed to be magnetic layers.

All layers roughly parallel to the surface except igneous rocks are assigned to extend infinity in  $X^+$  and  $X^-$  directions. This assumption let us be avoided from the edge effects.

## **CHAPTER V**

### **RESULTS AND INTERPRETATIONS**

A bouguer gravity map, and pole-reduced magnetic intensity map were constructed to interpret crustal and basin structures of the area. Since gravity and magnetic maps do not show all the structural features of the area effectively, filtered maps were prepared by using data enhancement methods. In addition, three 2-D gravity modeled cross sections, ranging from 470 to 650 km – long, through the uplifts were constructed.

#### **5.1. QUALITATIVE INTERPRETATIONS**

Bouguer gravity values over the study area range from -110 to 50 mGal (figure 5.1). The variations of the gravity values are combined effect of variable crustal thickness and Moho depth, basins and uplifts, igneous rocks and sedimentary rocks. Four main gravity ranges are appeared as -50 to -25 mGal; -25 to -5 mGal; -5 to 15 mGal and 15 to 50 mGal. Sabine Uplift, Monroe Uplift, and Jackson Dome are mostly characterized by -5 to 15 mGal range which are superimposed by 15 to 50 mGal circular anomalies (Figure 5.2). These gravity maximas are mostly related with igneous rocks over the uplifts. La

Salle Arch is also characterized by the values of -5 to 15 mGal. Long wavelengths -50 to -25 mGal values are associated with deeper Moho and thick crust as shown over Wiggins Arch and the minima located at the southern part of Sabine Uplift. The -25 to -5 mGal values are observed over East Texas Salt Basin and North Louisiana Salt Basin.

Reduced – to – pole magnetic intensity values over the study area range from -1600 to 6200 nT (Figure 5.3). To generalize magnetic value ranges for different structures are not as easy as we did for the gravity values but main ranges are appeared as -200 to -50 nT; -50 to 10 nT; 10 to 100 nT; and 100 to 300 nT. East Texas Salt Basin and southern part of the basin, central part of Wiggins Arch are characterized by -200 to -50 nT. Sabine Uplift, Monroe Uplift, and Jackson Dome are mostly characterized by -50 to 10 nT which are superimposed by 10 to 100 nT and 100 to 300 nT anomalies (Figure 5.4). La Salle Arch is also observed as in 10 to 100 nT range. 100s nT magnetic values are produced by lithological boundaries. 100 to 300 nT is observed over Sabine Uplift, Monroe Uplift and Jackson Dome in a circular shape which is an evidence of igneous rocks beneath the structures.

Short wavelength, high amplitude circular gravity and magnetic anomalies coincide (Figure 5.2; Figure 5.4). Gravity values of these anomalies are up to 50 mGal where magnetic anomalies are up to 800 nT. The most straightforward interpretation for these anomalies is igneous rocks because these kinds of anomalies can be created by sharp lithological changes. Such changes with high magnetic characteristics are due to igneous rocks whose anomalies also circular in general.

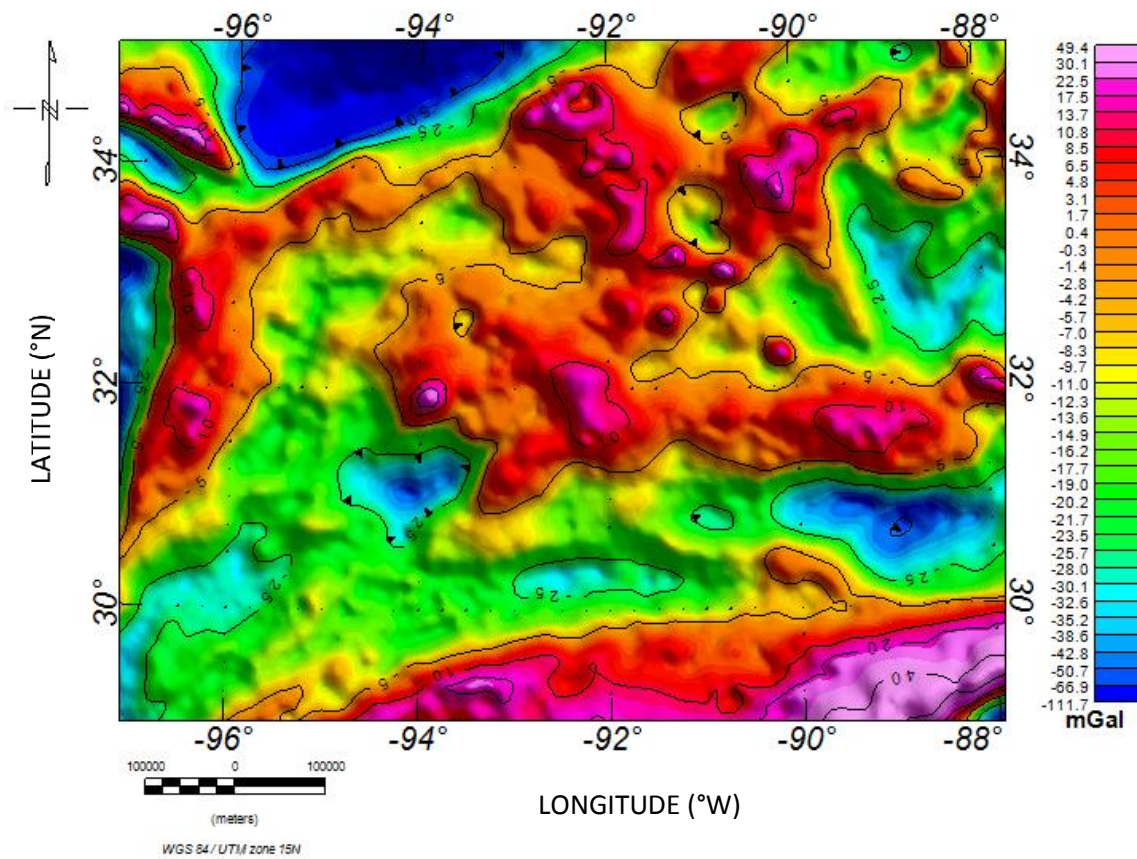


Figure 5.1: Contoured Bouguer Gravity Anomaly Map (Contours are in mGal.).

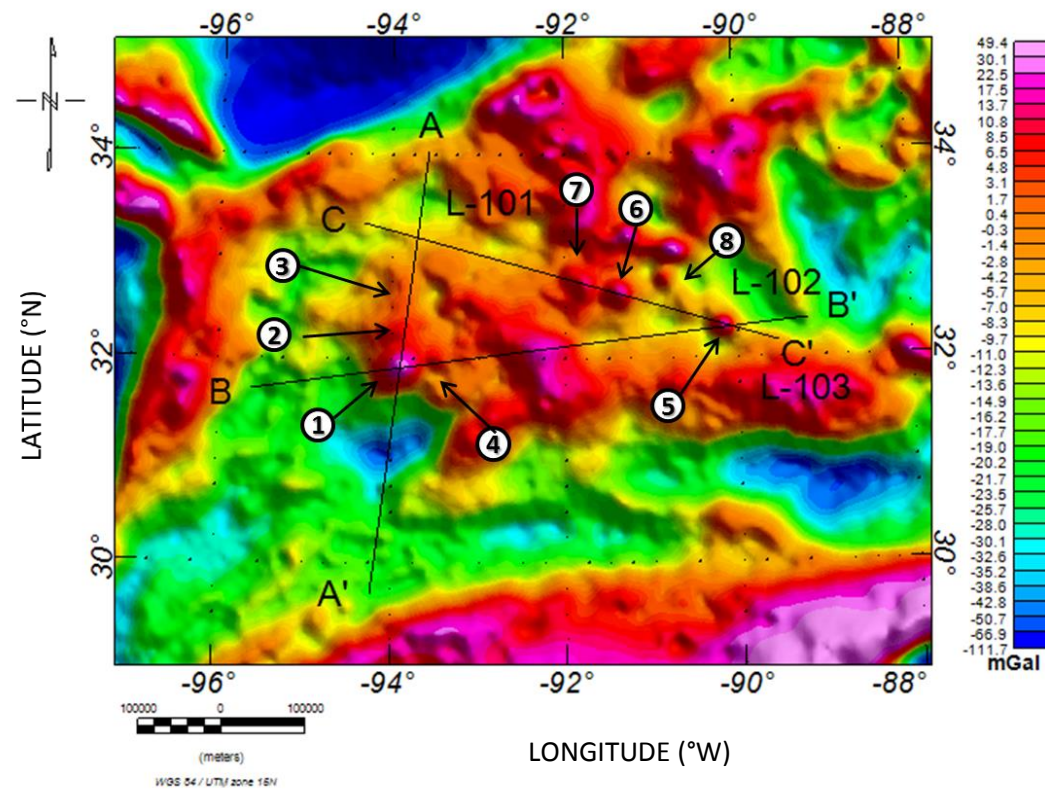


Figure 5.2: Interpreted anomalies of Sabine, Monroe and Jackson Uplifts on Bouguer Gravity Map. Black solid lines show the locations of 2-D gravity models.

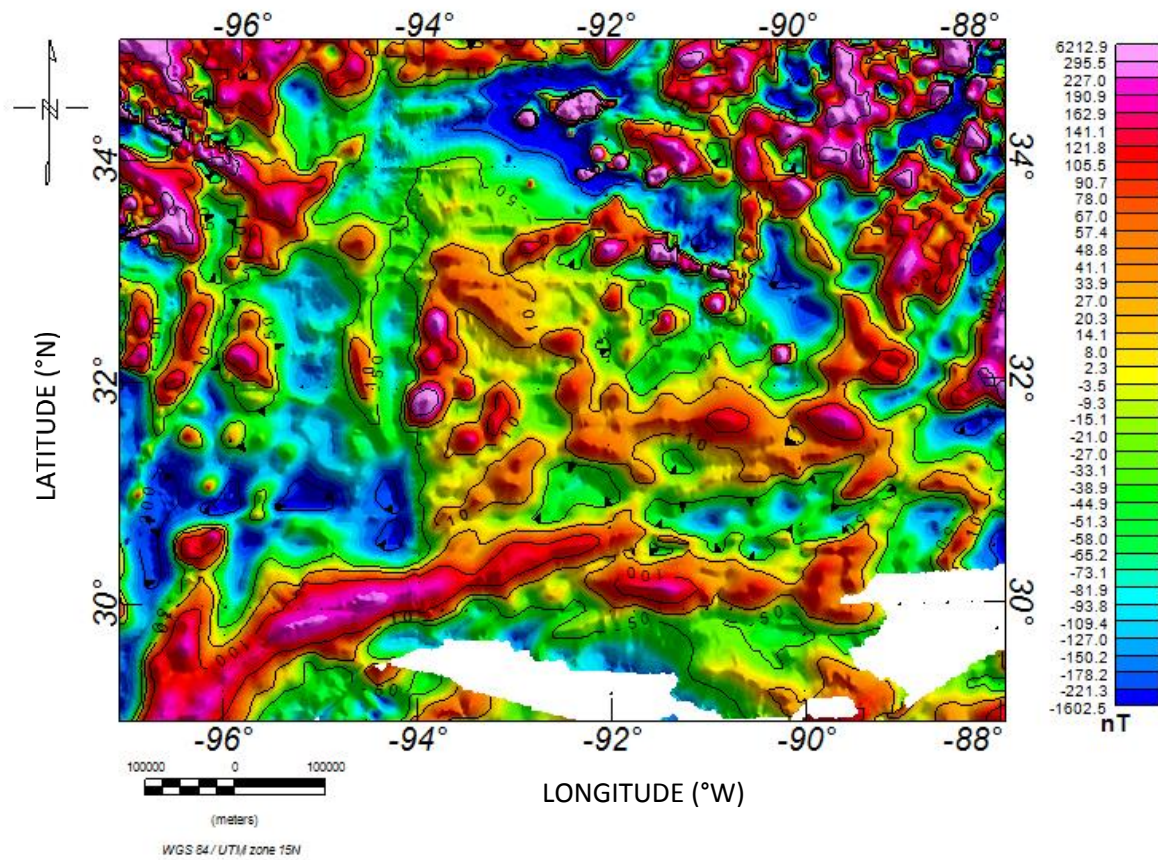


Figure 5.3: Contoured reduced to pole magnetic intensity map (Contours are in nT).

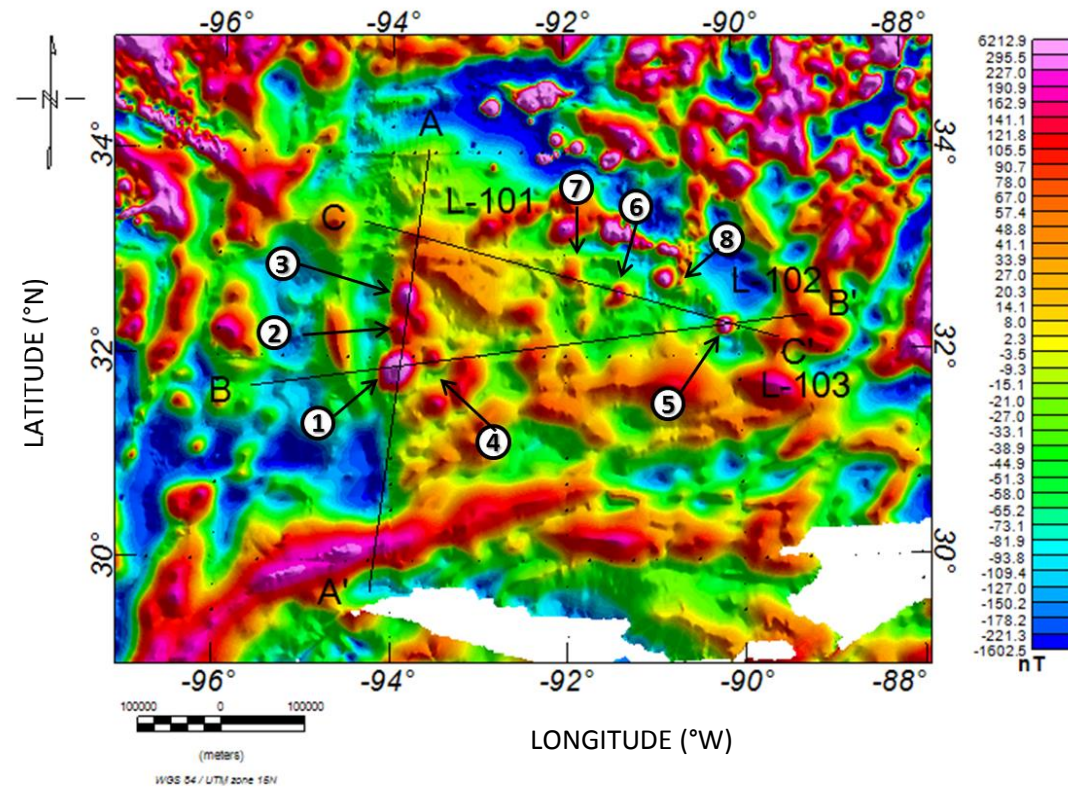


Figure 5.4: Interpreted anomalies of Sabine, Monroe and Jackson Uplifts on reduced to pole magnetic anomaly map. Black solid lines show the locations of 2-D gravity models.

### **5.1.1. Sabine Uplift**

Sabine Uplift produces a broad gravity high which is superimposed by short wavelength high amplitude gravity anomalies. Short wavelength magnetic anomalies over the structure are evidence for a shallow basement. Circular short wavelength magnetic high anomalies correlate with the gravity maximas.

On the southern part of Sabine Uplift, there is a circular maxima for both gravity and magnetic data over the Sabine Uplift that has been interpreted to be produced by an igneous body (Kruger and Keller, 1986; Mickus and Keller, 1992). Previous studies in the area document occurrences of igneous rocks (Byerly, 1991; Kidwell, 1951; Moody, 1949; Griffin, 2010; Ewing, 2009; Baksi, 1997; Nichols et al., 1968) that have been discussed and sampled in deep exploration wells. In addition, geophysical signatures were interpreted as an evidence of subsurface igneous activity.

High gravity and magnetic anomalies on the structure could be interpreted as igneous body because high amplitude magnetic values more than 100s of nT which we see around the maximas can be produced by lithological boundaries. When it is considered by the potential field point of view with previous works, interpretation of filtered maps; igneous body is the most promising one as a source body for those anomalies.

There are three roughly circular short wavelength magnetic high anomalies next to each other at the northern part of uplift. Magnetic point values of these anomalies from north to south are 372, 220, and 750 nT, respectively (Figure 5.4). Those magnetic high

anomalies also have similar magnetic intensity values with the southern maxima. Those anomalies have most likely same origin with the southern maxima.

A long wavelength gravity minima on the outside southern Sabine Uplift has the lowest gravity and magnetic values in the Sabine Uplift area. Gravity and magnetic anomaly amplitudes are  $-44.51$  mGal and  $-84.12$  nT, respectively. The shape of the gravity anomaly is roughly ellipsoidal and the length of longer axis is approximately 70 km. This kind of anomalies where gravity low coincides with a long wavelength magnetic anomaly, are produced by deep basement or Moho topography. Relatively deeper and thicker crust, where we expect crust-mantle boundary deeper, most likely produces this anomaly.

### **5.1.2. Monroe Uplift**

Monroe Uplift is located in parts of mainly north-east Louisiana, south-central Mississippi and southern Arkansas. It is a roughly circular structure. The uplift consists of several circular isolated circular gravity and magnetic maximas. Gravity anomalies on the Monroe Uplift vary between  $-8$  to  $28$  mGal whereas magnetic intensity anomalies vary between  $-21$  to  $774$  nT. However, isolated circular anomalies have gravity values range from  $23$  to  $27$  mGal. On the other hand, produced significant isolated magnetic anomalies range from  $120$  to  $975$  nT.

Instead of a dome or homogenous uplift, Monroe Uplift consists of several different buried igneous bodies which produce isolated circular gravity and magnetic high

anomalies. Variety of igneous bodies as compositional, depth and rock type is the main reason why each maxima has a different kind of anomaly in a relatively small area. Previous works also support this idea. The Monroe Uplift has largest volume of magma and greatest compositional diversity in the Northern Gulf of Mexico Basin and at least four major igneous rock groups were defined so far: i) intermediate rocks; ii) alkaline rocks; iii) basalts; iv) lamprophyres (Ewing, 2009; Byerly, 1991; Kidwell, 1951). Igneous rocks are encountered in more than 50 wells in and around the Monroe Uplift (Baksi, 1997). Since each of those rock types has a characteristic density and magnetic property, they also produce specific anomalies.

### **5.1.3. Jackson Dome**

Jackson Dome is a structural feature at the northeastern edge of the Mississippi Salt Basin and it is geographically located below the City of Jackson, Mississippi. This structure produces a circular short wavelength high frequency gravity anomaly. A magnetic maximum also correlates with the gravity anomaly. Magnetic anomalies on the maxima vary between 150 – 840 nT whereas the anomalies surround the maxima range from -20 to 20 nT. There is more than 300 nT difference between the maxima and the anomalies surround it. Gravity values on the maxima vary from 15 to 20 mGal whereas average gravity value over the structure is around -15 mGal.

The most straightforward interpretation for the gravity and magnetic anomalies over Jackson Dome is a relatively deep crust and Moho superimposed by igneous rocks. The only possibility that produce around 300 nT magnetic anomaly difference is an igneous

body for this area. This structure also generates gravity anomaly difference on the area. Therefore, igneous rocks buried under sedimentary section produced this circular high amplitude gravity and magnetic anomaly. Previous studies and models also support this idea. Jackson Dome has a similar structural style with the most of the salt domes in the Gulf Coast. It has a core built by igneous rocks of Cretaceous age instead of salt stacks (Saunders and Harrelson, 1992; Ewing, 2009). There was abundant igneous activity in the Late Cretaceous which was followed by deposition of reefal carbonates, called as Jackson Gas Rock, associated with the uplift (Ewing, 1991).

## **5.2. FILTERED MAPS**

Gravity and magnetic maps of the region do not give a clear image of all the structural features of the area. High amplitude, short wavelength anomalies on Sabine, Jackson and Monroe Uplifts are visible. However, to obtain clear images of the edges and sources of anomalies produced by structures; upward continuation, upward continuation residual, total horizontal gradient, analytic signal and low pass maps were constructed. To obtain magnetic filtered maps, reduced – to – pole magnetic intensity data was used as an input data. Filtered maps are shown in Figure 5.5 through 5.15.

Deep seated structures as crustal and Moho depth variations are observed in the upward continuation maps (Figure 5.5.a; Figure 5.6.a), anomalies at elevation greater than 15 km; and 100 km low – pass maps (Figure 5.15). These maps enhance relatively deeper anomalies by attenuating the effect of shallower anomalies. Crustal structures of Sabine Uplift, La Salle Arch, and Monroe Uplift are clear in these maps. Upward continued

maps indicate shallower crust beneath La Salle Arch, Sabine Uplift and northwestern part of Monroe Uplift. Low-pass maps also support this idea. It was also observed that there is a relatively deeper basement and Moho under the structures of Wiggins Arch, southern off-limit of Sabine Uplift and East Texas Salt Basin.

Residual maps of 15 km upward continuation (Figure 5.5.b; Figure 5.6.b, and 5.7), accentuate the effect of shallower source bodies by minimizing anomalies of deeper sources. Short-wavelength, high-frequency circular anomalies, interpreted as intrabasinal and intra-crustal igneous bodies are observed better in these residual maps. Locations of pronounced circular gravity and magnetic anomalies coincide.

Total horizontal gradient maps for Bouguer gravity and reduce – to –pole magnetic intensity maps (Figure 5.8 through Figure 5.10) identify edges of the structures which produce anomalies. Edges of the circular anomalies on Sabine Uplift, Monroe Uplift and Jackson Dome are better resolved in the total horizontal gradient maps. The most straightforward interpretation for the anomalies is igneous rocks. They all have maxima on gravity and magnetic filtered maps in a circular shape. In addition, anomalies have similar characteristics with well-known igneous locations as Magnet Cove and Little Rock.

Interpreted anomalies as a result of igneous rocks are shown on the figures (5.7, 5.8, 5.10, 5.12, and 5.14). Locations of these anomalies coincide in all gravity, magnetic anomaly and data enhancement maps. Their causative bodies are also modeled in the 2-D gravity models and shown with same assigned numbers (Figure 5.19, 5.21, 5.24).

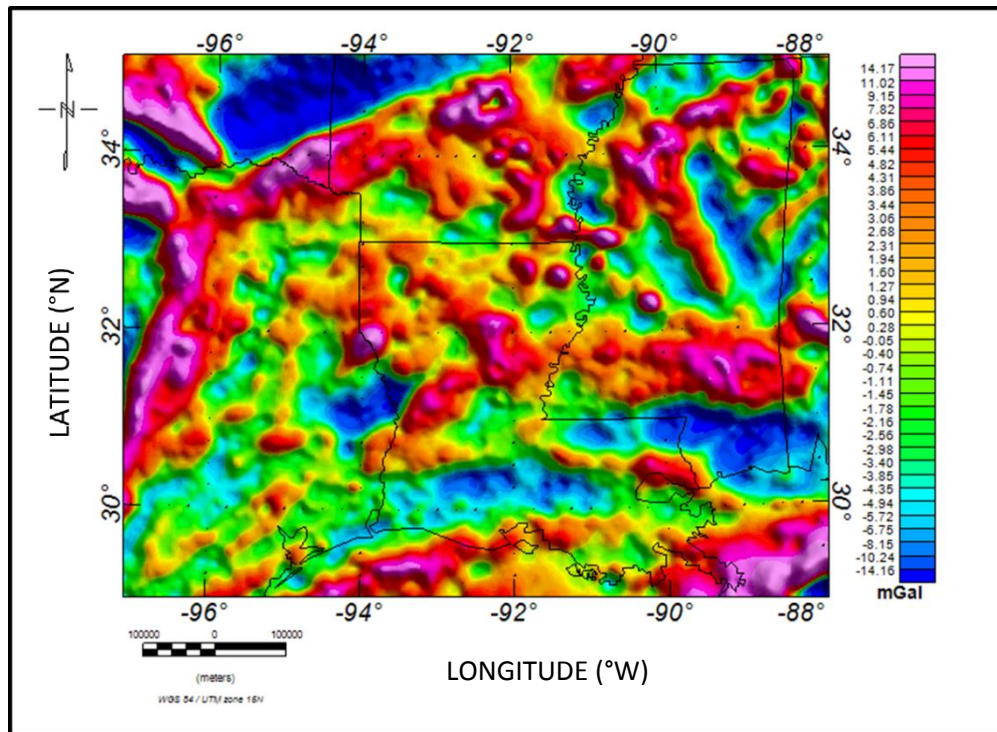
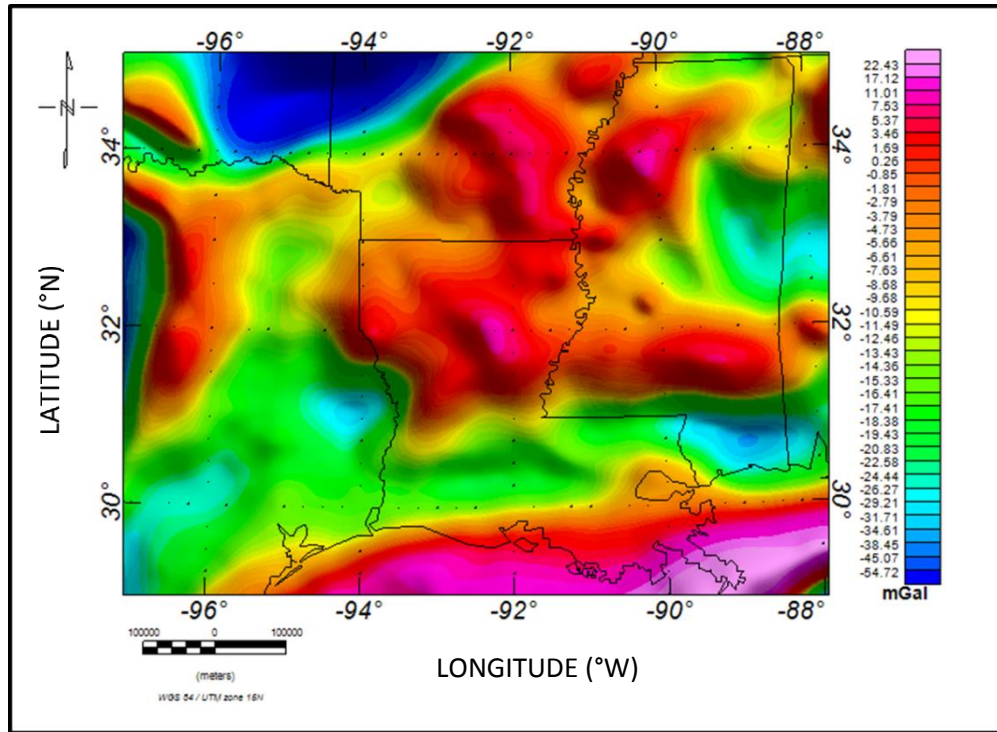


Figure 5.5: A) 15 km upward continuation Bouguer gravity map B) 15 km upward continuation Bouguer gravity residual map.

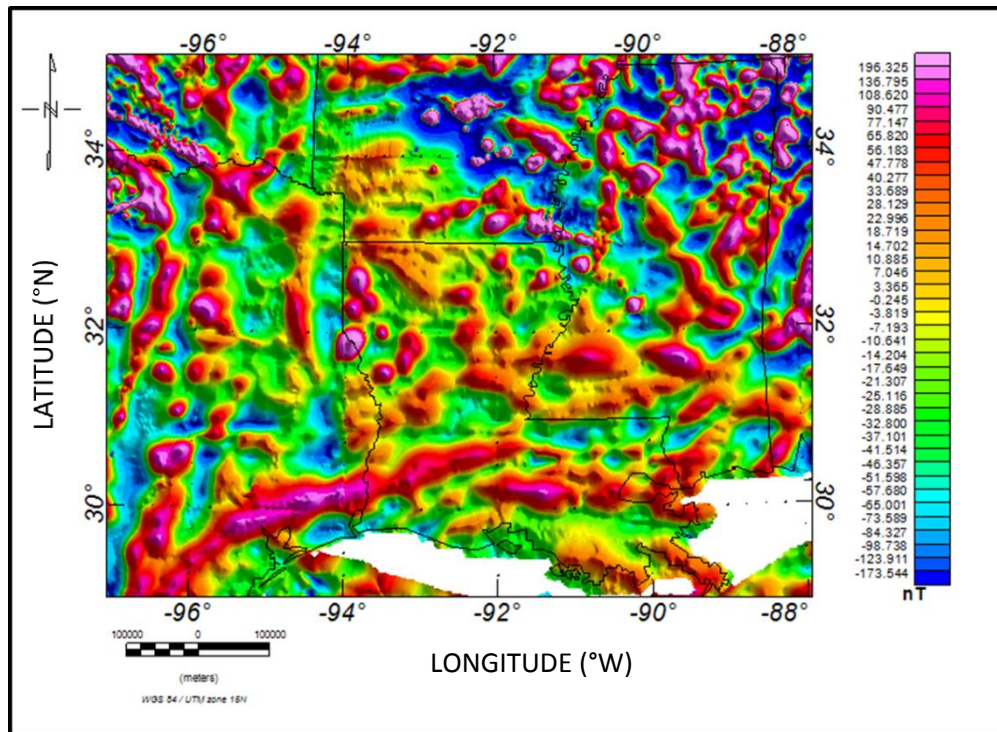
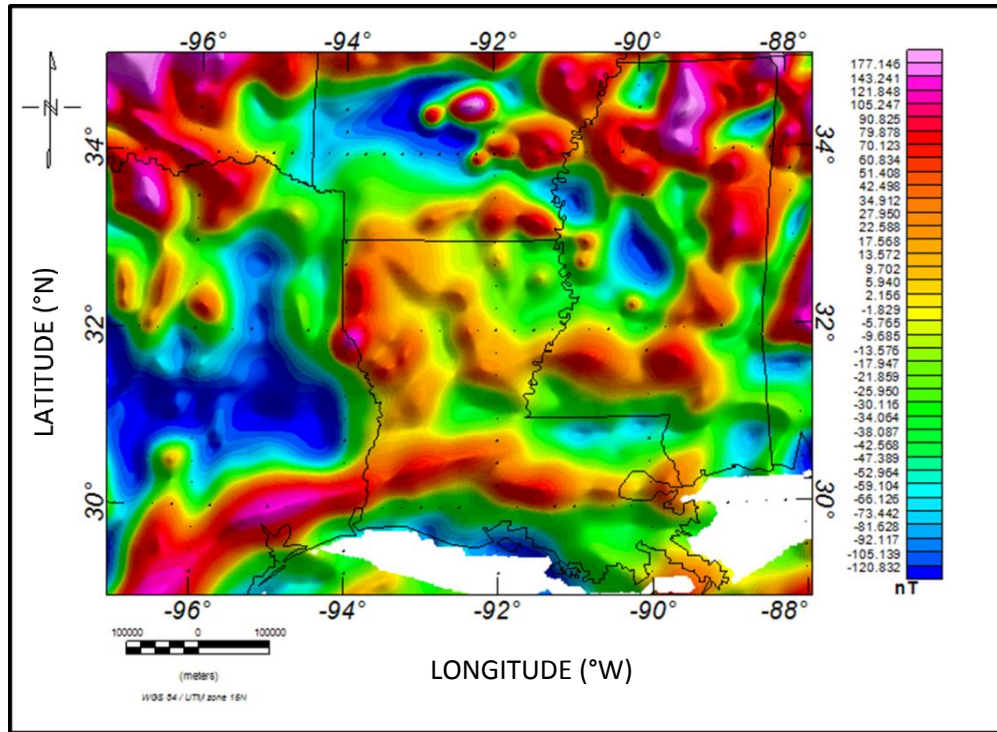


Figure 5.6: A) 15 km upward continuation reduced – to – pole magnetic intensity map B) 15 km upward continuation reduced – to – pole magnetic intensity residual map.

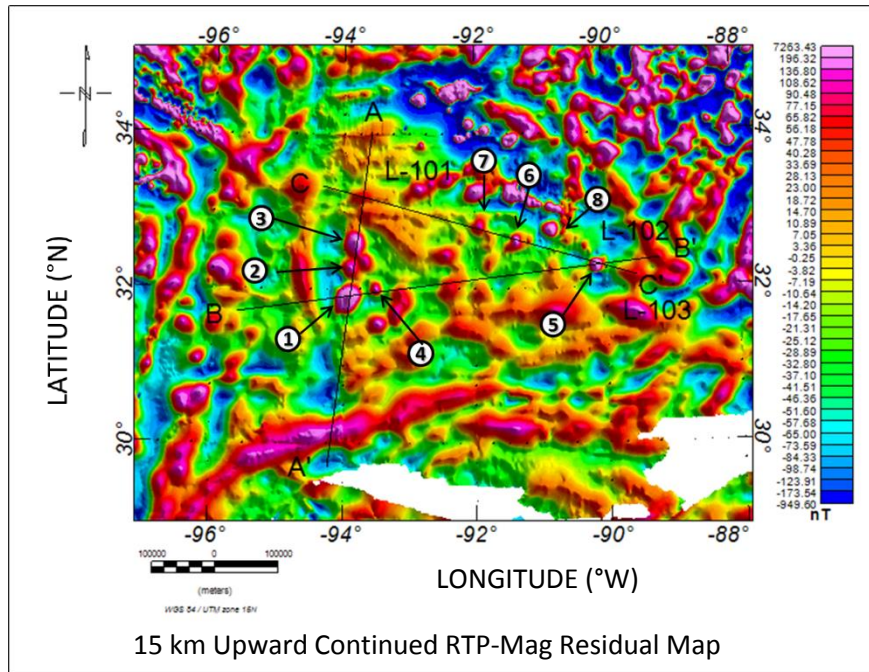
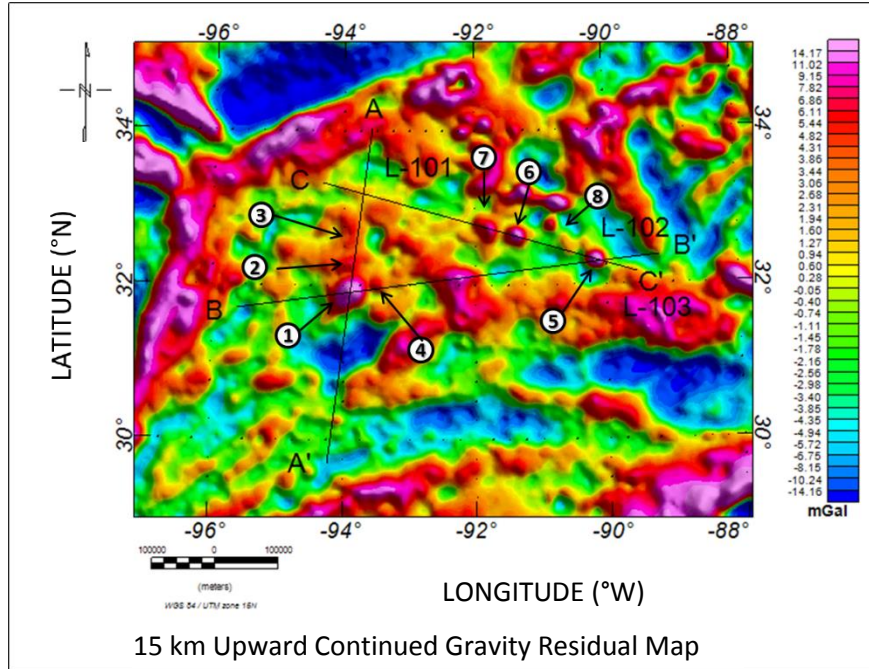


Figure 5.7: Residual Maps of 15 km upward magnetic and gravity data. Assigned numbers are interpreted anomalies over Sabine, Monroe and Jackson Uplifts. Black solid lines show the locations of 2-D gravity models.

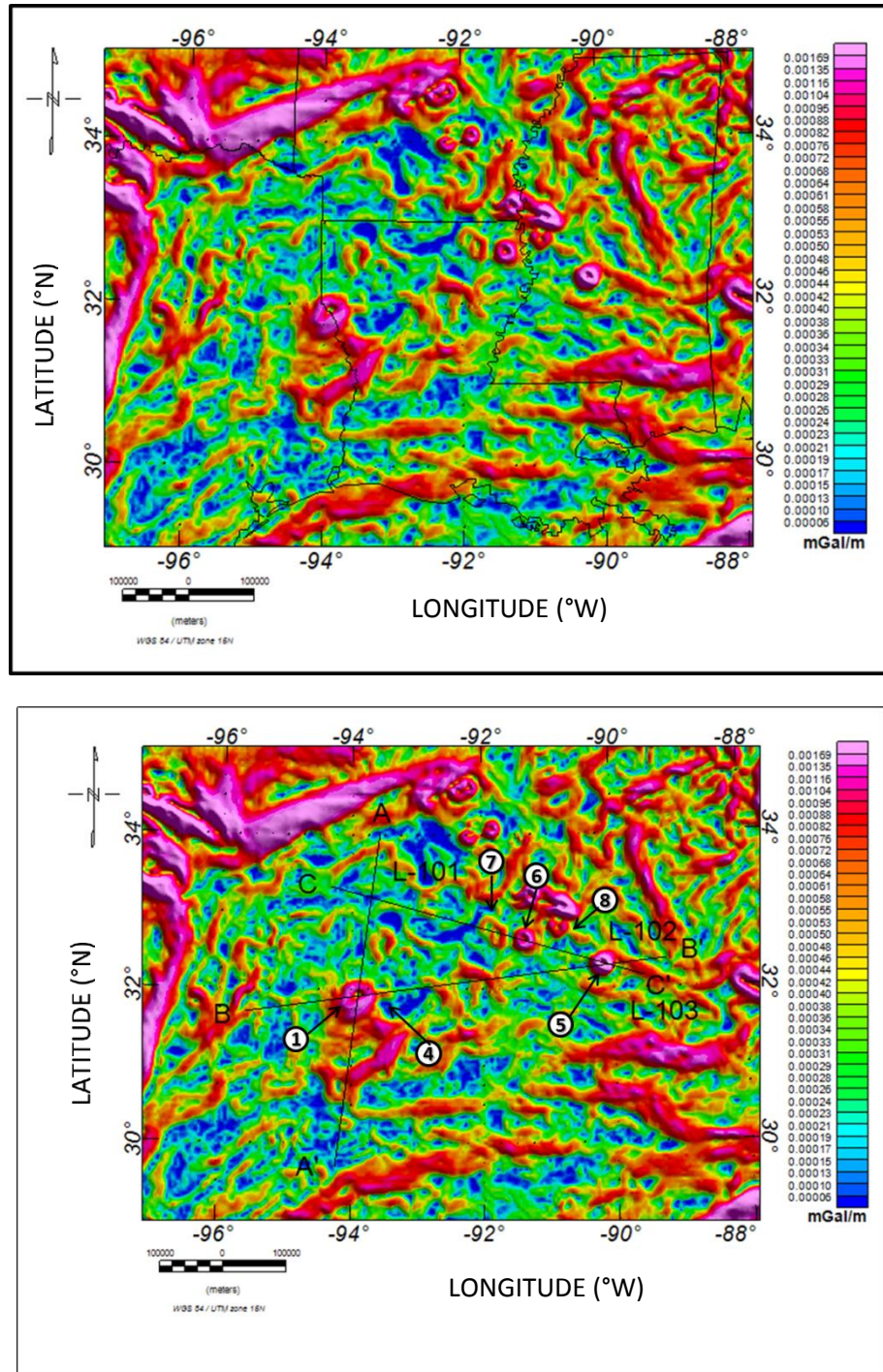


Figure 5.8: Total horizontal gradient (THG) of Bouguer Gravity Data. Assigned numbers are interpreted anomalies over Sabine, Monroe and Jackson Uplifts. Black solid lines show the locations of 2-D gravity models.

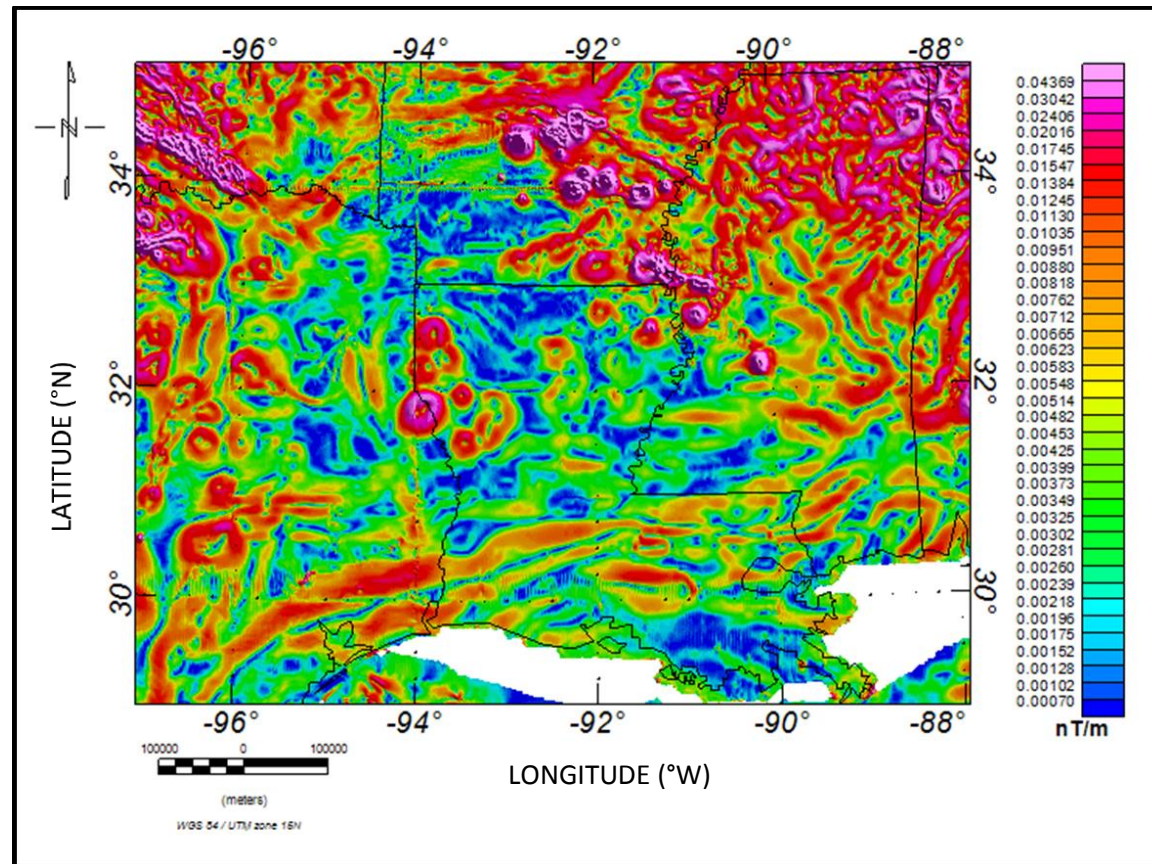


Figure 5.9: Total horizontal gradient (THG) of Reduced – to – pole magnetic intensity

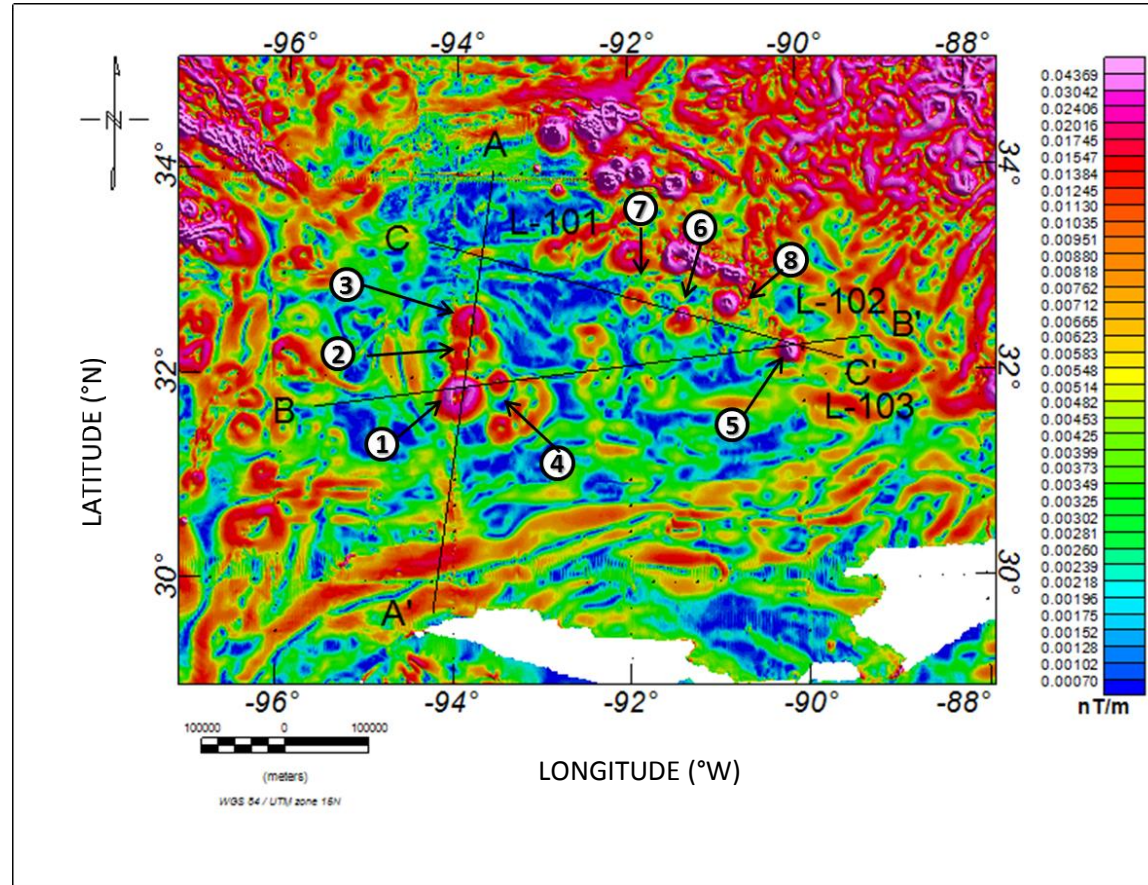


Figure 5.10: Total horizontal gradient (THG) of Reduced – to – pole magnetic intensity with interpreted anomalies of Sabine, Monroe and Jackson Uplifts. Black solid lines show the locations of 2-D gravity models.

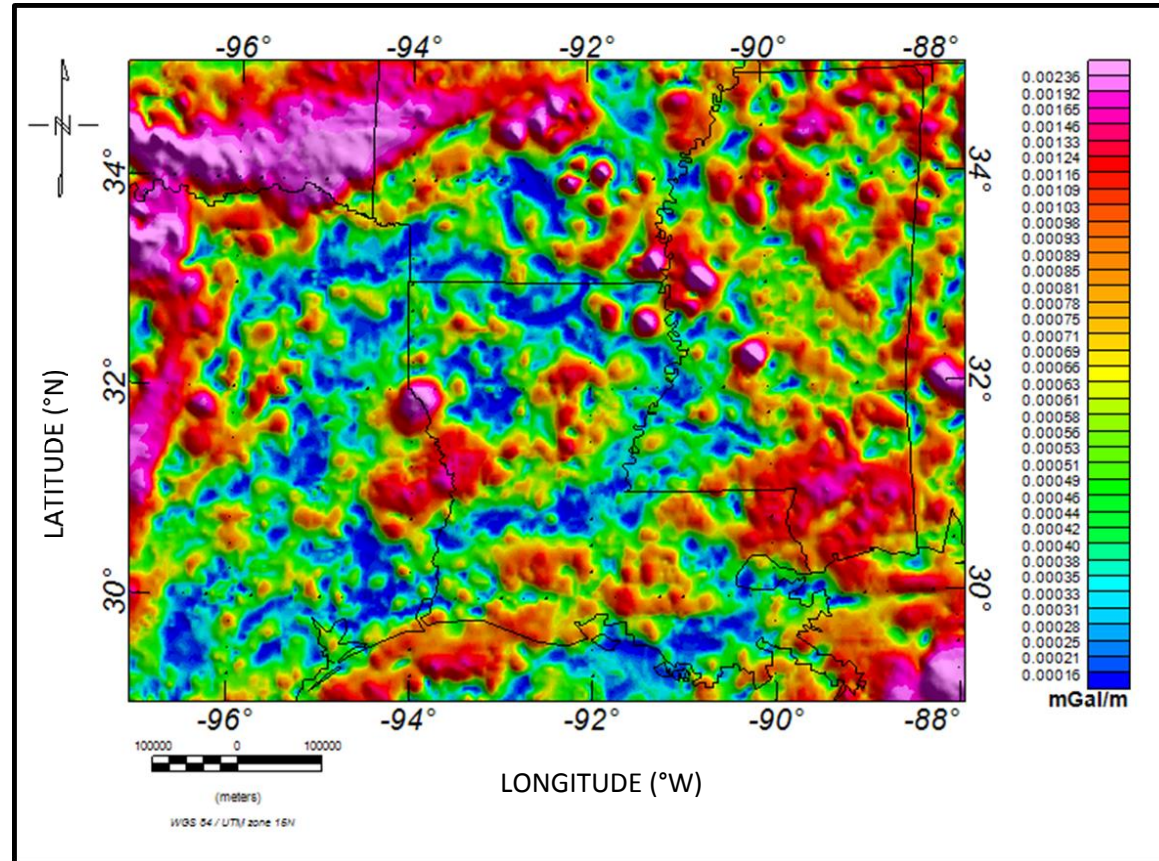


Figure 5.11: Analytic Signal of Bouguer gravity data

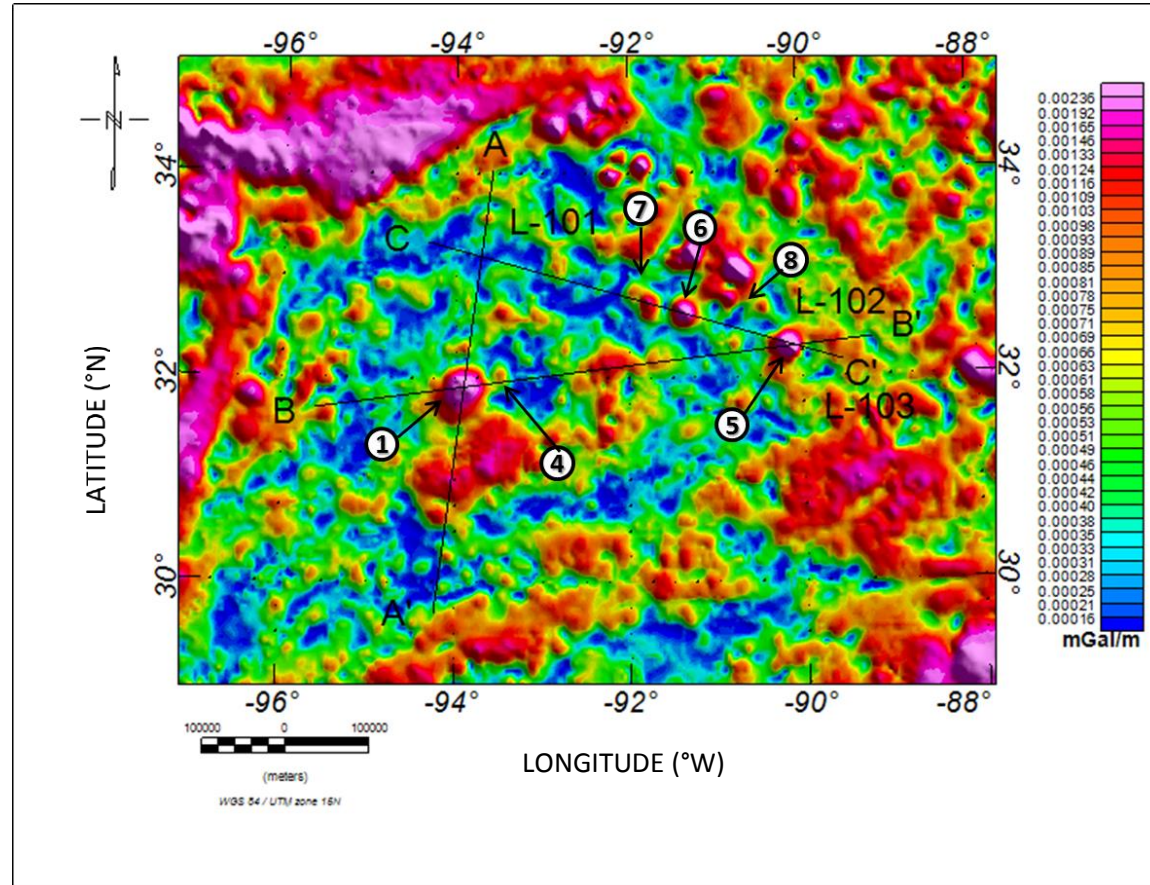


Figure 5.12: 2-D Gravity model locations through the interpreted anomalies of Sabine, Monroe and Jackson Uplifts on the analytic signal map of Gravity data.

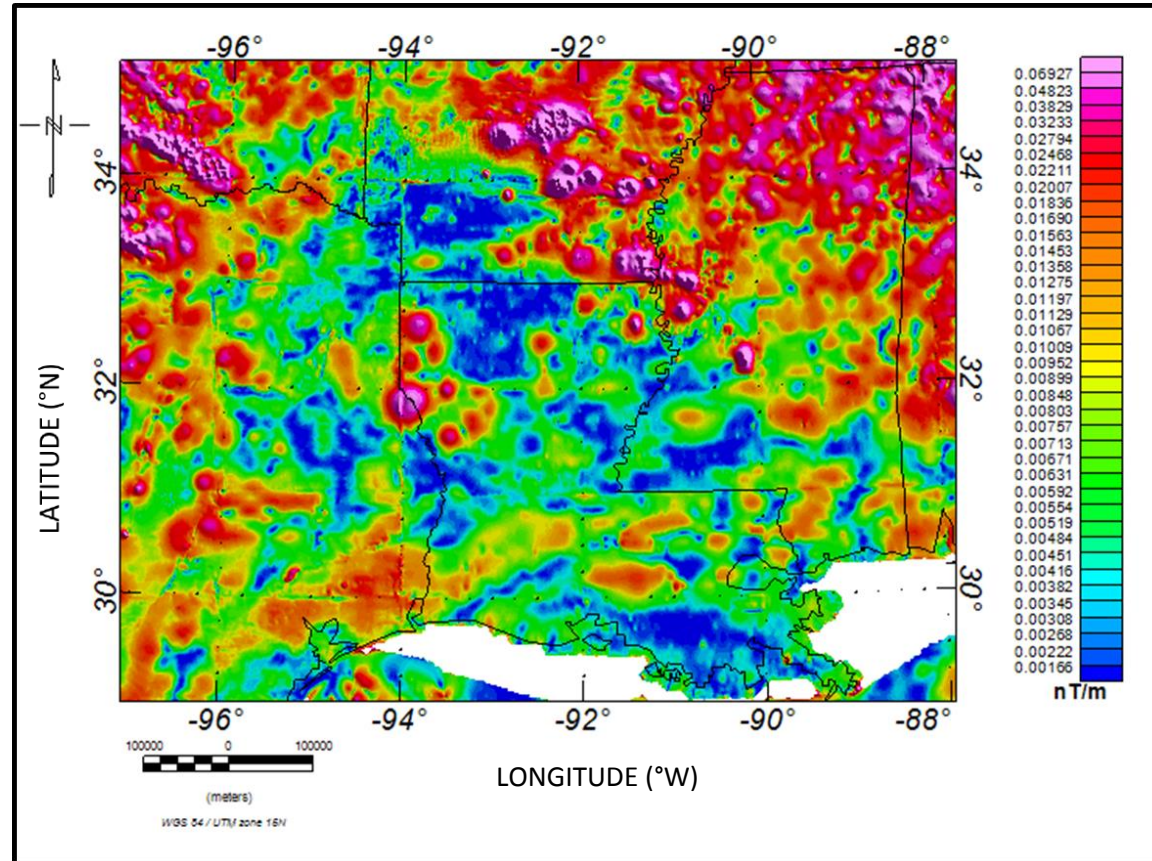


Figure 5.13: Analytic signal of reduced – to – pole magnetic intensity data

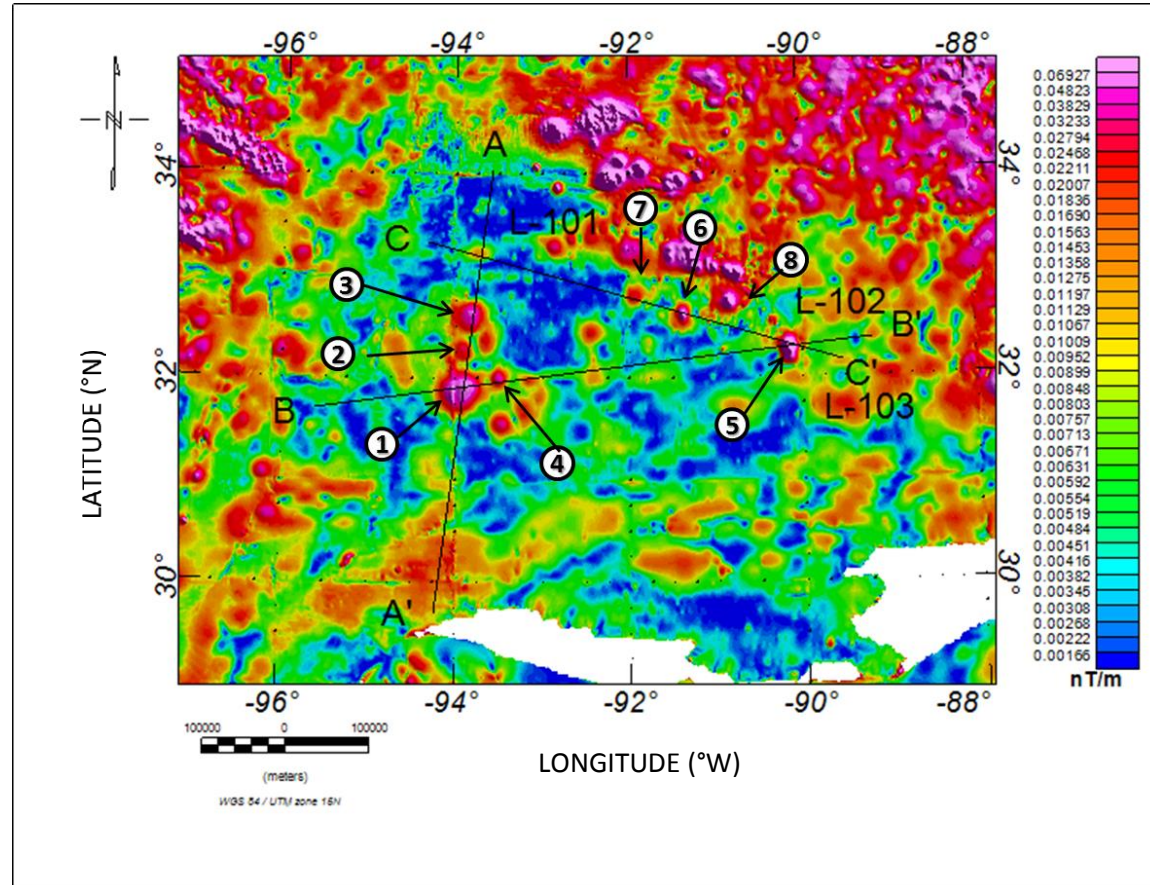


Figure 5.14: 2-D Gravity model locations through the interpreted anomalies of Sabine, Monroe and Jackson Uplifts on the analytic signal map of magnetic data.

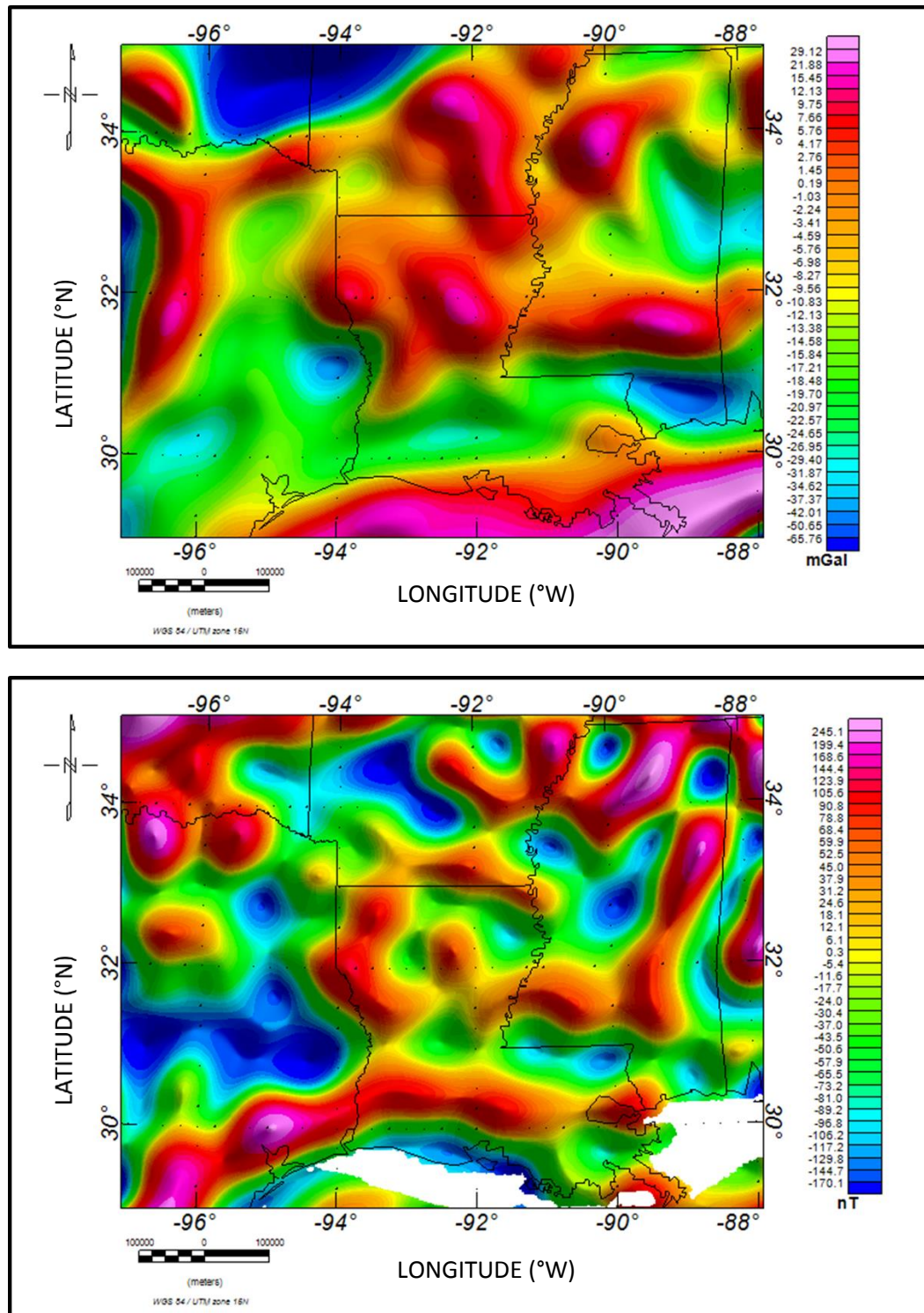


Figure 5.15: 100 km low pass of a) Bouguer gravity data; b) reduced – to – pole magnetic intensity data.

Analytic signal maps produces gravity and magnetic enhancement maps to show clear images of boundaries of geologically anomalous source bodies. Analytic signal maps of the area (Figure 5.11. through Figure 5.14) give noticeable anomalies over Sabine Uplift, Monroe Uplift and Jackson Dome. Four circular distinct isolated anomalies over Monroe Uplift locate the possible Cretaceous volcanism and subsurface intrusive rocks. Buried volcano beneath Jackson Dome and intrusive igneous rocks of Sabine area also give similar anomalies with the anomalies located over Monroe Uplift. These gravity anomalies are roughly circular. Similar anomalies over the magnetic analytic signal map correlate with the anomalies in the gravity analytic signal map.

### **5.3. 2-D GRAVITY MODELS**

Three profiles, ranging from 470 to 650 km – long, were created through Sabine Uplift, Monroe Uplift and Jackson Dome. Figure 5.16 shows the locations of the profiles on Bouguer gravity map. These transects (AA`, BB`, and CC`) were developed and modeled by using Geosoft – Oasis Montaj and GM-SYS software.

Profile locations were chosen:

- Along Sabine Uplift, Monroe Uplift, Jackson Dome and other possible structures
- Where we have maximum control point data
- Through the possible locations where Cretaceous igneous activity had occurred
- To see the crustal variations to North – South and East – West

In order to construct measured gravity values of each profile, gravity data was sampled with 1000 m station spacing. Surface conditions of each profile were also sampled from topographic map with 1000 m spacing to integrate them to the models. Gtopo 30, which is a global onshore digital elevation model with a horizontal grid spacing of 30 arcs – seconds (approximately 900m), was used for topography of the area (Figure 5.18).

All models are composed of 9 layers as below:

- Unconsolidated Sediments
- Salt
- Cenozoic Sedimentary Rocks
- Cretaceous Sedimentary Rocks
- Pre – Cretaceous Sedimentary Rocks
- Igneous Rocks
- Upper Crust
- Lower Crust
- Upper Mantle

Color legend bar for the layers is shown on Figure 5.17.

All horizons of each model were designed to extend to the infinity in  $-x$  and  $+x$  directions to avoid edge effects.

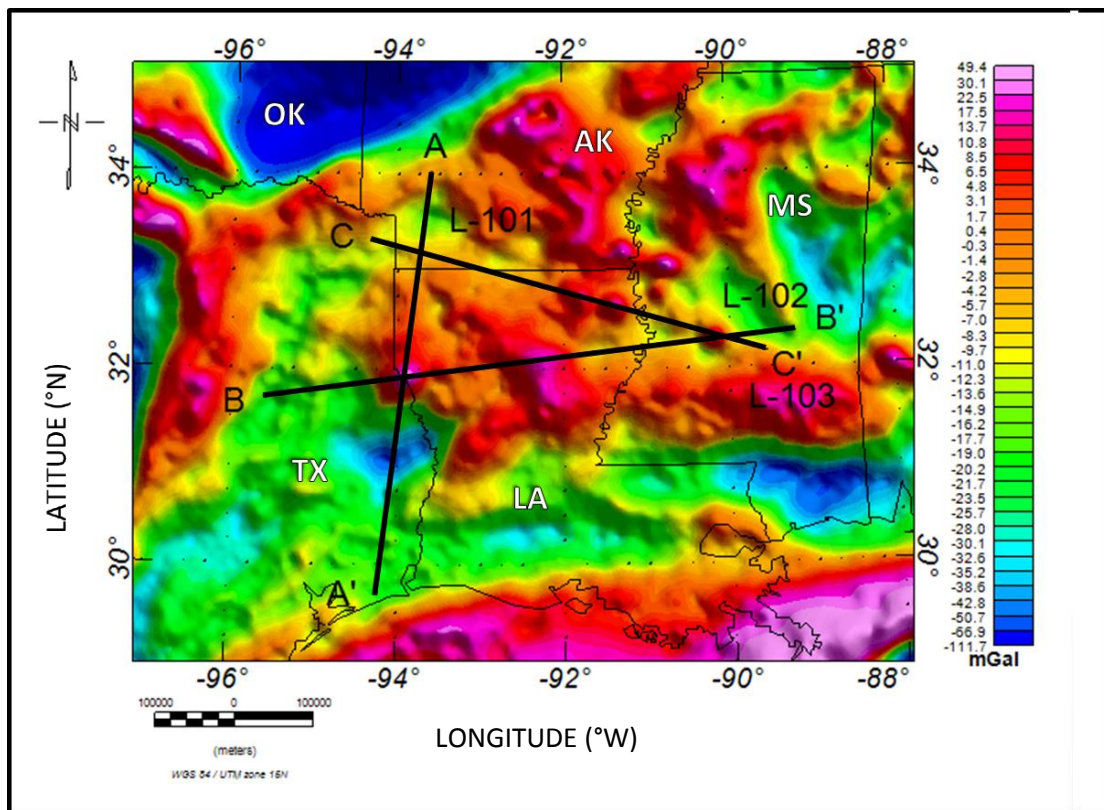


Figure 5.16: 2-D gravity model locations











Non-Mag		Unconsolidated Sediments – 2.1
Non-Mag		Louann Salt – 2.16
Non-Mag		Cenozoic Sedimentary Rocks (Mostly clastics) – 2.25
Non-Mag		Cretaceous Sedimentary Rocks (Clastics+Carbonates) – 2.5
Non-Mag		Pre-Cretaceous Sedimentary Rocks (Clastics) – 2.5
Magnetic		Igneous Rocks 1 – Mafic – 2.8
Magnetic		Igneous Rocks 2 – Intermediate – 2.7
Magnetic		Upper Crust – 2.7
Non-Mag		Lower Crust – 3.0
Non-Mag		Upper Mantle – 3.3

Figure 5.17: Properties of 2-D gravity model layers

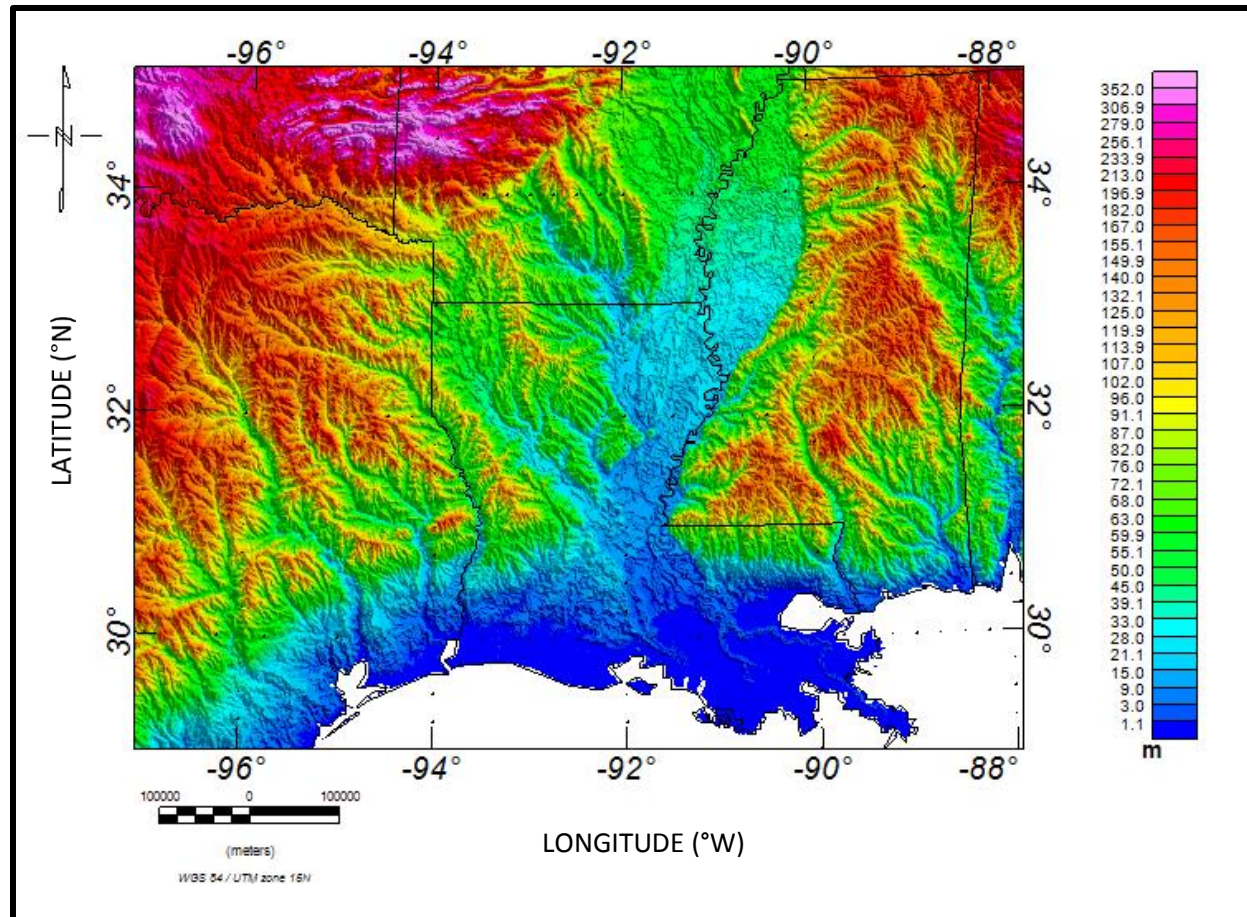


Figure 5.18: Topography of the area (GTOPO 30 digital elevation model was used to generate the map)

### **5.3.1. Model 1: L-101 (AA`)**

N-S, L-101 model was created roughly North – South with an azimuth of 187°. The transect extends from southwestern part of Arkansas, through northwest Louisiana and all the way south to the Texas coast. This model is constrained by seismic refraction observations for crustal structures (Hales et. al, 1970; Sawyer et. al, 1991); deep well data for sedimentary thickness (Rogers, 1968); regional cross – sections from well logs for basement structure and sedimentary thicknesses (Nichols et. al, 1966).

N-S, L-101 profile through Sabine Uplift was modeled to examine the crustal and basin architecture of the area. Alternative models were constructed to test different possible structures which might produce anomalies beneath the study area. One of the main focuses of the models is to clarify the high gravity and magnetic anomalies on the Sabine Uplift. Our geologically preferred model for L-101 (Figure 5.19 and 5.20) represents crustal intrusions which cause the gravity and magnetic maxima beneath the Sabine Uplift. It has a good fit with the data which constraints our models. The depth of basement varies from north to south. Main trends of basement depths are 7.0 to 7.5 km on the northern part of the profile, around 6.0 km beneath Sabine Uplift, 8.0 to 8.5 km in the southern part of the uplift, and up to 11 – 11.5 km beneath Texas Coastal Plain. Although there is a relatively shallower crust beneath Sabine Uplift, it is not enough to produce the gravity and magnetic maximas. Crustal structures produce the broad gravity high anomalies whereas short wavelength high amplitude gravity and magnetic anomalies are produced by igneous bodies. Crustal structure of the area varies to the north and south.

Different crustal thicknesses possibly result of differential extension during rifting. The thickest crust in the model is present beneath Sabine Uplift and the area located southern part of the uplift where broad gravity minima exist. From N to S, when we are getting closer to coastal areas; crustal thickness is decreasing dramatically which is an evidence of oceanic crust further in the south. This led a dramatic increase in the sedimentary thicknesses. Total sedimentary rock thicknesses are up to 7 km in the northern part of the profile whereas it goes up to 11 km in the southern part. Crustal extension which is followed by a passive margin subsidence should lead this change in the southern part of the profile.

The model shown in Figure 5.19 is our preferred model because of several reasons: 1) qualitative interpretations of the data and filter maps suggest an occurrence of igneous body; 2) igneous rocks give the best fit during the forward modeling by considering both gravity and magnetic anomalies; 3) pronounced circular gravity and magnetic anomalies in enhancement maps coincide; 4) some geophysical and geological indicators have been interpreted as magmatism in the previous studies.

Alternative models for the profile will be discussed in the next chapter.

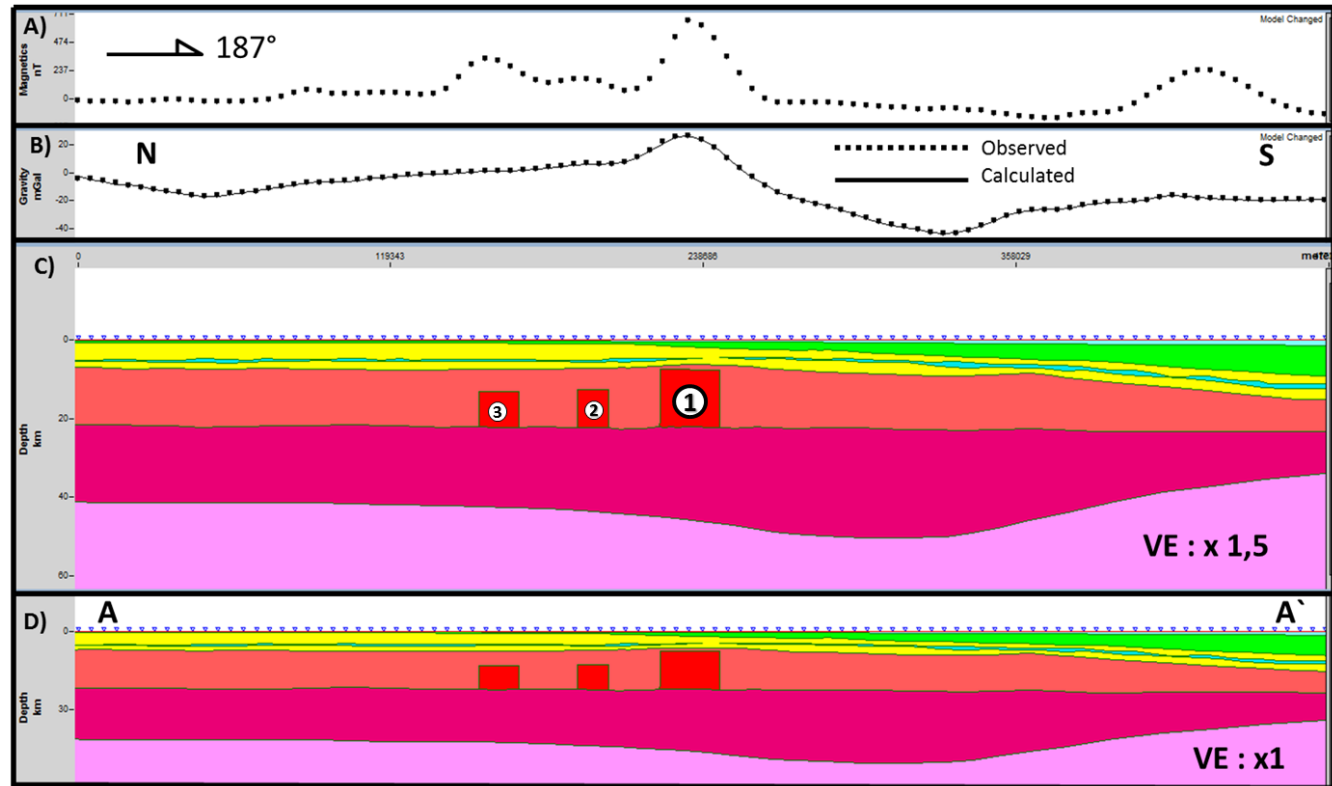


Figure 5.19: Crustal view of preferred 2-D gravity model for profile L-101 (see figure 5.17 for legend); A) Observed reduced – to – pole magnetic anomalies; B) Observed and calculated gravity values in mGal; C) 1,5 times vertically exaggerated version of final model; D) No vertical exaggeration. Locations of the assigned numbers are shown in anomaly and filter maps.

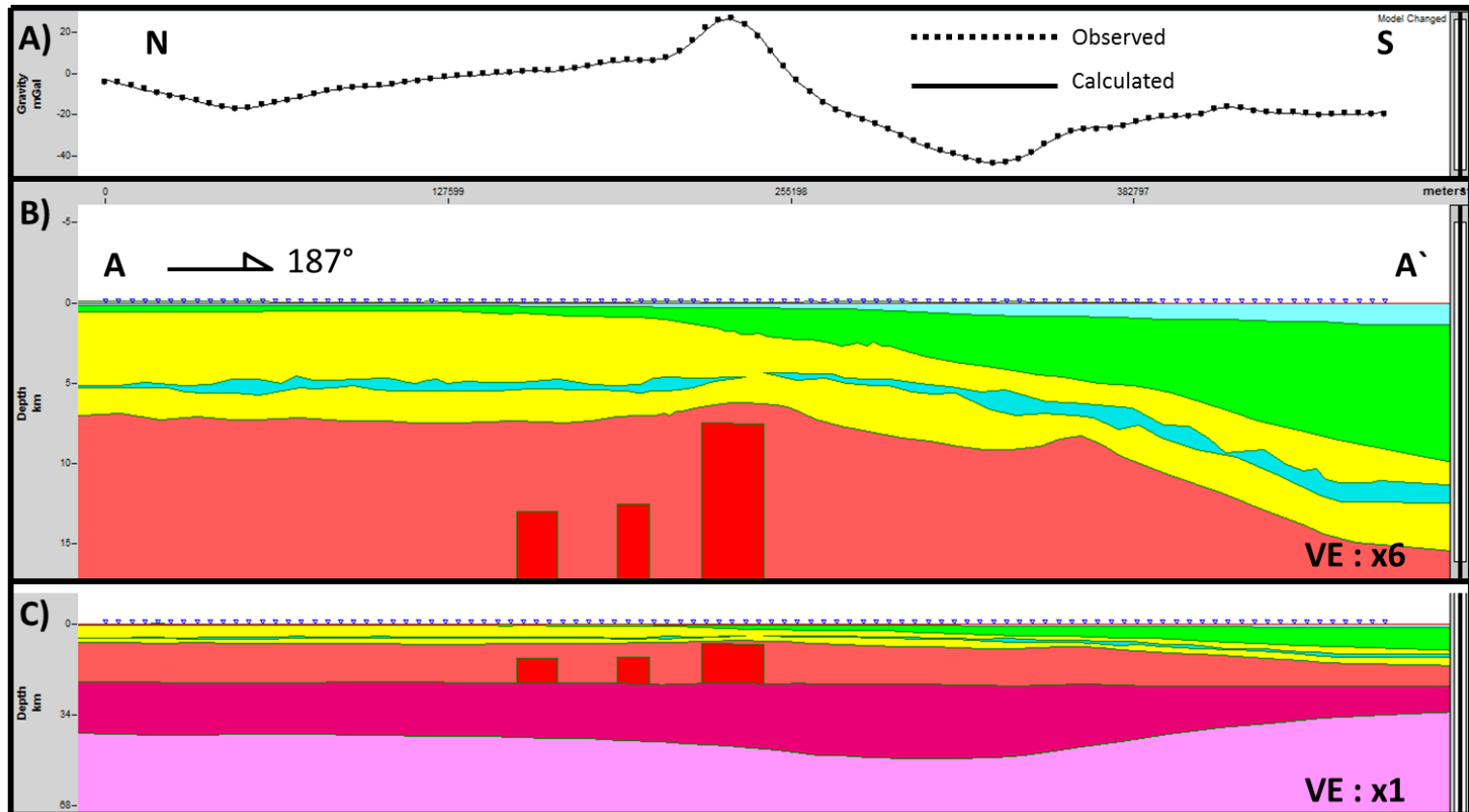


Figure 5.20: Basin view of preferred 2-D gravity model for profile L-101 (see figure 5.11 for legend); A) Observed and calculated gravity values in mGal; B) Basin view of model – 6 times vertically exaggerated C) No vertical exaggeration.

### **5.3.2. Model 2: L-102 (BB`)**

L-102 model was created roughly East - West with an azimuth of 82° (Figure 5.16). The transect extents from eastern part of East Texas Salt Basin, through Sabine Uplift, North Louisiana Salt Basin and La Salle Arch to the eastern part of Jackson Dome. This model is constrained by seismic refraction observations for crustal structures of east Texas and west Mississippi (Worzel and Watkins, 1973; Hales et. al, 1970); deep well data for sedimentary thickness from Carthage Field, TX (Rogers, 1968); regional cross – sections by using well logs for basement structure and sedimentary thicknesses of eastern Texas and western Louisiana (Nichols et. al, 1966); and geological cross – section by using well and geophysical data for sedimentary thicknesses and buried volcano of Jackson Dome vicinity (Dockery, 1997). This profile has an intersection with model 1 (L-101) where there is an anomaly of gravity and magnetic maxima. The model was also constrained by first model. Briefly, this model is well constrained by available data in the west and east but it has sparse data on the central part of the profile. However, there are also studies around La Salle Arch, considered during modeling stage, that crustal and basin structures of the area have been discussed (Lawless and Hart, 1990).

The main goals of this model are to test the structure of crust and basin beneath the profile. Possible igneous bodies, which have been discussed in the previous studies, (Byerly, 1991; Kidwell, 1951; Moody, 1949; Griffin, 2010; Ewing, 2009; Baksi, 1997; Nichols et al., 1968) were also modeled to get the best fit between the observed and

theoretically calculated gravity anomalies. In addition, we had a chance to double check the crustal structure and igneous rocks of Sabine Uplift where two models are intersected.

The gravity model of profile BB` (Figure 5.21 and Figure 5.22) suggests that relatively thick and shallow crust under east Texas and west Louisiana produce broad gravity high anomalies of the area. Gravity maximas produced by Sabine Uplift and La Salle Arch are caused by shallow crust. In addition, intruded igneous rocks of Sabine Uplift produce short wavelength gravity and magnetic anomalies (up to 800 nT) that superimpose the regional high. East Texas Salt Basin is located on the westernmost part of the model and the anomalies on the area are characterized by broad gravity low which is superimposed by several short wavelength anomalies. The crust beneath this area is relatively more attenuated (thinned). Regional gravity low anomaly is produced by thick sedimentary rocks including salt layer. Short wavelength gravity anomalies correlate where salt layer is thickening.

Cenozoic and Mesozoic sedimentary rocks between La Salle Arch and Jackson Dome are thickening. This part of the model is going across the northern edge of Mississippi Salt Basin where basement is deep. This area produces roughly flat gravity anomalies without any major change in the trend until Jackson Dome.

There is a major change in the gravity and magnetic anomalies where Jackson Dome is located. The buried volcano of Jackson Dome (Baksi, 1997; Saunders and Harrelson, 1992; Ewing, 2009; Ewing, 2001; Byerly, 1991) produces an isolated short wavelength, high amplitude gravity and magnetic anomaly. Gravity and magnetic anomalies vary up

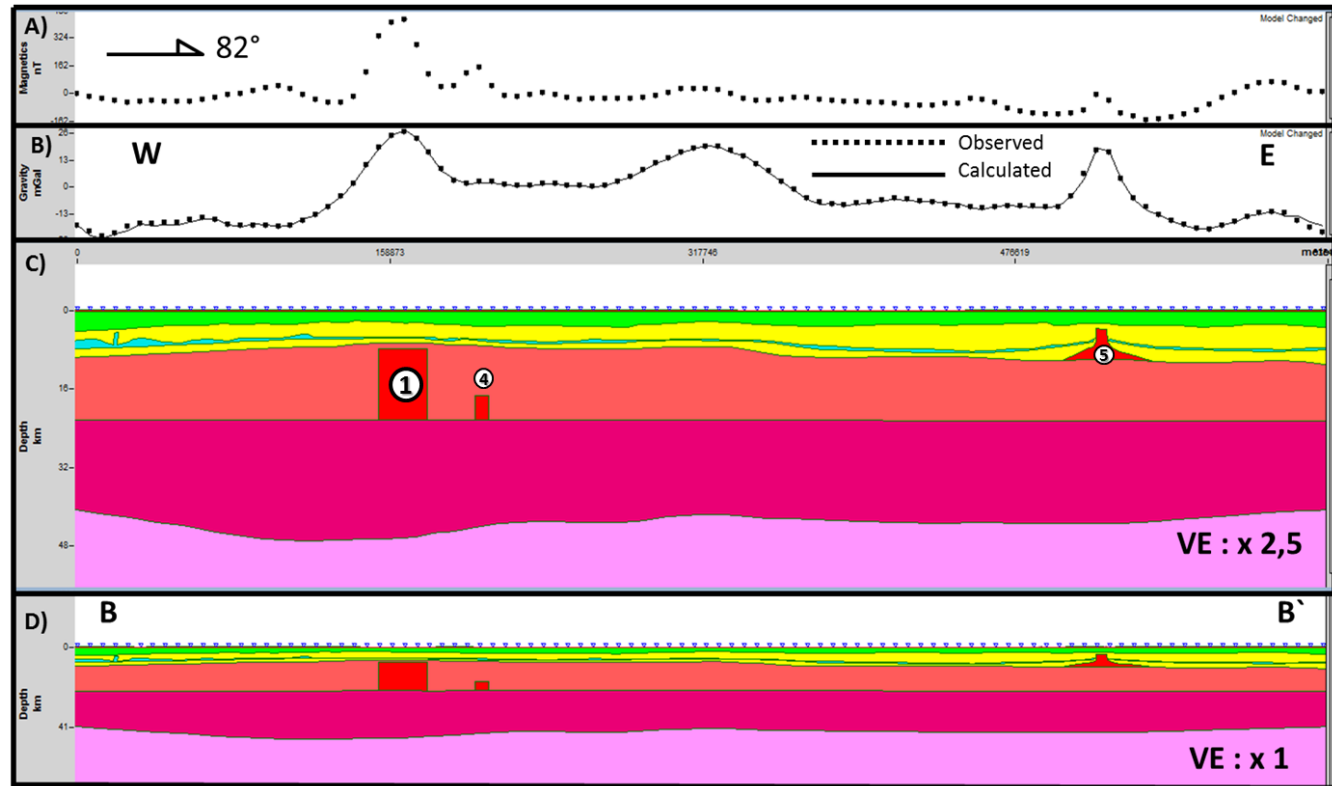


Figure 5.21: Crustal view of preferred 2-D gravity model for profile L-102 (see figure 5.17 for legend); A) Observed reduced – to – pole magnetic anomalies; B) Observed and calculated gravity values in mGal; C) 2,5 times vertically exaggerated version of final model; D) No vertical exaggeration. Locations of the assigned numbers are shown in anomaly and filter maps.

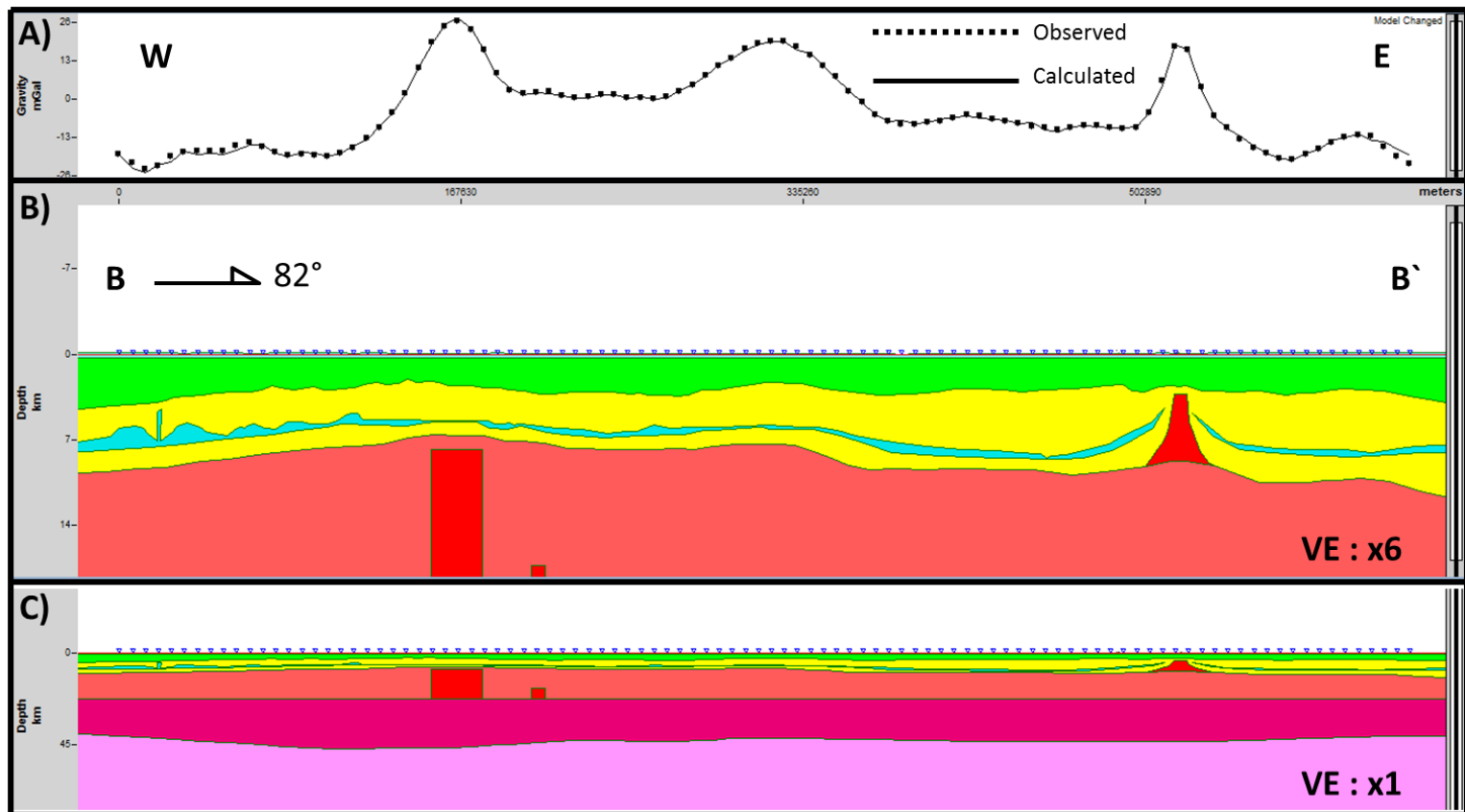


Figure 5.22: Basin view of preferred 2-D gravity model for profile L-102 (see figure 5.11 for legend); A) Observed and calculated gravity values in mGal; B) Basin view of model – 6 times vertically exaggerated; C) No vertical exaggeration.

to 25 mGal and 850 nT, respectively. Shape and dimensions of igneous bodies, where we do not have control points to constraint, were assumed to have regular shapes as in the first model. However, shape and dimensions of Jackson Volcano were integrated from a detailed section of the area by Dockery (1997) (Figure 5.23). Calculated anomalies produced by integrated structure and igneous rocks of Jackson Dome were fitted well with the observed gravity anomalies.

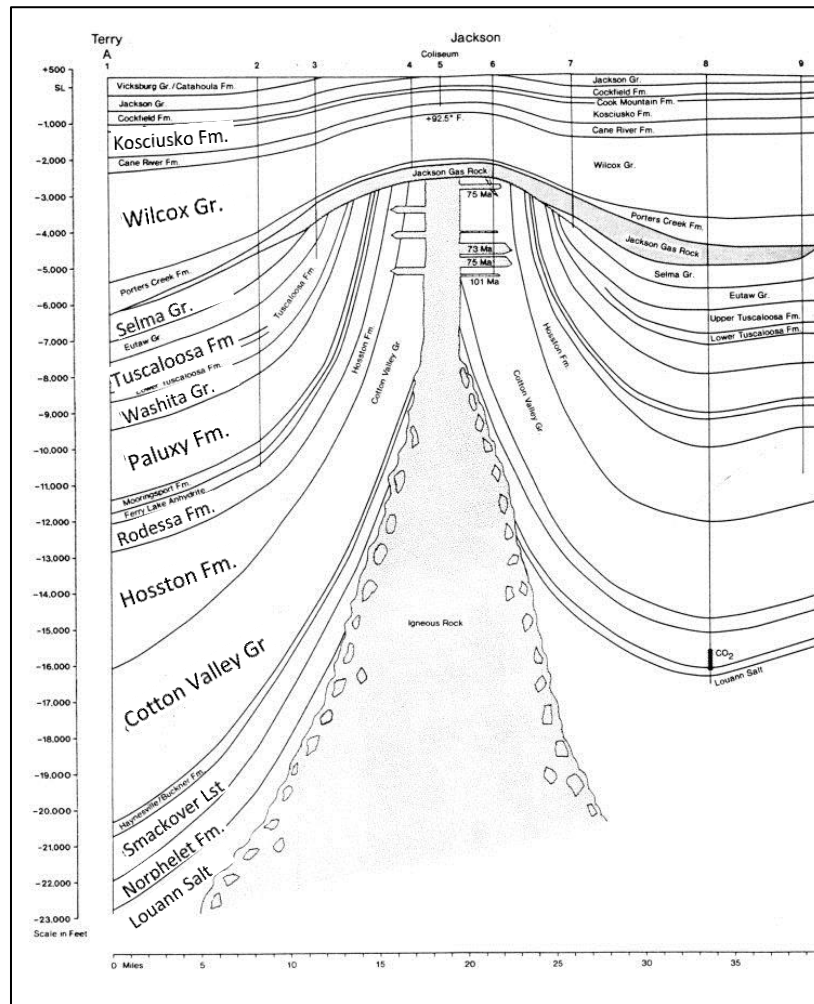


Figure 5.23: Cross – section through Jackson Dome, constructed by well data (Dockery, 1997)

### **5.3.3. Model 3: L-103 (CC`)**

L-103 profile was created roughly Northwest - Southeast with an azimuth of  $115^{\circ}$  (Figure 5.16). The transect extends from northeastern edge of Texas through north - central Louisiana – Arkansas boundary to southern part of Monroe Uplift and it is over after Jackson Dome. This model is the only one which is not well constrained by seismic data due to lack of available data is around this profile. It is constrained by two edges of the profile by (Worzel and Watkins, 1973; Sawyer et. al, 1991) refraction data. However, the results of other two models (L-101; L-102) were integrated to this model where they intersect. Shape and dimensions of Jackson Volcano were integrated from a detailed section of the area by Dockery (1997) (Figure 5.23). Calculated anomalies produced by integrated structure and igneous rocks of Jackson Dome were again fitted well with the observed gravity anomalies which verifies that model parameters are acceptable.

The main focus of the model is to test and locate subsurface Mesozoic igneous rocks of the area. Igneous rocks of Monroe Uplift and Jackson Dome were modeled through the profile. Previously modeled buried volcano of Jackson Dome was modeled again and the theoretically calculated data has a good fit with observed gravity anomalies (Figure 5.24). Since we do not have control points or previous studies about igneous bodies of Monroe Uplift, they are modeled as in regular shapes conceptually to the specified locations (Figure 5.24 and 5.25). Shape and dimensions of the igneous bodies vary at the subsurface.

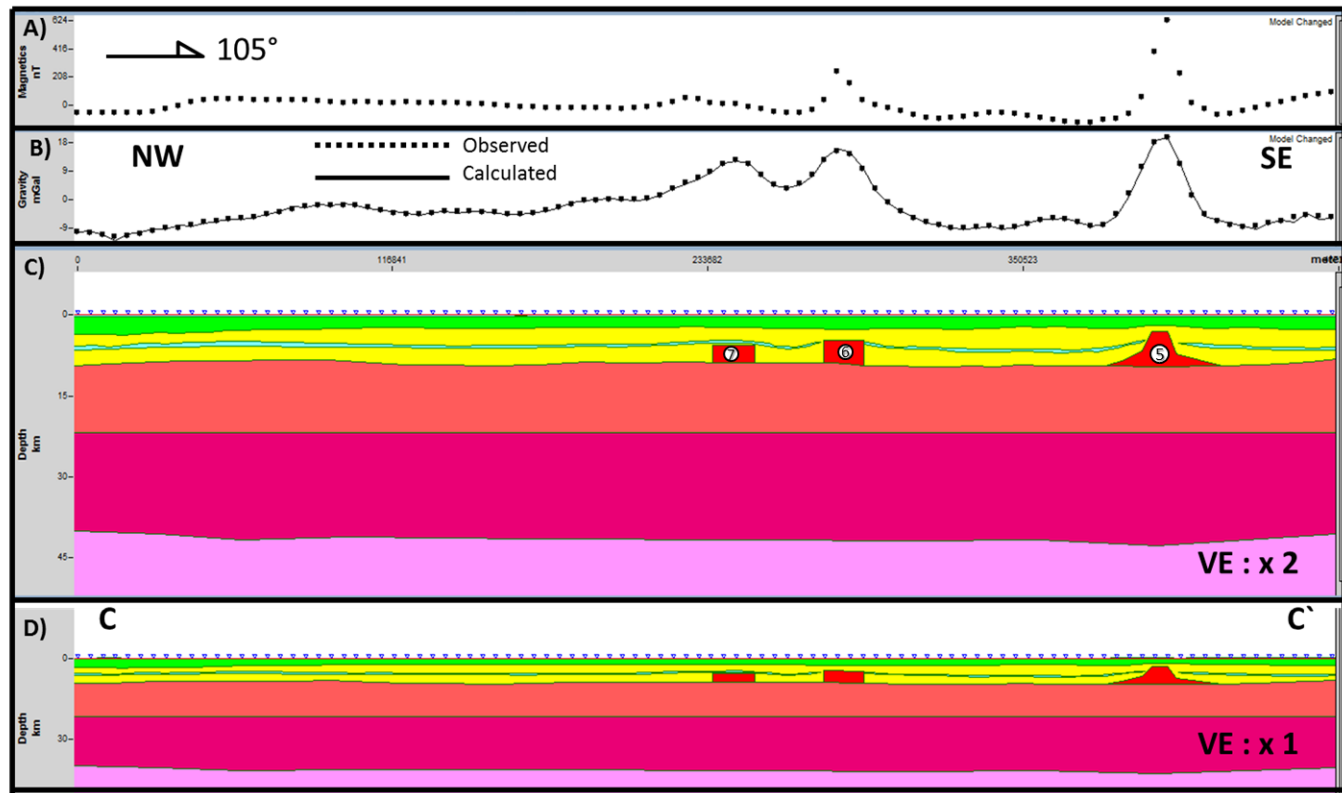


Figure 5.24: Crustal view of preferred 2-D gravity model for profile L-103 (see figure 5.17 for legend); A) Observed reduced – to – pole magnetic anomalies; B) Observed and calculated gravity values in mGal; C) 2 times vertically exaggerated version of final model; D) No vertical exaggeration. Locations of the assigned numbers are shown in anomaly and filter maps.

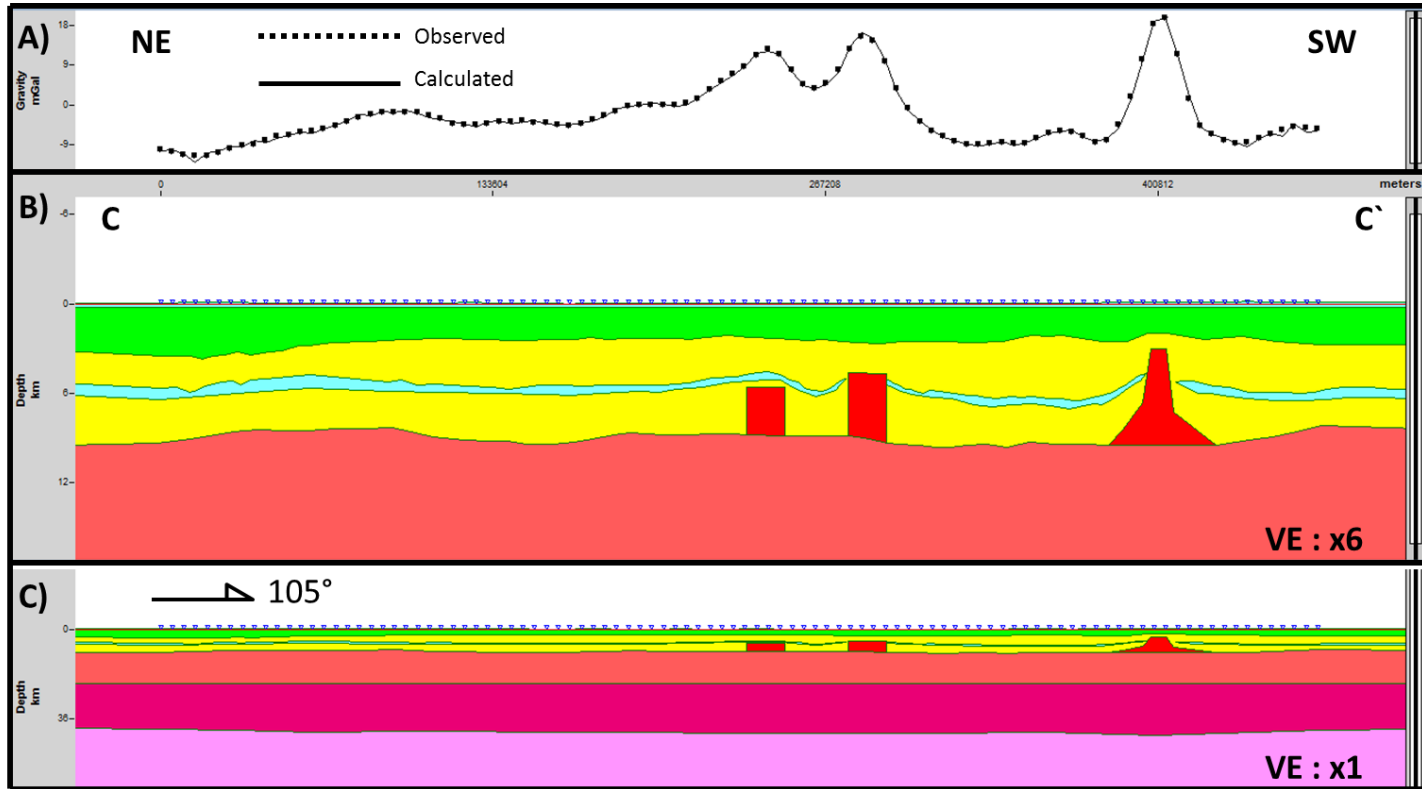


Figure 5.25: Basin view of preferred 2-D gravity model for profile L-103 (see figure 5.11 for legend); A) Observed and calculated gravity values in mGal; B) Basin view of model – 6 times vertically exaggerated C) Crustal view – no vertical exaggeration.

#### **5.4. CRUSTAL THICKNESS, DEPTH TO MOHO AND DEPTH TO BASEMENT MAPS**

Crustal-thickness map, depth-to-Moho and depth-to-basement maps, shown in Figure 5.26 to Figure 5.28, were constructed by using the results of 2-D gravity models and interpretations of the data. The mapped area is limited by the coverage of 2 – D models. Models were sampled systematically and the areas between these lines were correlated with available data and interpretations.

Thickness of the crust beneath the mapped area varies between 26 and 41 km (Figure 5.26). The largest area from east Texas through north Louisiana to west Mississippi has a crustal thickness of 34 – 38 km. The thickest crust exists beneath southern part of Sabine Uplift and the outside of south Sabine Uplift with a thickness of 38 – 41 km. western part of East Texas Salt Basin and northern part of east Texas and west Louisiana coastal areas have a relatively thinner crust varying from 30 – 34 km. The thinnest crust, 26 to 30km, exists beneath the southern edge of model L-101.

Major Moho depth variation is from North to South (Figure 5.27). In the models, L – 102 and L – 103, there is not a major change in depth to Moho. There are only minor smooth changes in a large area. However, in the North – South model, L – 101, there is a sharp variation from Sabine Uplift to the south. First, Moho is deepening beneath the Sabine Uplift and south of this uplift, and then it is shallowing again in a short distance. In addition, the shallowest Moho exists in the southern edge of the area and around western

East Texas Salt Basin where the crust was most likely attenuated more during the rifting stages.

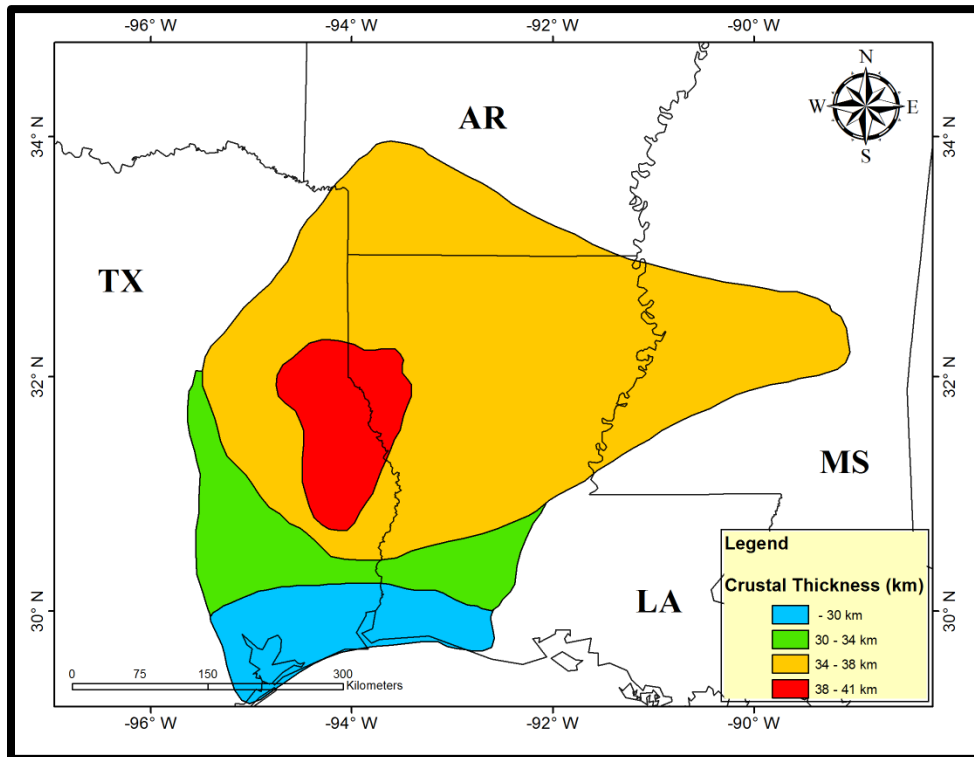


Figure 5.26: Crustal-Thickness Map of the area

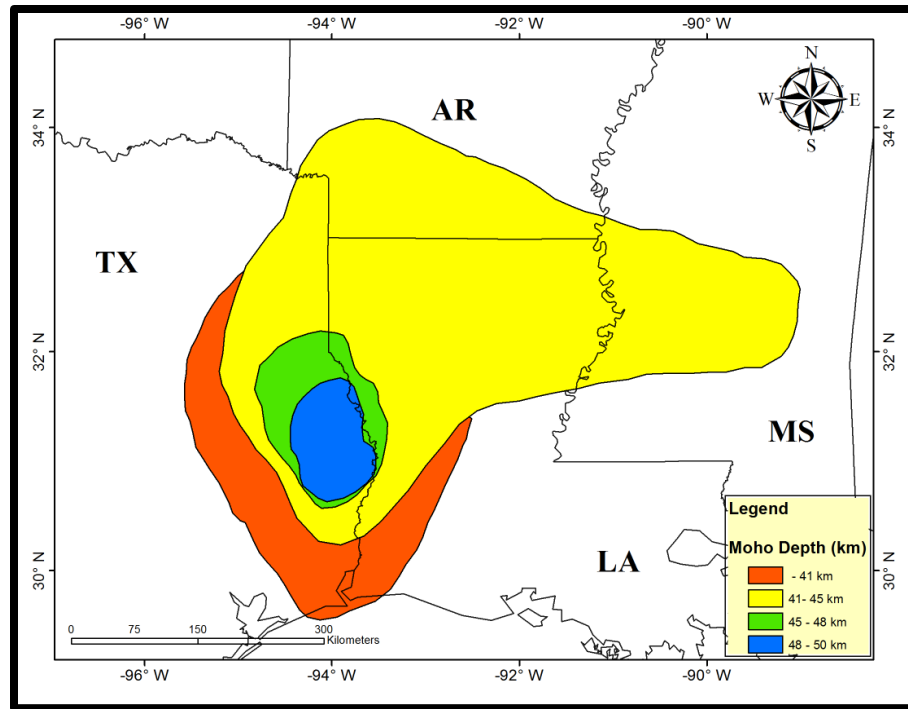


Figure 5.27: Depth-to-Moho Map

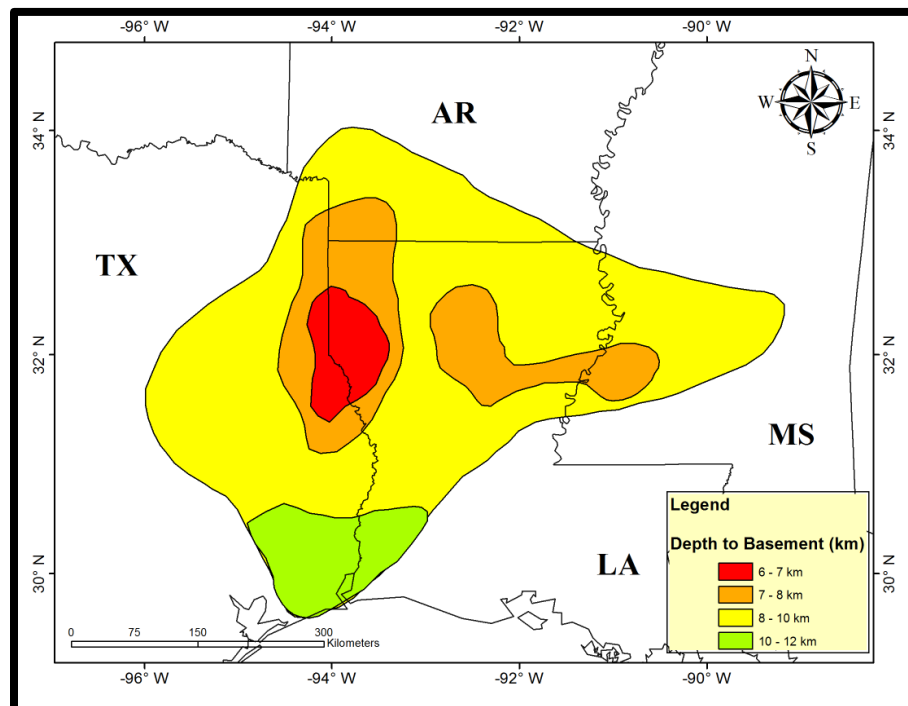


Figure 5.28: Depth-to-Basement Map

Basement depth of the mapped area is shallowing around Sabine Uplift and La Salle Arch. In the southern edge of the area, sedimentary thickness is increasing, in the other words, depth to basement values are increasing to the south up to 11 km (Figure 5.28). From west to east, basement depth values are undulating. Basins with deeper basement are located between high relief structures. From west to east, basement is deepening in East Texas Salt Basin, North Louisiana Salt Basin and northern edge of Mississippi Salt Basin on the contrary basement is shallowing in Sabine Uplift and La Salle Arch.

### **5.5. SUBSURFACE IGNEOUS ROCKS**

Figure 5.28 shows the subsurface igneous rocks of the area especially beneath the Sabine Uplift, Monroe Uplift and Jackson Dome.

Results of this study suggest that the existence of deep seated intrusive igneous bodies beneath the Sabine Uplift which have never reached the surface. Jackson Dome has a relatively very shallow buried volcano beneath the structure. The age of the youngest igneous rocks is latest Upper Cretaceous. The Monroe Uplift has largest volume of magma and greatest compositional diversity in the Northern Gulf of Mexico Basin. It contains both volcanic and intrusive igneous rocks. Igneous rocks that were interpreted during forward modeling in northeastern Louisiana and western Mississippi are interpreted as sub- volcanic and volcanic rocks, respectively. However, igneous rocks of the Monroe Uplift in the southern Arkansas were located by interpretation of potential field data and enhancement of this data.

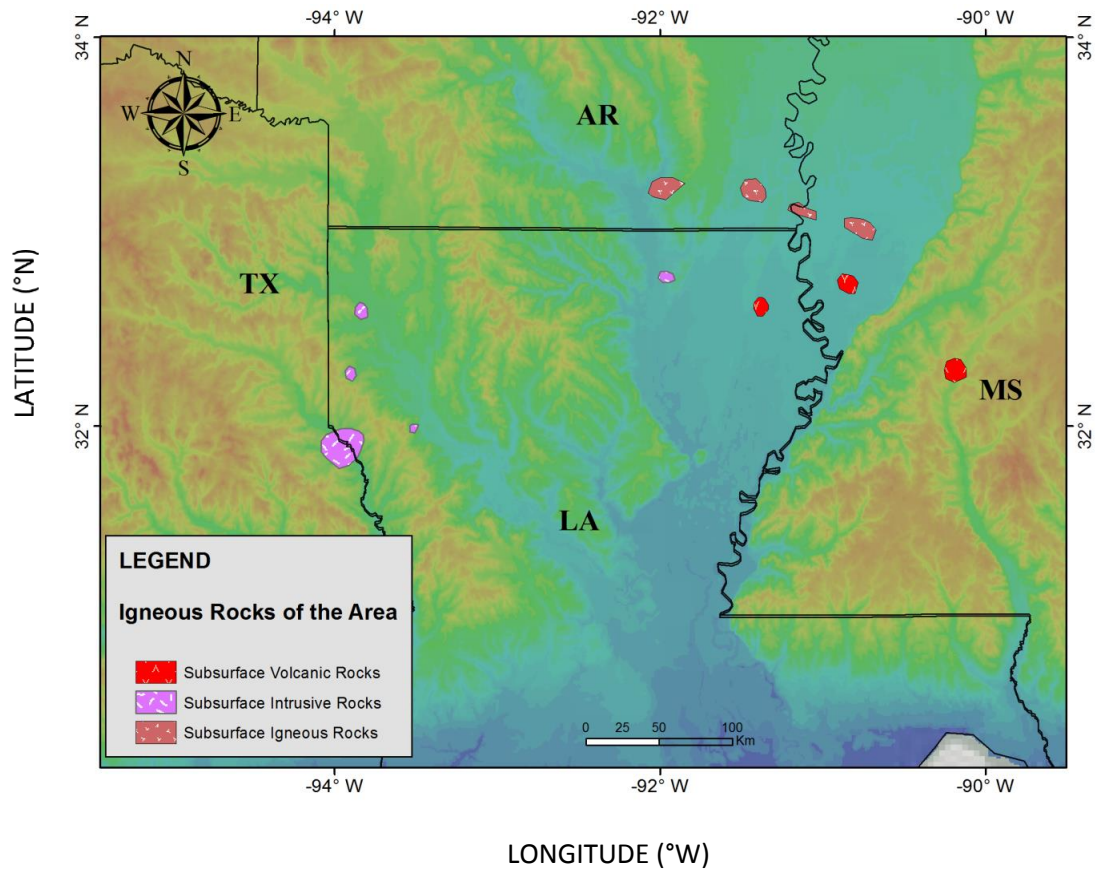


Figure 5.28: Subsurface Igneous Rocks of the Sabine Uplift, Monroe Uplift and Jackson Dome

## **CHAPTER VI**

### **DISCUSSION**

#### **6.1. INTERPRETATIONS AND MODELS**

Results from our study suggest that gravity anomalies in the study area are produced by variably extended crystalline crust, Moho topography, differential sedimentary thicknesses, salt structures, and igneous rocks. From East Texas Salt Basin in the west through Jackson Dome in the east, there are several structural highs and lows caused by variable crustal attenuation during the rifting stage. Relatively more extended thin crust, beneath the basins with thicker sedimentary rocks and salt, is represented by gravity low and long wavelength magnetic anomalies as we see in East Texas Salt Basin. On the other hand, structural highs with relatively shallower basement are represented by gravity high as we see in La Salle Arch. Moreover, gravity and magnetic anomalies of Sabine, Monroe, and Jackson structures are modified and superimposed by large igneous bodies. Two regional gravity minima, Wiggins Arch and South of Sabine Uplift, are produced by less attenuated thick crust with deep Moho. Subsurface Mesozoic igneous rocks of Gulf

Coast Plain are characterized by circular gravity maxima where magnetic high anomalies correlate. Igneous bodies interpreted in this study are parallel with the existing geologically accepted ideas (Moody, 1949; Kidwell, 1951; Byerly, 1991; Ewing, 2009).

Three 2 – D gravity modeled sections, through the structural highs and lows, were constructed. Big scale subsurface Mesozoic igneous rocks of the area were also taken place with crustal structures in the models. Our models are constrained by available seismic refraction, well and geological data. To locate igneous bodies in the models, detailed literature review about the igneous activity during Mesozoic Era were conducted. Cross-cutting relationships and available petrological analysis were obtained for Monroe and Jackson structures (Baksi, 1997; Halbouty and Halbouty, 1982; Nichols et. al, 1968). This information was also considered during modeling stage. Shape and dimension of the buried volcano beneath Jackson Dome was integrated to the models from a previous study (Dockery, 1997). Since there is no available study defining the shape and size of the igneous rock bodies beneath Sabine and Monroe Uplifts, theoretically cylindrical bodies were used in the models. Although igneous rocks of Sabine Uplift have been discussed in the literature, there is not any age determination and specific cross-cutting relationship information in the previous studies. Therefore, position of igneous bodies in the models were decided where calculated anomalies gave the best fit with the observed anomalies with a consideration of magnetic anomalies. Our preferred 2 – D models are shown in chapter 5 (Figure 5.19, 5.21, 5.24). However, before we obtained our preferred models, other alternative models had also been created.

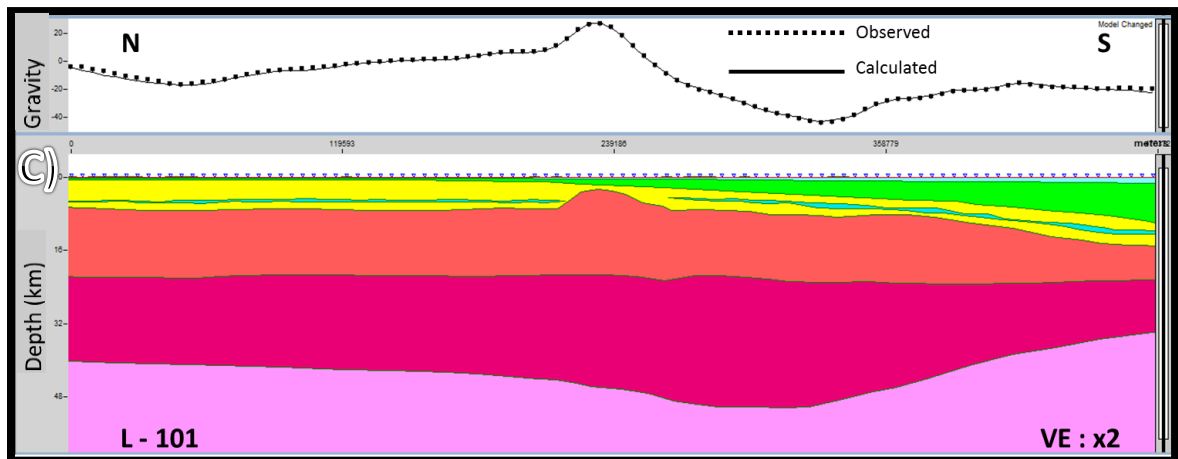
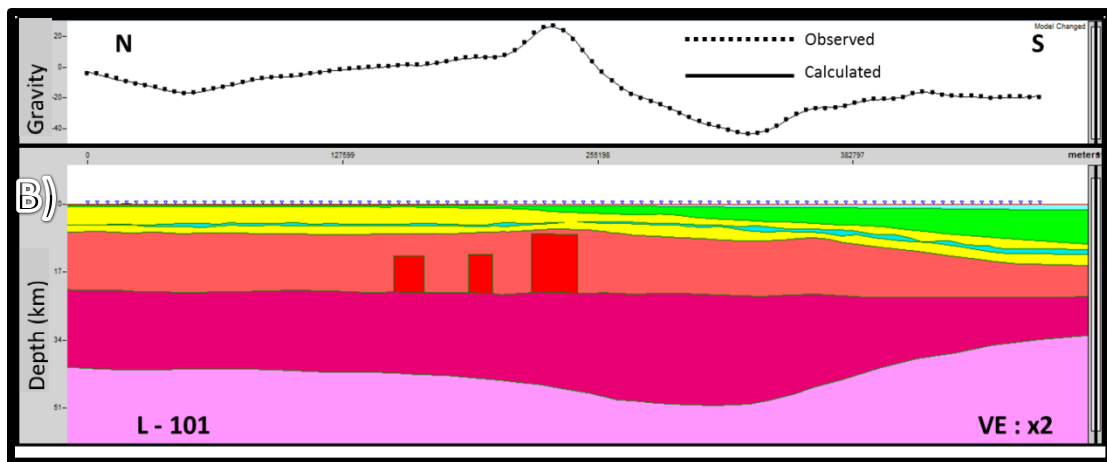
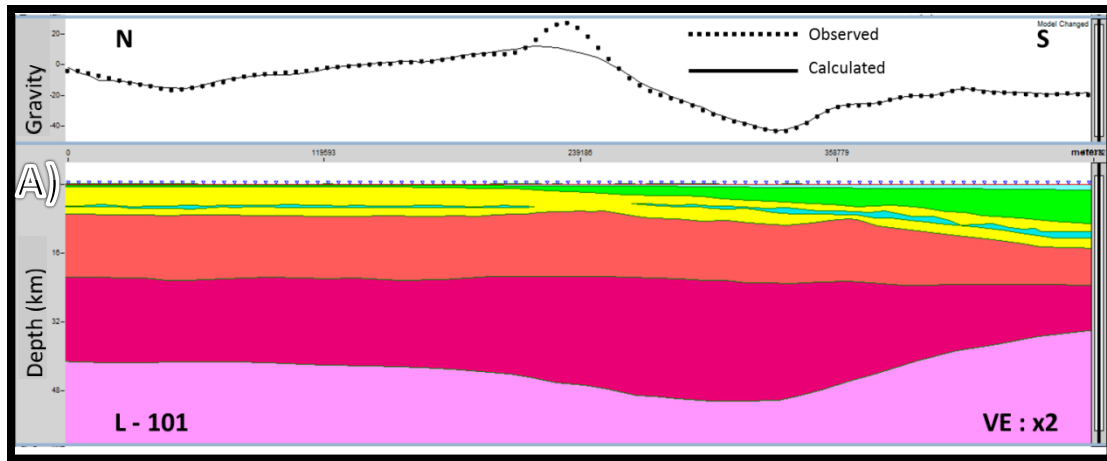


Figure 6.1: Alternative 2 – D gravity models for model 1: L-101; A) Gravity anomalies without igneous bodies; B) Our preferred model with igneous bodies; C) Gravity anomalies with an uplifted crust beneath Sabine Uplift

Figure 6.1.A shows the calculated and observed gravity curve for the model in the absence of igneous rocks. In such a situation, there are two geologically reasonable possibilities to generate the gravity maxima. The first one is an intruded igneous body which we discuss in our preferable model (Figure 6.1.B). Model B is our preferred model which correlates the anomalies produced by Cretaceous intrusions in the upper crust that has been discussed by Flawn et. al, 1961. The second one is a crustal uplift to match observed anomalies.

This hypothesis was modeled as a crustal uplift (Figure 6.1.C) on the area. However, it was hard to fit the observed anomaly without ruling out already known depth of sedimentary rock section and crust. Depth of the uplifted crust would have to be 2.5 – 2.7 km to match the curve but it is very shallow and none of the existing ideas and studies supports this. However, there is not any evidence or observation in the area that shows so shallow basement. In addition, our results also show that there is a relatively shallower basement beneath Sabine Uplift about 6 km but 2.5 km basement depth is not acceptable for this area. This model is speculative. Although it is geologically possible, it is not as plausible as the preferred model.

The model in the Figure 6.1.B is preferred because of several reasons: 1) qualitative interpretations of the data and filter maps suggest an occurrence of igneous body; 2) igneous rocks give the best fit during the forward modeling by considering both gravity and magnetic anomalies; 3) some geophysical and geological indicators have been interpreted as magmatism in the previous studies. Results of our models are mainly

parallel with other studies in the area (Kruger and Keller, 1986; Mickus and Keller, 1992). Some of our model parameters as basement depth, sedimentary thicknesses and igneous bodies of Sabine Uplift match with the results of Kruger and Keller, 1986. However, Moho depth in their model is shallower than ours in the first model (L-101; Figure 5.20). Shallower basement as up to 34 km beneath Sabine Area does not agree with the results of the seismic refraction results of Hales, 1970.

There are disadvantages of our models and interpretations. Horst and grabens of buried rift basins are not shown in our models. Large spacing control data in the area does not allow us to locate this kind of structures. In addition, salt structures of the area; especially in East Texas Salt Basin, North Louisiana Salt Basin, and Mississippi Salt Basin; were not modeled in detail. We believe that interpreted high resolution seismic refraction data can help to improve details of models because GM-SYS modeling software let you load and tie the seismic refraction data to the models.

## **6.2. CRUSTAL STRUCTURE**

Results of crustal thickness map, depth to Moho and depth to basement maps, are discussed in chapter 5 and figures are shown in Figure 5.20 to Figure 5.22. According to our results, Sabine Uplift and south of Sabine Uplift have a relatively thicker crust than the surrounded areas. Moho is deep and basement is shallow. East Texas Salt Basin has a thin crust, deep basement, shallow Moho and thick salt layer where crust is attenuated more during the rifting. After rifting stopped, high amount of subsidence took place during the cooling stage of crust that enabled the deposition of thick sedimentary

packages. To the east, there is another structural high, La Salle Arch, in which basement is shallower and salt layer is very thin. Between this structure and Sabine Uplift, North Louisiana Salt Basin is located. Salt layer is thicker than the surrounded areas. There is a small relief in the crustal topography of Monroe Uplift but there is not a major change. Small amount of flexural bending of the plate beneath buried igneous rocks of Jackson Dome appears in the models especially to the west and northwest. There is not a direct evidence or previous study related with that. However, dense igneous rocks in a sedimentary basin can cause this kind of flexure according to its lithospheric properties as flexural rigidity. We see examples of this kind of structures at the present time like Hawaii Islands and Colorado River Basalts. There is a major change in the crustal structure to the south. Coastal line of the Texas – Louisiana border has a thin crust, shallower Moho and thick sedimentary basin up to 11 km.

Crustal structure of the area was also discussed in previous studies (Bassin et. al, 2000; Sawyer et. al, 1991; Salvador, 1991). Figure 6.2 shows the crustal thickness map of CRUST 2.0. Crustal thickness map of our study is shown in Figure 5.20. Crust 2.0 is a global crustal model by 2 x 2 degree grid. Since it is a global model it lacks the detail of crustal structures. However, the crustal thickness values do not match with our models especially around Sabine Uplift where control points in our models including seismic refraction data, well data and regional cross sections are available. Trend of thinning crust in the south is almost similar with our results.

Crustal thickness map of Sawyer et. al, 1991 is shown in Figure 6.3 which is a result of a total tectonic subsidence analysis study. General trend of the crustal thicknesses show similarities with our results (Figure 5.20). Thickening of the crust around Sabine Uplift is obvious and parallel with our results. In addition, trend of thinning of the crust in the south is roughly parallel to the coast line where we have similar results. However, crustal thicknesses have different values with our results. Our results show that thicknesses of the crust beneath Sabine and Uplifts are 38 – 41 km and 34 – 38 km, respectively. Whereas Sawyer et al.'s map shows that crustal thicknesses for the same areas are 30 – 35 km. Since results of this study are based on subsidence analysis, they used some assumptions for this method. Original crustal thickness was assumed 40 km. In addition, they defined the basement of the area all the rocks beneath Middle Jurassic Unconformity, including Upper Triassic and Lower Jurassic sediments. However, onshore drilling results had proved the occurrences of sedimentary rocks beneath Louann Salt in Northeast Texas and Northwest Louisiana. The following results are gathered

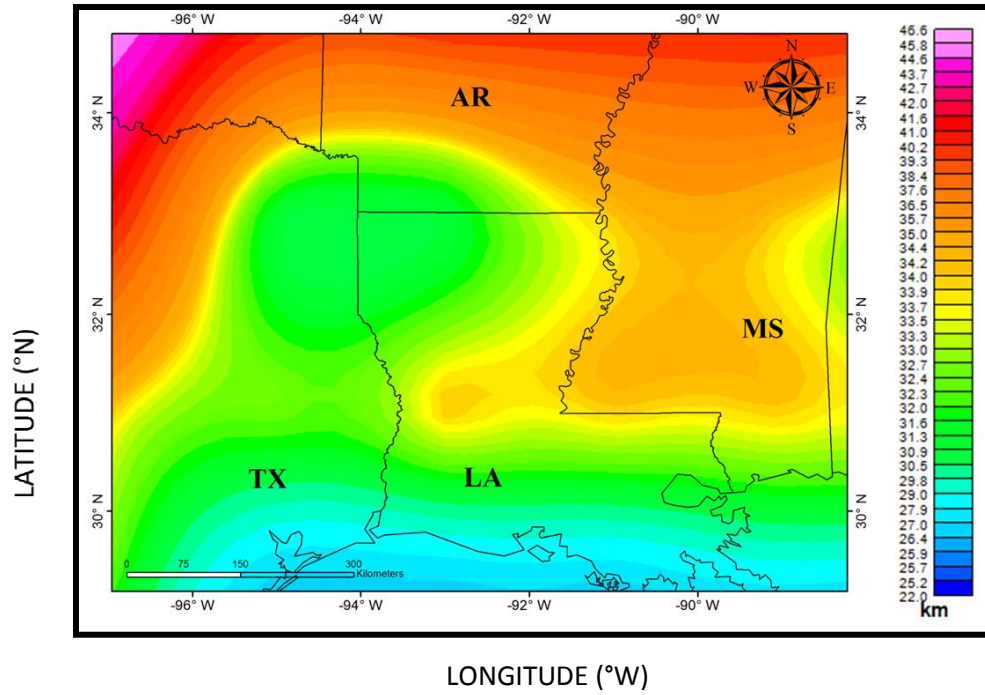


Figure 6.2: Crustal thickness map of CRUST 2.0 for the area

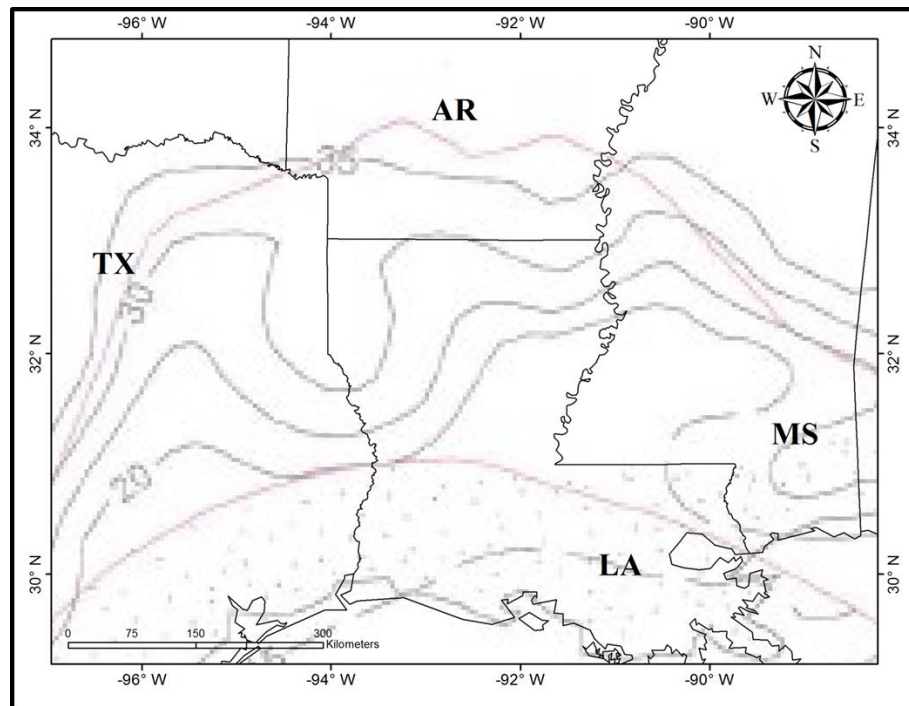


Figure 6.3: Crustal thickness map by Sawyer et. al, 1991 (Contours are in km)

from Nichols et. al, 1968 and Nicholas and Waddell, 1989. Penetration of sedimentary rocks beneath Upper Jurassic Salt is reported in Placid Oil Co. H. A. Dunn No. 2, Harrison County location. Exxon Boise Southern No. 1 well drilled around 700 m of rocks beneath Jurassic Unconformity, including late Paleozoic sedimentary rocks. 240 m of sedimentary rocks beneath Jurassic Unconformity, was drilled in Shell Southern No. 1 well location. These results show that the crystalline basement under this area should be located deeper than Upper Jurassic rocks. The assumptions of this model might lead the differences between the results of ours and this study. Although our results are not neither unique nor the only solution, they are compatible with the results of previous seismic refraction studies.

### **6.3. STRUCTURAL EVOLUTION OF THE UPLIFTS**

After the Gulf of Mexico basin had taken its final form during the Berriasian age, it was tectonically stable until the end of Early Cretaceous. Regional uplifts, tilting, erosion, and igneous activity, were started to occur with the beginning of Late Cretaceous time and continued until Paleocene. Sabine Uplift, Monroe Uplift and Jackson Dome were formed within this period.

Tectonostratigraphic chart of the uplifts (Figure 6.4) shows the unconformities, eroded and deposited formations, and igneous activity in detail. This chart is prepared by combining information of previous studies and our results. Depositional history and dated

age of igneous rocks were obtained from previous studies (Mancini et. al, 2005; Mancini et. al, 2008; Halbouty and Halbouty, 1982; Nichols et. al, 1968, Ewing, 2009; Baksi, 1997; Sundeen and Cook, 1977; Salvador, 1991).

Clastic rocks of the Woodbine and time – equivalent Tuscaloosa formations were deposited in the Northern Gulf of Mexico Basin overlying the Early Cenomanian unconformity. The entire region was affected from this pronounced regional unconformity. The maximum uplift occurred in the Southern Arkansas up to 3000 m in the center where Cenomanian sedimentary rocks were deposited over pre-Upper Jurassic rocks (Ewing, 2009). Abundant volcanic material of Woodbine and Tuscaloosa strata could be derived from the erosion in this region.

Igneous activity in the area started during Cenomanian and Turonian. Figure 6.5 shows the paleogeography of the region with igneous activity during this time. Volcanos were interpreted in the area of present Monroe Uplift and Jackson Dome (Salvador, 1991). As a result of emplacement of igneous rocks, these structural features were formed or at least enhanced.

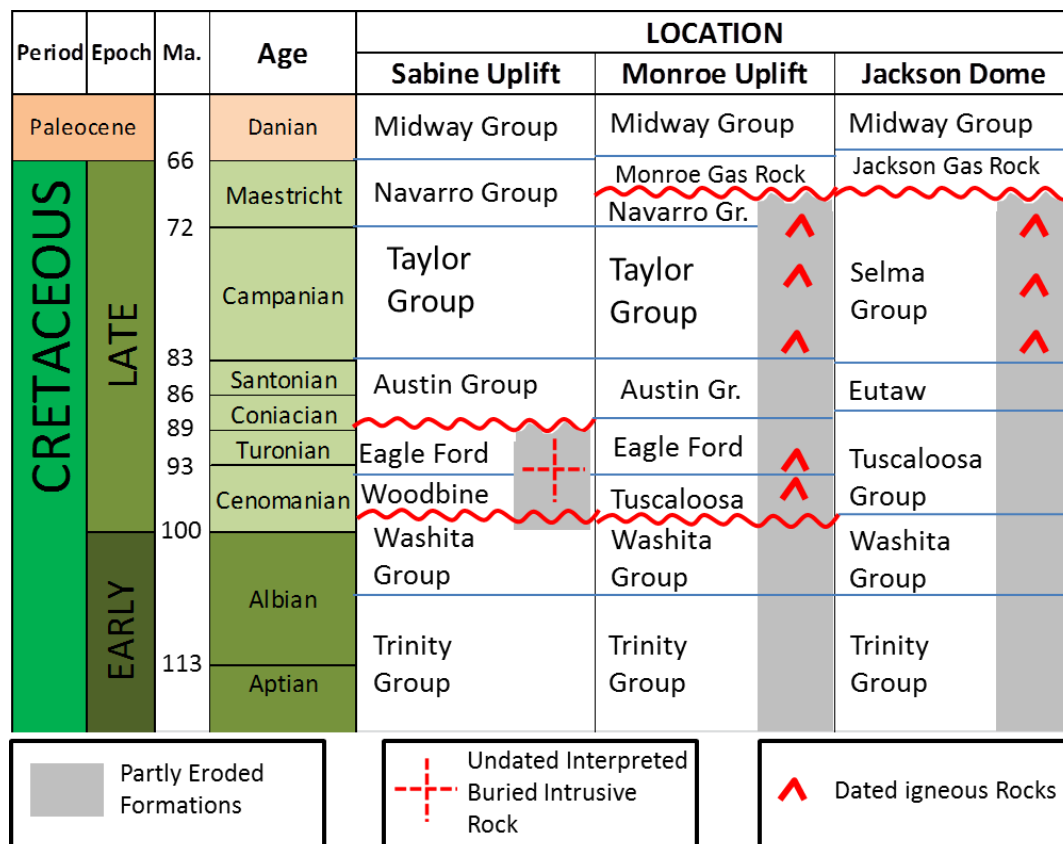


Figure 6.4: Tectonostratigraphic chart of the uplifts. Depositional history and dated age of igneous rocks were obtained from previous studies (Mancini et. al, 2005; Mancini et. al, 2008; Halbouty and Halbouty, 1982; Nichols et. al, 1968, Ewing, 2009; Baksi, 1997; Sundeen and Cook, 1977; Salvador, 1991).

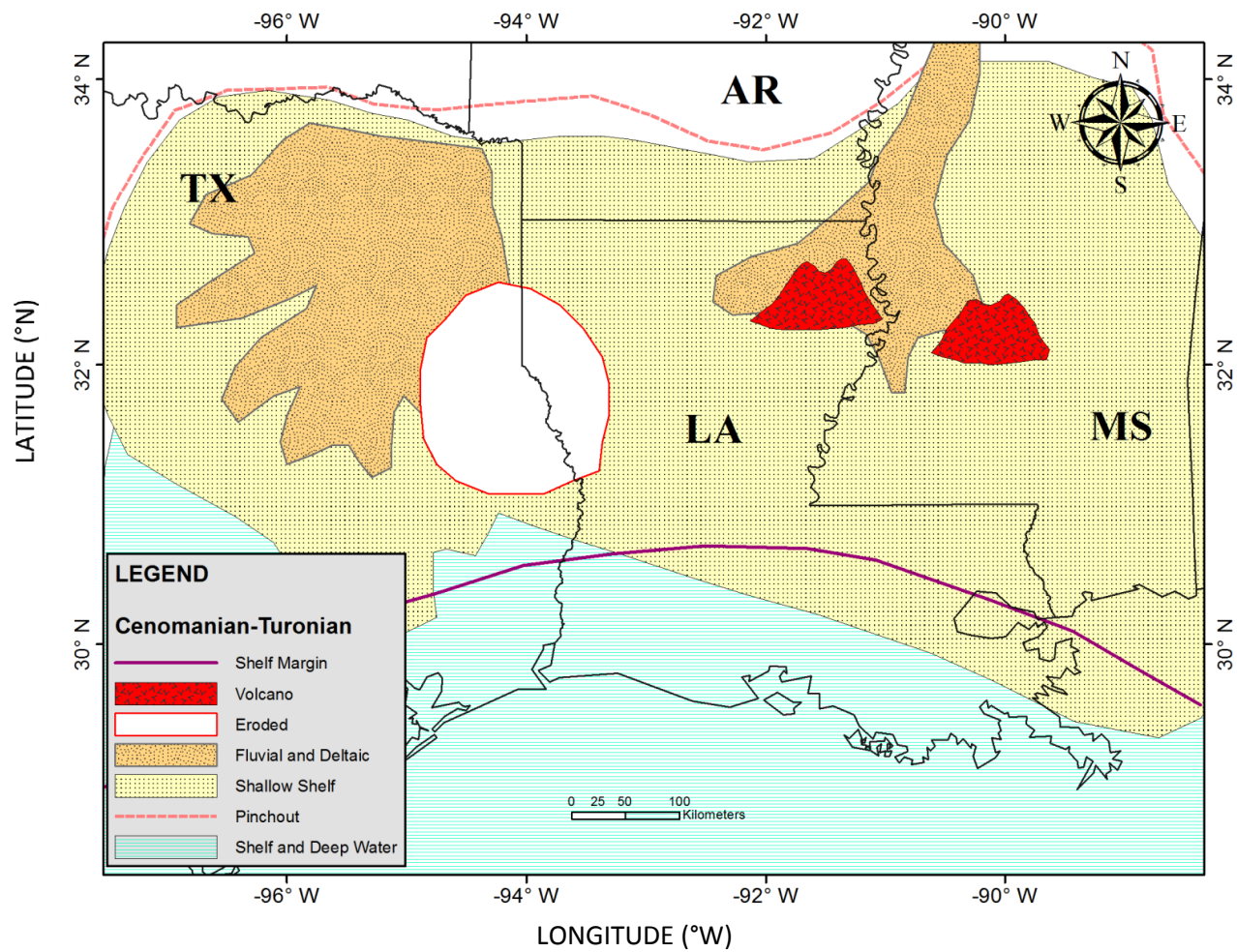


Figure 6.5: Paleogeography of the region during Late Cenomanian – Turonian (modified from Salvador, 1991).

Sabine Uplift area was uplifted and eroded during late Cenomanian and Turonian time (Figure 6.5). Rise of the area resulting with an angular unconformity is a local event. The unconformity does not exist in further west and east. Figure 6.6 shows the rise of Sabine Uplift based on position of James Limestone (Early Cretaceous in age) during that period. During rise of Sabine Uplift, Woodbine and Eagle Ford Formations were partly eroded and Austin Chalk of Coniacian age overlaid these formations with an angular unconformity as a trap. The truncation of the Woodbine Formation on the western flank of the Sabine Uplift formed East Texas Field which is one of the most prolific petroleum fields of the North America. As we discussed in the Chapter 5, our results show the occurrence of intrusive igneous rocks beneath Sabine Uplift. The most potential explanation for the rise of the Sabine Uplift during the deposition of Woodbine and Eagle Ford Formations is the thermal doming caused by the igneous rocks beneath this structure. It is shown in the tectonostratigraphic chart as an interpreted igneous rocks formed during Cenomanian and Turonian. This interpretation is plausible because the rise of the Sabine Uplift followed by erosion is limited in a circular area where our results show the occurrence of igneous rocks. Although it is missing the direct evidence (dated sample) of igneous activity in this age, it had been discussed in the previous studies (Ewing, 2009; Salvador, 1991, Jackson and Laubach, 1988).

Volcanic activity in the Monroe Uplift continued during the entire Upper Cretaceous. Age of the dated samples and diversity of igneous rocks has been discussed (Baksi, 1997; Sundeen and Cook, 1977; Ewing, 2009). Schematic interpretive section through Monroe Uplift is shown in Figure 6.7.

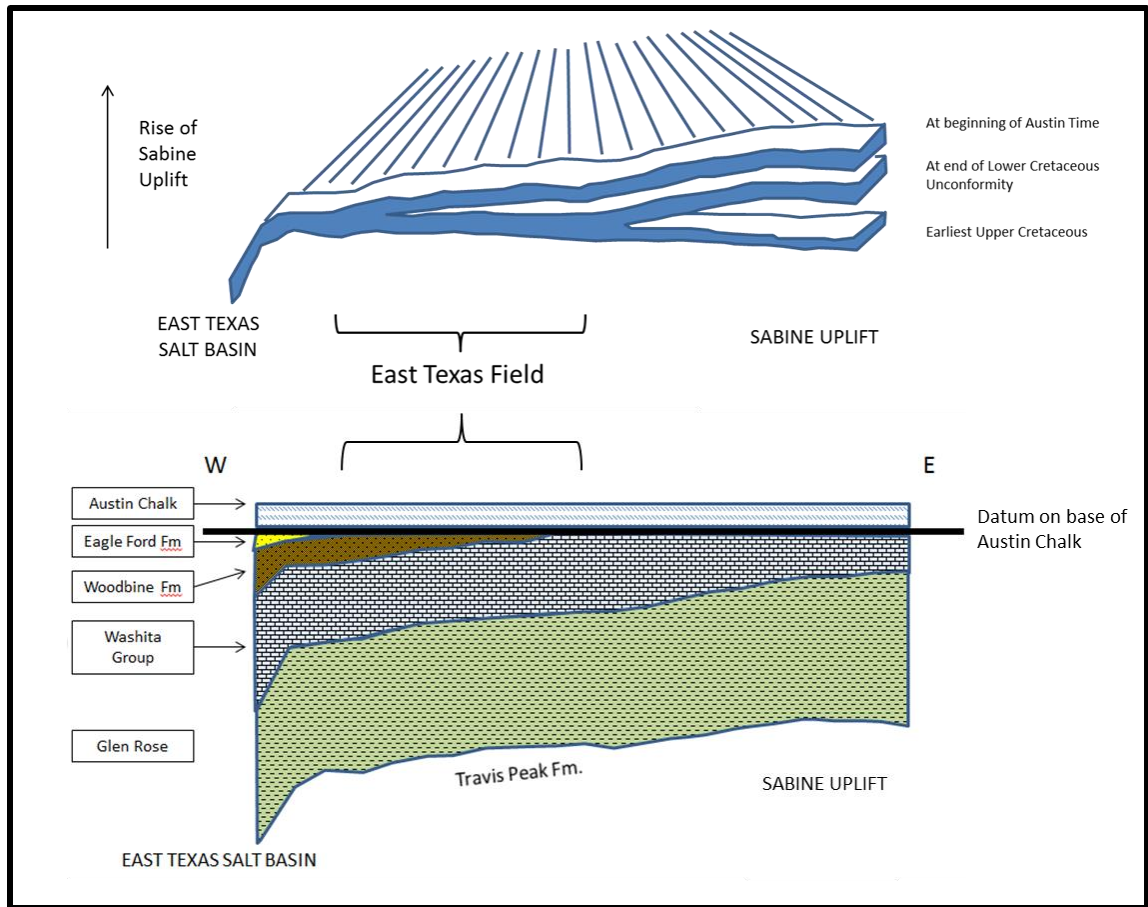


Figure 6.6: Rise of the Sabine Uplift based on the position of James Formation and cross – section with datum on base of Austin Chalk. Truncation of Woodbine Formation created stratigraphic trap of East Texas Field (modified from Halbouty and Halbouty, 1982).

There are two major uplifts which are followed by erosion resulting with angular unconformities as shown in tectonostratigraphic chart. The older unconformity is a result of regional uplift and erosion. However, the younger unconformity where latest Upper Cretaceous and Paleocene rocks are overlying older units unconformably is a local uplift

associated with igneous activity. On the top of high standing structure, carbonate shoals of Monroe Gas Rock was deposited.

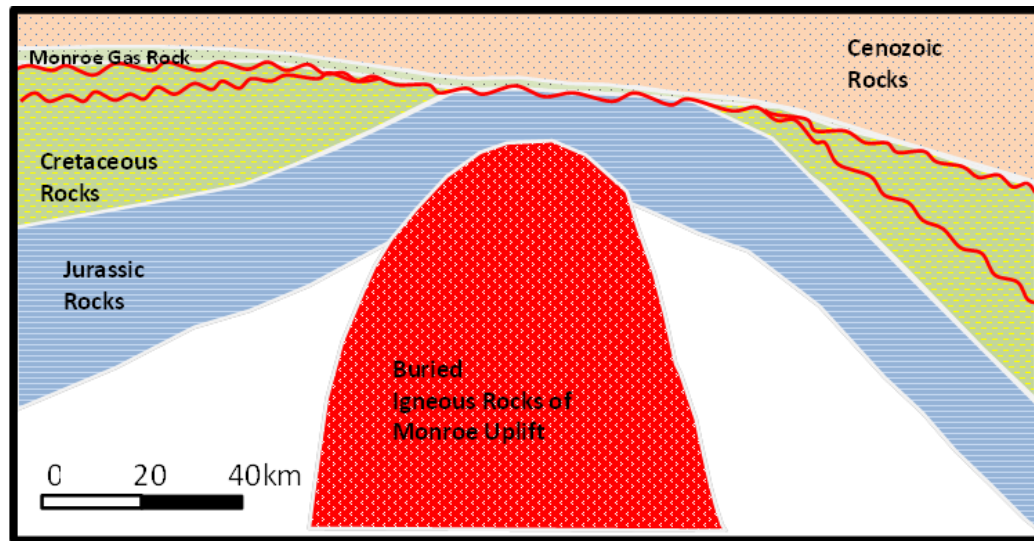


Figure 6.7: Interpretative cross section through Monroe Uplift. The lower unconformity where Upper Cretaceous rocks are overlying older Lower Cretaceous rocks unconformably is a regional unconformity. The upper unconformity where Monroe Gas Rock is overlying Cretaceous and Jurassic rocks unconformably is a result of a local rise of this structure (modified from Johnson, 1958).

Buried volcano of the Jackson Dome was discussed in our results. In addition, dated samples from the area and its cross – cutting relationship with surrounded rocks prove that igneous activity in this locality was active until latest Upper Cretaceous. Tilting of the Jurassic and Cretaceous rocks due to volcanic activity was followed by erosion of uplifted (up to 2000 m) sedimentary rocks. The rocks in Latest Upper Cretaceous and Paleocene age were deposited on this high standing structure. Carbonate shoals of latest

Cretaceous Jackson Gas Rock formed a major natural gas reservoir on top of this structure.

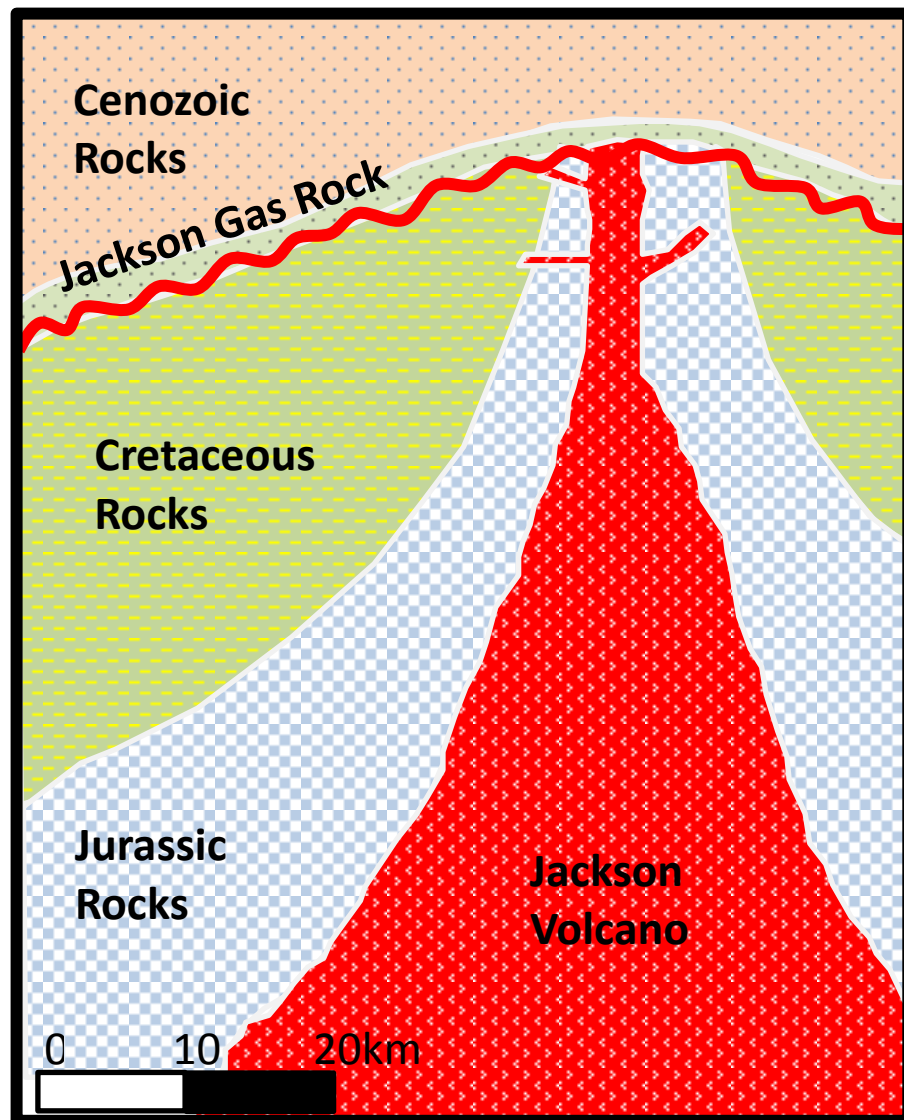


Figure 6.8: Cross – section through Jackson Dome (modified from Dockery, 1997).

## **CHAPTER VII**

### **CONCLUSION**

The Gulf of Mexico Basin is one of the richest hydrocarbon basins in the world. It is well-studied especially in the areas of active and successful exploration. Onshore Northern Gulf of Mexico Basin contains major petroleum – producing trends of Upper Jurassic, Upper Cretaceous and Lower Cretaceous in the areas of North East Texas, North Louisiana and west-central Mississippi. Moreover, development of shale gas plays in these areas revived the recent exploration projects. Rising of the Sabine Uplift during Late Cretaceous provide major traps for oil and gas accumulation in East Texas Field and natural gas plays have been discovered related with Monroe and Jackson structures. Understanding of the crustal architecture of the region and relationship between the structural elements and the interior basins are crucial. There are still different ideas about crustal architecture, structural elements of the basin, and presence or absence of magmatism in some of the areas.

Interpretation of the potential field data and 2 – D models constrained by all available data are useful tools in tectonic and geological studies to determine basement structures and locations of magmatism. Our results suggest that the crystalline crust of the northern onshore Gulf of Mexico Basin was variably extended beneath the Sabine, Monroe and Jackson Uplifts. There is a thick crust beneath Sabine Uplift with a shallow basement and deep Moho. Thickness of the crust is decreasing to the south through Texas – Louisiana coast line where differential subsidence led thickening of the sedimentary rocks in Cenozoic and Mesozoic age sharply. From west to east interior basins are located between high standing structures with deeper basement and they are characterized by structures and thick accumulations of salt layer. Upper Cretaceous igneous activity modified and superimposed the crustal and basinal structures. Our results suggest that large-scale igneous bodies beneath Sabine, Monroe and Jackson Uplifts are present. This activity was followed by partly erosion of the uplifted formations resulting in angular unconformities. Sabine and Monroe Uplifts show multiple stages of uplifting marked by regional and local unconformities. On the other hand, Jackson Dome shows only one pronounced single stage uplift where latest Upper Cretaceous and Paleocene rocks are underlain by Upper Jurassic sedimentary rocks. Late Cretaceous stage of uplifts and age of igneous rocks in Monroe and Jackson structures suggest that rise of the structures during this time are associated with igneous activity. Local rise of the Sabine Uplift, during Woodbine and Eagle Ford Gulf Stages, was interpreted as a result of igneous activity modeled in this study. Unraveling the complex relationship between this

structuring and magmatism requires a solid understanding of the crustal architecture of the region.

This study is important because all existing ideas and available data were considered during analysis and interpretations as a result of a detailed literature review. Models and results of this study are an integrated synthesis of available data. They show similarities and differences with previous studies and existing ideas. Results and models can be tested and improved by further studies and higher resolution data.

## **CHAPTER VIII**

### **REFERENCES**

- Baksi, A. K., 1997, The timing of Late Cretaceous alkalic igneous activity in the northern Gulf of Mexico Basin, southeastern USA: *Journal of Geology*, v. 105, p. 629-643.
- Bassin, C., Laske, G. and Masters, G., The Current Limits of Resolution for Surface Wave Tomography in North America, *EOS Trans AGU*, 81, F897, 2000.
- Bird, D.E., Burke, K., Hall, S.A., and Casey, J.F., 2005, Gulf of Mexico tectonic history: Hotspot tracks, crustal boundaries, and early salt distribution: *American Association of Petroleum Geologists Bulletin*, v. 89, p. 311–328.
- Blakely, R.J., 1995, *Potential theory in gravity and magnetic applications*: New York, Cambridge Univ. Press 441 p.

- Blakely, R., and Simpson, R., 1986, Approximating edges of source bodies from magnetic or gravity anomalies, *GEOPHYSICS*, 51(7), 1494–1498.
- Buffler, R. T., 1991, *Early Evolution of the Gulf of Mexico Basin*, in D. Goldthwaite, ed., pp. 1-15, Introduction to Central Gulf Coast Geology, New Orleans Geological Society, New Orleans, Louisiana.
- Byerly, G. R., 1991, Igneous activity, *in* A. Salvador, ed., The Gulf of Mexico Basin: The geology of North America, v. J: Geological Society of America, Boulder, Colorado, p. 91-108.
- Christensen, N.I., 1989, Pore pressure, seismic velocities, and crustal structure, In Pakiser, L.C., and Mooney, W.D., (eds.), Geophysical framework of the continental United States: Geological Society of America Memoir, v.172, 783–798.
- Cox, R. T., and R. B. Van Arsdale, 2002, The Mississippi Embayment, North America: A first order continental structure generated by the Cretaceous superplume mantle event: *Journal of Geodynamics*, v. 34, p. 163-176.
- Dockery, D.T., Marble, J.C., Henderson, J., 1997, The Jackson volcano. Mississippi Geology 18, 33–45.

Ewing, T. E., 1991, Structural features, *in* A. Salvador, ed., The Gulf of Mexico Basin: The geology of North America, v. J: Geological Society of America, Boulder, Colorado, p. 31-52.

Ewing, T. E., 2009, The ups and downs of the Sabine Uplift and the northern Gulf of Mexico Basin: Jurassic basement blocks, Cretaceous thermal uplifts, and Cenozoic flexure: Gulf Coast Association of Geological Societies Transactions, v. 59, p. 253-269.

Ginzburg, A., W. D. Mooney, A. W. Walter, W. J. Lutter, and H. H. Healy (1983). Deep structure of northern Mississippi Embayment: Am. Assoc. Petr. Geol. Bull., 67, 2031- 2046.

Griffin, W.R., Foland, K. A., Stern, R.J., Leybourne, M.I., 2010. Geochronology of Bimodal Alkaline Volcanism in the Balcones Igneous Province, Texas: Implications for Cretaceous Intraplate Magmatism in the Northern Gulf of Mexico Magmatic Zone. Journal of Geology 118, 1-21.

Halbouty, M. T., and J. J. Halbouty, 1982, Relationships between East Texas Field region and Sabine Uplift in Texas: American Association of Petroleum Geologists Bulletin, v. 66, no. 8, p. 1042-1054.

Hales, A. L., Helsley C. E., and Nation J. B., 1970a, Crustal structure study on Gulf Coast of Texas: AAPG Bulletin, v. 54, p. 2040–2057.

Jackson, M. P. A., and Laubach, S. E., 1988, Cretaceous and Tertiary compressional tectonics as the cause of the Sabine Arch, East Texas and northwest Louisiana: Gulf Coast Association of Geological Societies Transactions, v. 38, p. 245–256.

Jacobsen, 1987, A case for upward continuation as a standard separation filter for potential-field maps, Geophysics, v. 52, #8, p. 1138 – 1148.

Johnson, O. H., Jr., 1958, The Monroe Uplift: Gulf Coast Association of Geological Societies Transactions, v. 8, p. 24-26.

Keller, G. R., L. W. Braile, G. A. McMechan, W. A. Thomas, S. H. Harder, W.-F. Chang, and W. G. Jardine, 1989, Paleozoic continent-ocean transition in the Ouachita Mountains imaged from PASSCAL wide-angle seismic reflection-refraction data: Geology, v. 17, p. 119-122.

Kidwell, A. L., 1951, Mesozoic igneous activity in the northern Gulf Coastal Plain: Gulf Coast Association of Geological Societies Transactions, v. 1, p. 182-189.

Laubach, S. E., and Jackson, M. L. W., 1990, Origin of arches in the northwestern Gulf of Mexico basin: Geology, v. 18, no. 7, p. 595–598.

Lawless, P.N. and G.F. Hart, 1990, The LaSalle Arch and its effects on Lower Paleogene genetic sequence stratigraphy, Nebo-Hemphill Field, LaSalle Parish, Louisiana: Gulf Coast Association of Geological Societies Transactions: v. 40, p. 459-473.

Mancini, E. A., P. Li, D. A. Goddard, and R. K. Zimmerman, 2005, Petroleum source rocks of the onshore interior salt basins, north central and northeastern Gulf of Mexico: Gulf Coast Association of Geological Societies Transactions, v. 55, p. 486 – 504.

Mancini E. A., P. Li., V. O. Ramirez, D. A. Goddard, and S. C. Talukdar, 2008a, Mesozoic (Upper Jurassic–Lower Cretaceous) deep gas reservoir play, central and eastern Gulf Coastal Plain, USA: American Association of Petroleum Geologists Bulletin, v. 92, p. 283-308.

Macleod, I. N., Vieira, S., & Chaves, A. C., 1994., Analytic signal and reduction-to-pole in the interpretation of total magnetic field data at low magnetic latitudes.

Milligan, P.R., Gunn, P. J., Enhancement and presentation of airborne geophysical data, AGSO Journal of Australian Geology and Geophysics, v. 17, p. 63-75, 1997.

Moody, C. L., 1949, Mesozoic igneous rocks of the northern Gulf Coastal Plain: American Association of Petroleum Geologists Bulletin, v. 33, p. 1,410-1,428.

- Nichols, P. H., Peterson, G. E., and Wuestner, C. E., 1968, Summary of subsurface geology of northeast Texas, *in* Beebe, B. W., and Curtis, B. F., eds., Natural gases of North America: American Association of Petroleum Geologists Memoir 9, v. 2, p. 982–1004.
- Nunn, J. A., 1990, Relaxation of continental lithosphere: An explanation for Late Cretaceous reactivation of the Sabine Uplift of Louisiana-Texas: *Tectonics*, v. 3, p. 341-359.
- Nunn, J. A., A. D. Scardina, and R. H. Pilger, Jr., 1984, Thermal evolution of the north-central Gulf Coast: *Tectonics*, v. 3, p. 723-740.
- Rogers, R.E., 1968. Carthage field, Panola County, Texas. In: B.W. Beebe (Editor), Natural Gases of North America. Am. Assoc.
- Salvador, A., 1987, Late Triassic – Jurassic paleogeography and origin of Gulf of Mexico Basin: *AAPG Bulletin*, v. 71, p. 419–451.
- Salvador, A., 1991, Origin and development of the Gulf of Mexico Basin, *in* A. Salvador, ed., The Gulf of Mexico Basin: Geological Society of America, The geology of North America, v. J, p. 389– 444.

Saunders, J. A., and D. W. Harrelson, 1992, Age and Petrology of the Jackson Dome Igneous-Volcanic Complex, Mississippi: Implications for the Tectonic History of the Mississippi Salt Dome Basin, Gulf Coast Association of Geological Societies, Transaction

Sawyer, D. S., R. T. Buffler, and R. H. Pilger, Jr, 1991, The crust under the Gulf of Mexico Basin, *in* A. Salvador, ed., The Gulf of Mexico Basin: The geology of North America, v. J: Geological Society of America, Boulder, Colorado, p. 53-72.

Sundeen, D. A., and Cook, P. L., 1977, K-Ar dates from Upper Cretaceous volcanic rocks in the subsurface of west-central Mississippi: Geol. Soc. America Bull., v. - 88, p. 1144–1146.